Modelling and Control of Floating Wind Turbines

Iosu García de Baquedano, B.Sc.

Master-Thesis – 30. September 2016

Supervisor: Bastian Ritter, M.Sc.

TECHNISCHE
UNIVERSITÄT
DARMSTADT

REGELUNGSTECHNIK
UND MECHATRONIK rtm

Scope of the work

Floating wind turbines shall harvest the large amount of far-offshore wind energy. The offshore wind conditions are in general more predictable wind low turbulence intensities and higher mean wind speeds. However, there are still technological challenges for operational control due the rough offshore climate as well as maintenance and installation of power plants. One central part of the operating control is the actual wind turbine controller which regulates mainly the power production, stabilizes the system and keeps it within the allowable limits. For the design of advanced controllers a mathematical representation is required which serves as so called design model. This thesis shall develop such an engineering model for floating turbines that incorporates the drive-train, platform pitch and roll movement as well as the wind speed model. After the equations have been derived theoretically, it needs to be parametrized and validated against FAST code. Based on the valid design model advanced linear/nonlinear controllers shall be developed and tested in order to regulate the power and the mechanical vibrations actively, and compensate the pitch instability by a multivariable approach. The results and findings of the thesis need to be documented completely and critically within a scientific report. The consecutive research topics shall be discussed in an outlook.

Beginn:	01. April 2016
Ende:	30. September 2016
Seminar:	11. October 2016

Prof. Dr.-Ing. Ulrich Konigorski

Bastian Ritter, M.Sc.

Technische Universität Darmstadt
Institut für Automatisierungstechnik und Mechatronik
Fachgebiet Regelungstechnik und Mechatronik
Prof. Dr.-Ing. Ulrich Konigorski

Landgraf-Georg-Straße 4
64283 Darmstadt
Telefon 06151/16-4167
www.rtm.tu-darmstadt.de

Erklärung

Hiermit versichere ich, dass ich die vorliegende Arbeit ohne Hilfe Dritter und nur mit den angegebenen Quellen und Hilfsmitteln angefertigt habe. Alle Stellen, die aus den Quellen entnommen wurden, sind als solche kenntlich gemacht. Diese Arbeit hat in gleicher oder ähnlicher Form noch keiner Prüfungsbehörde vorgelegen.

Darmstadt, den 30. September 2016

Iosu García de Baquedano, B.Sc.

Abstract

Due to the fast development of wind energy and exponential growing of installed wind turbines, the number of places with optimal wind conditions is limited and wind turbines are installed in the sea. For deep sea levels a concept known as floating offshore wind turbine has been developed. There are diverse types of turbines documented with different structures and ways of reaching stability.

In this thesis the wind turbine spar buoy concept is analyzed, modeled and validated against FAST, an already developed and non linear complex model of a floating offshore wind turbine. In order to design a controller which guarantees the stable operation of the turbine and will achieve to obtain the maximum energy of it, different controllers are developed and used for this task. Finally the performance of the system with all the controllers is tested and compared.

Keywords: Modeling, FAST, hydrodynamics, Morison's equation, state feedback, LQR, parallel path modification, non minimum phase zeros compensator.

Contents

Symbols, Abbreviations and Parameters

Latin symbols

Symbol	Description	Units
c_{blade}	Blade chord length	m
C_{D}	Drag force coefficient	-
C_{L}	Lift force coefficient	-
C_{M}	Torque coefficient	-
C_{P}	Power coefficient	-
C_{T}	Thrust coefficient	-
E_{k}	Wind kinetic energy	J
F_{t}	Wind thrust force	N
F_{ax}	Wind axial force	N
F_{buoy}	Buoyancy force	N
F_{weight}	Weight force	N
F_{tan}	Aerodynamic tangential force	N
F_{nor}	Aerodynamic normal force	N
GK	Sensitivity of power to blade pitch angle correction factor	-
h	Height from SWL to the point where the force acts on the blade	m
h_{buoy}	Center of buoyancy below SWL	m
H_{wave}	Wave height	m
K_{I}	Blade pitch PI controller integral gain	-
K_{P}	Blade pitch PI controller proportional gain	-
$K_{\text{I,LQR}}$	Integral action gain applied to LQR controller	
L	Lift force	N
D	Drag force	N
M_{nor}	Aerodynamic tangential moment	N m
M_{tan}	Aerodynamic normal moment	N m
$M_{\text{y,n}}$	Bladeroot flap moment of blade n	kN m
$M_{\text{z,n}}$	Bladeroot pitch moment of blade n	kN m
$M_{TTP,x}$	Tower top roll moment	N m
$M_{TTP,y}$	Tower top pitch moment	N m
$M_{TTP,z}$	Tower top yaw moment	N m
$M_{TB,x}$	Tower base roll moment	N m
$M_{TB,y}$	Tower base pitch moment	N m
$\dot{m}_{\text{wind}}$	Wind flow mass	Kg/s
P	Mechanical power	W
P_{av}	Available wind power	W
P_{lim}	Available maximum wind power	W

P_{Gen}	Generator mechanical power	W
T_{aero}	Aerodynamic torque	N m
T_{Gen}	Generator torque	N m
T_{mec}	Mechanical torque	N m
T_{Rot}	Low-speed shaft torque	N m
$V_{TTP,x}$	Tower top velocity in x direction	m/s
$V_{TTP,y}$	Tower top velocity in y direction	m/s
U_{∞}	Wind speed for upstream	m/s
v	Relative wind speed	m/s
W	Relative wind speed	m/s
x_{CM}	CM surge	m
y_{CM}	CM sway	m
z_{CM}	CM heave	m
$\boldsymbol{a}$	FOWT linear acceleration vector	m/s^2
$\boldsymbol{a}_{\text{b}}$	Floating platform acceleration vector	m/s^2
$\boldsymbol{a}_{\text{f}}$	Water particle acceleration vector	m/s^2
$\boldsymbol{F}_{\text{T}}$	Vector of applied forces on the wind turbine	N m
$\boldsymbol{F}_{\text{aero}}$	Aerodynamic forces and moments vector	N m
$\boldsymbol{F}_{\text{Hydro}}$	Hydrodynamic and hydrostatic forces and moments vector	N m
$\boldsymbol{F}_{\text{lines}}$	Mooring lines forces and moments vector	N m
$\boldsymbol{F}_{\text{mor}}$	Morison's force and moments vector	N m
$\boldsymbol{f}_{\text{u}}$	Nonlinear input vector	-
$\boldsymbol{F}_{\text{waves}}$	Waves forces and moments vector	N m
$\mathbf{K}_{\text{LQR}}$	LQR controller matrix	-
$\boldsymbol{q}$	Degrees of freedom vector	-
$\mathbf{Q}$	Matrix of nonlinear forces	N m
$\boldsymbol{u}$	Input vector	-
v_{b}	Floating structure velocity vector	m/s
v_{f}	Water particle velocity vector	m/s
$\boldsymbol{x}$	States vector	-
$\boldsymbol{y}$	Outputs vector	-

Greek symbols

Symbol	Description	Units
β	Blade pitch angle	rad
β_{waves}	Waves direction angle	rad
ω	Wave frequency	rad/s
Ω	Rotor speed	rad/s
Ω_{Gen}	Generator speed	rpm
ρ	Air density	kg/m^3
λ	Tip speed ratio	-
θ_{r}	CM roll angle	rad
θ_{P}	CM pitch angle	rad
θ_{y}	CM yaw angle	rad
θ_{yaw}	Nacelle yaw angle	rad
φ	Rotor azimuth	rad
$\omega_{\varphi n}$	Blade pitch PI controller natural frequency	rad/s
$\zeta_{\varphi n}$	Blade pitch PI controller damping ratio	-
$\boldsymbol{\alpha}$	Vector of FOWT angular acceleration vector	rad/s^2
$\boldsymbol{\tau}^{\boldsymbol{T}}$	Vector of applied moments on the FOWT	Nm

Wind Turbine Parameters

Parameter	Description	Value	Units
A	Rotor area	12,468.98	m^2
C_A	Normalized hydrodynamic-added-mass coefficient in Morison's equation	0.969954	-
C_D	Normalized viscous-drag coefficient in Morison's equation	0.6	-
$C_{P,opt}$	Optimal Betz coefficient	0.482	-
$C_{P,U_\infty=15}$	Betz coefficient for a wind speed of 15m/s	0.2087	-
$C_{T,U_\infty=15}$	Thrust coefficient for a wind speed of 15m/s	0.2484	-
c_{T,U_∞}	Gradient of thrust force with respect to effective local wind speed	$8.0181 \cdot 10^4$	Ns/m
c_{P,U_∞}	Gradient of thrust force with respect to effective local wind speed	$1.7281 \cdot 10^4$	Ns/m
$c_{T,\beta}$	Gradient of aerodynamic torque with respect to effective local wind speed	$-6.6026 \cdot 10^4$	Ns/m
$c_{P,\beta}$	Gradient of aerodynamic torque with respect to effective local wind speed	$-1.0185 \cdot 10^4$	Ns/m
D_T	Floating platform diameter	9.4	m
H	Hub height	87.6	m
h_{buoy}	Buoyancy center distance from SWL	62.06	m
h_T	Wind turbine and floating platform center of mass	76.55	m
i_{GB}	Gearbox ratio	93	-
I_T	Wind turbine mass moment of inertia	$1.9731 \cdot 10^{10}$	$kg\,m^2$
J_{DT}	Drivetrain inertia with respect to the low-speed shaft	43,785,000	$kg\,m^2$
k	Wave number	155	-
K_{opt}	Torque optimal parameter	0.0255764	Nm/rpm^2
m_T	Turbine and platform total mass	$8.163 \cdot 10^6$	Kg
N	Number of blades	3	Blades
R	Blade radius	63	m
P_{rated}	Rated generator power	5.296	MW
ρ_{air}	Air density	1.125	kg/m^3
ρ_{water}	Water density	1,025	kg/m^3
λ_{opt}	Optimal tip speed ratio	7.55	-
Ω_{rated}	Rated rotor speed	1.267	rad/s
$\left.\frac{\partial C_T}{\partial \lambda}\right\|_{U_\infty=15}$	Betz coefficient gradient with respect to tip speed ratio with a wind speed of 15m/s	-0.0425	-
$\left.\frac{\partial C_P}{\partial \lambda}\right\|_{U_\infty=15}$	Thrust coefficient gradient with respect to tip speed ratio with a wind speed of 15m/s	-0.039	-

$\left.\frac{\partial C_T}{\partial \beta}\right\|_{U_\infty=15}$	Betz coefficient gradient with respect to blade pitch angle with a wind speed of 15m/s	-2.2345	rad^{-1}
$\left.\frac{\partial C_P}{\partial \beta}\right\|_{U_\infty=15}$	Thrust coefficient gradient with respect to blade pitch angle with a wind speed of 15m/s	-1.9154	rad^{-1}
$\frac{\partial P}{\partial \beta}$	Sensitivity of power to the blade pitch angle		
$\mathbf{A}$	State matrix		
$\mathbf{A}^{\text{Hydro}}$	Hydrodynamic added mass matrix		
$\mathbf{A}^{\text{lin}}$	Linearized state matrix for a wind speed of 15m/s		
$\mathbf{A}^{\text{red}}$	Reduced model state matrix		
$\mathbf{B}$	Input matrix		
$\mathbf{B}^{\text{Hydro}}$	Hydrodynamic damping matrix		
$\mathbf{B}^{\text{lin}}$	Linearized input matrix for a wind speed of 15m/s		
$\mathbf{B}$	Input matrix		
$\mathbf{C}$	Output matrix		
$\mathbf{C}^{\text{lin}}$	Linearized output matrix for a wind speed of 15m/s		
$\mathbf{C}^{\text{red}}$	Reduced model output matrix		
$\mathbf{C}^{\text{Hydro}}$	Hydrodynamic restoring matrix		
$\mathbf{D}$	Feedforward matrix		
$\mathbf{D}^{\text{lin}}$	Linearized feedforward matrix for a wind speed of 15m/s		
$\mathbf{D}^{\text{red}}$	Reduced model feedforward matrix		
$\mathbf{D}$	Damping matrix		
$\mathbf{K}$	Stiffness matrix		
$\mathbf{M}$	Added mass matrix		

Abbreviations

Contraction	Full name
CB	Center of buoyancy
CM	Center of mass
DOF	Degrees of freedom
FOWT	Floating Offshore Wind Turbine
NREL	National Renewable Energy Laboratory
NMPZ	Non minimum phase zeros
SWL	Sea water level
LQR	Linear quadratic regulator

1 Introduction

The rapid development of wind energy and rising amount of installed wind farms are trending the wind turbine industry to go offshore. The problem is that not all the countries have shallow waters near the coast, hence a good solution needs to be found for waters deeper than 60 m. The development of the floating offshore wind turbine (FOWT) offers a feasible solution for those cases where the water is so deep.

Motions and forces in this kind of turbines are different from onshore or even fixed offshore wind turbines. Forces induced by wind and wave conditions are almost impossible to eliminate. That is why the design of FOWT and its controllers have to be adapted to these new conditions. Even though the control of FOWT is a relatively new area of research, there have been very interesting and promising developments.

The aim of this master thesis is to develop a mathematical model of the turbine and an optimized control that will improve the generation of energy and the operational life of these turbine. These concepts are very important because nowadays FOWT are not yet economically feasible. If designs and controllers keep improving, it will be a day when the inversion will not suppose a problem to install FOWT.

1.1 Objectives

Principle objectives of this thesis are the following

- Introduction to wind energy and the concept of floating offshore wind turbines (in particular the spar buoy concept).
- Identification of model relevant degrees of freedom and the usable actuators from a control point of view.
- Perform a white-box modeling approach based on existing preliminary work results.
- Identification of the relevant parameters of the derived semi-analytical model and derive/discover their numerical values for a 5MW reference wind turbine.
- Validation of the design model against FAST code and perform simulations with different wind fields.
- Formulate the control objectives verbally and develop a concept how to reach them with the given actuators, implement the controller in Matlab/Simulink.
- Evaluation and parametrization of the advanced controller and testing with the design model/FAST code.

- Testing and evaluation of different controller performance.

1.2 Overview

The report is structured in six chapters. The first one is an introduction to the thesis. In the second chapter, a basic introduction to the global energetic situation is given, focusing on the global wind energy situation. Some basic principles of wind energy and wind turbines are introduced and finally, a review of FOWT concepts is provided, emphasizing in the spar buoy concept.

In the next chapter, the turbine used to develop the model is described. Afterwards, all the calculus of the dynamics, kinematics and kinetics is carried out and explained. Once the model has been developed, it is validated against an existing accurate model called FAST. The behavior of the system in addition to the validation results are subsequently discussed.

The fourth chapter begins with an introduction to the basic wind turbine control. After that, the problems related to the application of this control to the FOWT are explained. New controllers are proposed to overcome these problems.

Eventually, chapter number five compares and analyzes implemented controllers performance and success is discussed.

Finally, the last chapter summarizes the entire project, analyzes the achievements and purposes topics for future research.

2 Wind energy

In this chapter an overview of the global situation of wind energy is presented. Wind turbine's basics are explained as well as different technologies in wind energy.

2.1 Worldwide energetic situation

The worldwide energetic situation has significantly changed in a brief period of time, especially with respect to electric energy. Some decades before there was not such a high electricity consumption as today and it was enough with the existing methods to produce it. Most of the energy and electricity was produced using fossil fuels. It was a relatively easy way of producing energy, not to mention that the amount of fuels was assumed to be infinite.

Nevertheless, the world has changed a lot in the last decades. The growing world population, the reduction of the amount of fossil fuels, political conflicts related to this short of resources, environmental damages produced by the use of fossil fuels, as well as the need of more ways of producing electricity, have led to the development of the renewable energies penetrating the global energetic market [1].

Countries started to use renewable energies to achieve different goals:

- Development of their own economies and technologies.
- Reduction of the energetic dependence.
- Security in the energetic supply.
- Protection of the environment.

Different kinds of renewable energies exist. Although some of them are more common used, it is worth mentioning all of them.

Hydropower. The production of electrical power through the use of the gravitational force of falling or flowing water. In 2015 hydropower generated 16.6 % of the world's total electricity and 70 % of all renewable electricity. [2]

Wind Power. Generation of electricity by extracting the kinetic energy of the wind. The air flow passes through the wind turbine in order to generate this electricity.

Solar Power. Conversion of sunlight into electricity, either directly using photovoltaic, or indirectly using concentrated solar power. When using concentrated solar power a thermal cycle is needed in order to make this conversion.

Bio energy. The production of energy by the use of biomass. Either directly via combustion to produce heat, or indirectly after converting it to various forms of bio-fuel. Biomass is the material derived from living or recently living organisms.

Geothermal energy. The production of both electricity and thermal energy by using the thermal energy stored in the Earth. Earth's geothermal energy originates from the original formation of the planet and from radioactive decay of minerals.

Marine energy. When one speaks about Marine energy, it refers to the energy carried by ocean waves, salinity and temperature gradients. This marine phenomena can be used to produce renewable energy. It is not as developed as the other technologies though.

Even though the use of the renewable energies is not prevailing, it is very significant. A 19.2 % of the world's primary energy and 23.7 % of the world's electricity is produced using different renewable energies, being hydropower the most used modern renewable technology, 3.9 % of the total primary energy and 16.6 % of the total amount of electricity generation [2]. Its enormous power density, low operating cost and good manageability, as well as high demand matching, have turn the hydropower into the most used renewable energy. However, constructing a hydro central has an enormous environmental and economic cost. This is why more environmentally friendly kinds of producing energy have been developed.

The appearance and development of modern renewable technologies, such as wind energy, solar energy, biomass energy, geothermal energy and ocean energy, has been very recent. Even though these technologies are newer and their presence in the worldwide energetic panorama is not as remarkable as traditional ways of producing energy and electricity, it is clear that they are being exploited, improved and growing year on year.

As this thesis focuses on wind turbines, a further analysis of the situation and basics of this technology is given.

2.2 Evolution of wind energy

Along the history, people have harnessed the force of the wind to propel ships. Another use of the wind can be found in the use of windmills to grind grain or to pump water. At the beginning of the twentieth century electricity came into use and windmills gradually became wind turbines as the rotor was connected to an electric generator.

The use of wind turbines to generate electricity can be traced back to the late nineteenth century. Charles F. Brush (USA) constructed a 12 kWDC windmill generator with 144 blades, a tower 17 meters high and a rotor diameter of 18 m. Professor Poul La Cour (Denmark) also made a huge contribution to this. Though, there was little interest in using wind energy. It was only used for battery charging, remote dwellings and low-power systems. [3]

It was not until 1973, when the price of oil increased dramatically, that a number of Government-funded programs of research were approved. There was considerable uncertainty

as to which architecture might prove most cost-effective and several innovative concepts were investigated at full scale. Finally, the horizontal axis and 3 bladed wind turbine was chosen as the most cost efficient and effective one. Since then, both the number of installed wind turbines and the size and power of turbines have grown exponentially.

Nowadays, the biggest wind turbines in serial production have powers of more than 8 MW, rotor diameters of around 180 meters and hub heights close to 160 m. Some examples of such enormous creations are *MHI Vestas V164* 8 MW*, Adwen AD-180* or *Siemens SWT-8.0-154* 8 MW. [4]

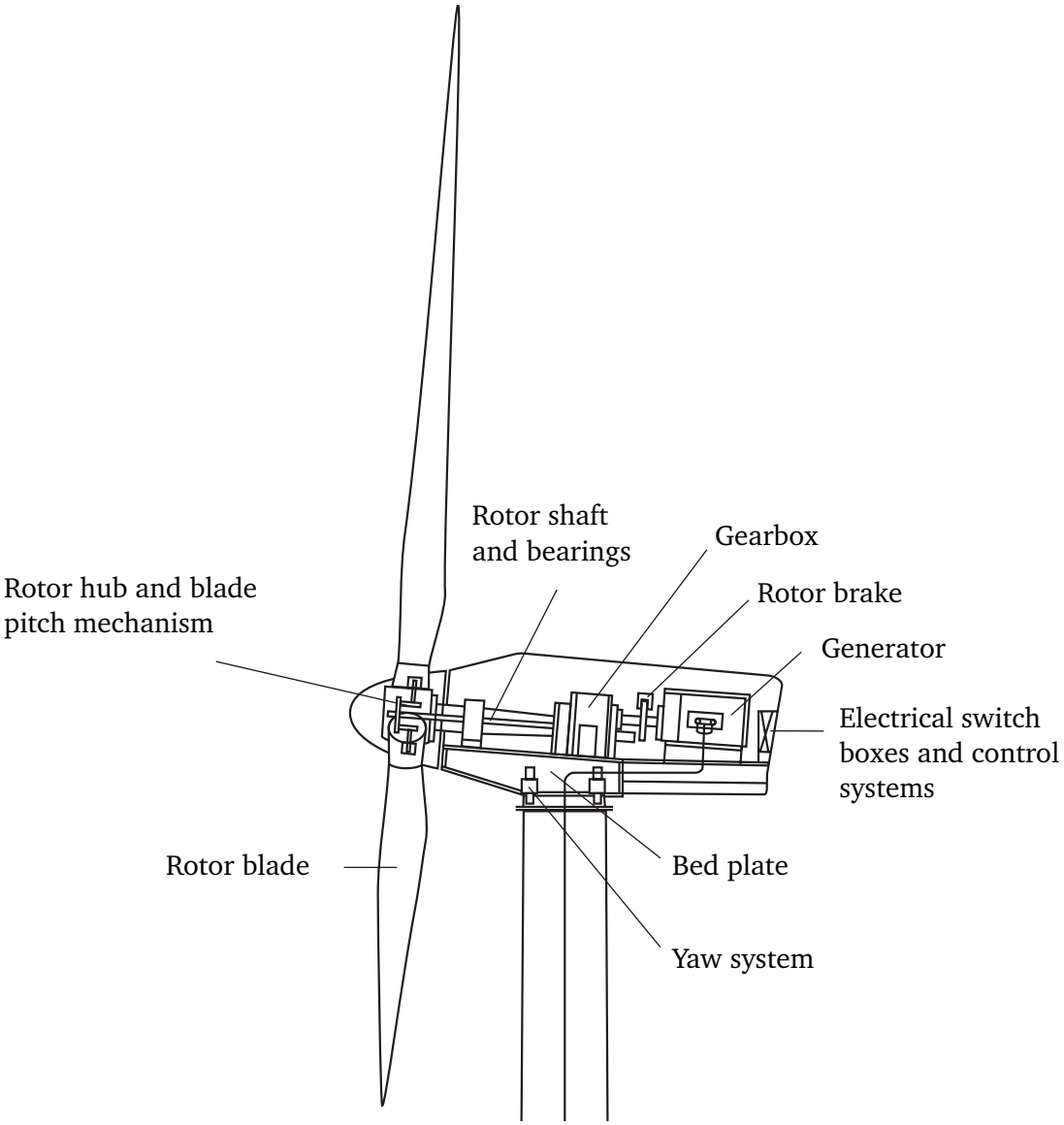

Figure 2.1.: Components of a wind turbine. [5]

2.3 Components of a wind turbine

Wind Turbines are very complex installations which have a lot of high technology components. Although all of the wind turbines have the same main components, depending on the location and work condition, these parts can be designed and developed differently. In Figure 2.1 the main components of a wind turbine are shown.

2.4 Basics of wind energy

Despite of the high number of different turbine types that have been brought into being over the years, the basic principle of all of them is the same. The mass of wind passes through the rotor and this mass slows down giving away some of its kinetic energy. The rotor, taking this kinetic energy, starts to rotate and an electric generator converts this rotation into electricity. Basically, what a wind turbine does is to convert the kinetic energy associated to the wind in electricity.

The mass of wind that passes through the rotor depends on the wind density, wind speed and rotor area:

$$\dot{m}_{\text{wind}} = \rho_{\text{air}} A U_{\infty} \tag{2.1}$$

The kinetic energy associated to this mass is:

$$E_{\text{k}} = \frac{1}{2}\dot{m}_{\text{wind}} U_{\infty}^2 \tag{2.2}$$

And the available wind power is:

$$P_{\text{av}} = \frac{\rho_{\text{air}}}{2} A U_{\infty}^3 \tag{2.3}$$

Nevertheless, not all the available power can be harvested. There is a physical limit, which is named Betz limit, that does not allow us to take advantage of all the wind power available:

$$P_{\text{lim}} = \frac{\rho_{\text{air}}}{2} A U_{\infty}^3 C_{\text{P,max}} \tag{2.4}$$

The maximum theoretical value of this limit is 0.59, therefore the maximum power it can extracted from the wind is the 59 % of the available power. In practice this percentage is smaller due to the design of the blades and constructive characteristics of the turbine. This is why the tip speed ratio λ is defined. This coefficient depends on the turbine number of blades, the rotor radius, the angular speed and the wind speed. This coefficient is defined as

$$\lambda = \frac{\Omega R}{U_{\infty}} \tag{2.5}$$

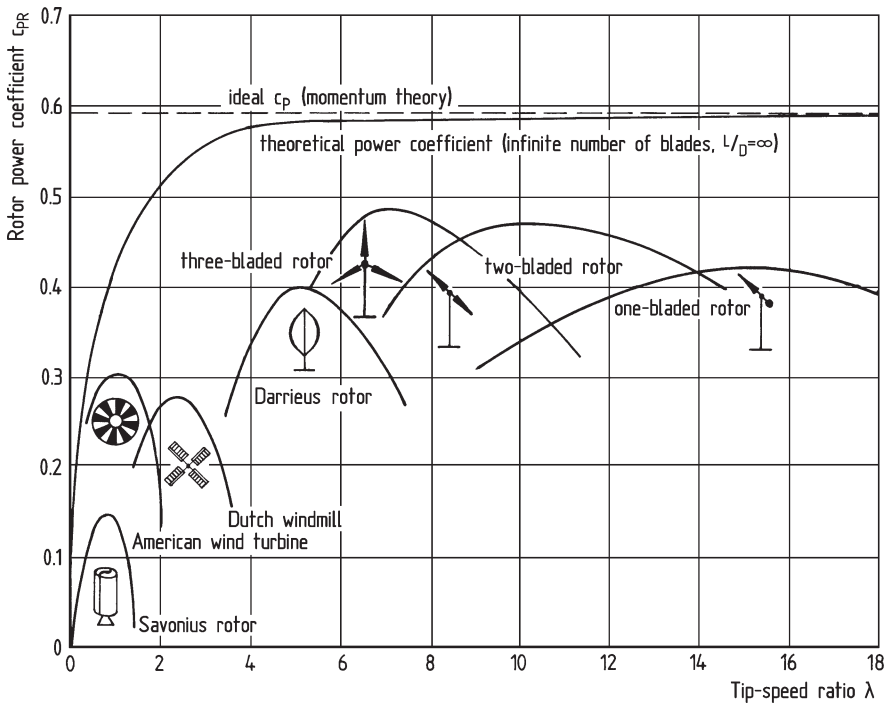

Figure 2.2.: $C_P(\lambda)$ coefficients for different wind turbines. [5]

Figure 2.2 shows how a big difference in power coefficients can be found on rotors of different configurations. The historical wind wheels were drag-type rotors with low tip speed ratio. Their power was mainly generated by the air drag of the surfaces moved by the wind. The aerodynamic characteristics of the blades themselves were of minor importance, achieving a modest power coefficient between the values of 0.2 and 0.3. Only a good power coefficient can be reached with faster-moving rotors. Current three blade rotors have maximum power coefficients very close to Betz coefficient's ideal value.

The situation regarding to the torque coefficient is the inverse. While the slow multi-blade rotors have a high torque, the torque is much lower for rotors with few blades. This is especially remarkable in the starting torque. Because of this poor starting torque, modern turbines can not start unless the pitch angle of the blades (a wider explanation of this concept will be provided) is changed to an optimum value.

2.5 Blade aerodynamics

To calculate the forces on a blade element the two dimensional aerofoil coefficients are used. These coefficients are related to an angle of attack determined from the incident resultant velocity in the cross-sectional plane of the element.

Studying the case of a turbine which has N blades of radius R each with chord c_{blade} and the pitch angle is set to β, both the blade chord length and the pitch angle may vary along the blade

span. The angular velocity of the blades is Ω and the wind speed is defined as U_∞. In Figure 2.4 all the velocities and forces relative to the blade chord line at radius r are represented.

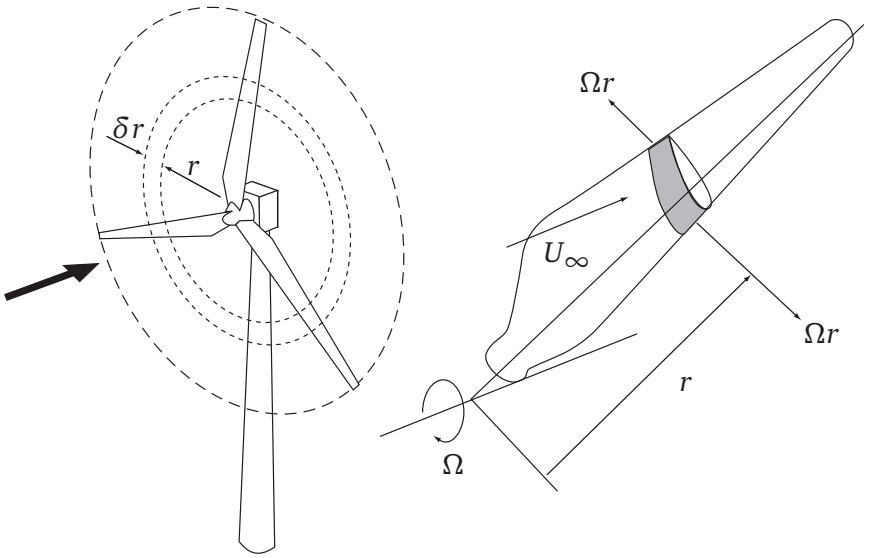

Figure 2.3.: A blade element sweeps out an annular ring. [6]

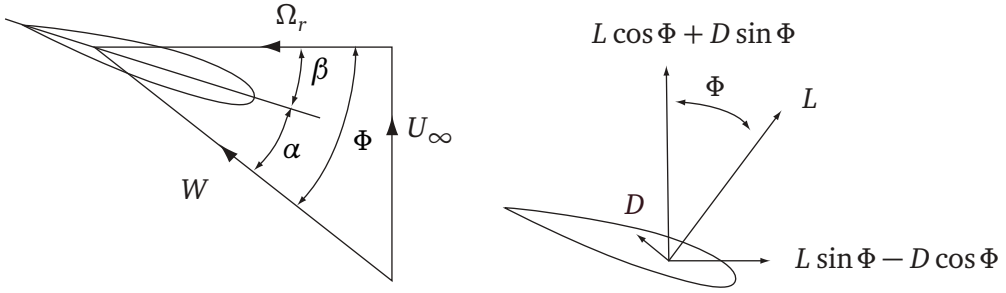

(a) Velocities (b) Forces

Figure 2.4.: Blade element velocities and forces. [6]

Since it is known how the aerofoil characteristics coefficients C_L and C_D varies with the angle of attack, the lift force L and the drag force D can be known [7]. The combination of both forces will give a tangential force and an axial force component. The sum of all the forces around the blade results in two resultants forces: the resultant tangential force, which contributes to the rotation of the rotor, and the resultant axial force, which contributes to the thrust of the wind turbine.

So it is clear that depending on the wind speed, rotor rotational speed and blades pitch angle there will be more or less forces and, as a consequence, more or less generated power. A deeper explanation of the way of controlling this power will be provided further in the control section.

2.6 Offshore wind turbines

When the idea of wind energy came up, wind turbines were though and designed in order to install them onshore. With the exponential evolution and growing of the installed power, most of the proper inland placements for the wind turbines have been occupied. This is the reason why, some years ago, different companies, governments and institutions proposed to install those turbines in the sea, designating them as offshore wind turbines.

The installation of the first offshore wind farm, named Vindeby, dates of 1991. SEAS and Elkraft installed this innovative wind farm in Denmark [8]. Since then, wind turbines are classified in two groups: onshore wind turbines (those installed in mainland) and offshore wind turbines (the ones installed in the sea). The main components are almost the same in both kind of turbines, but the installation, design and operation way truly differ.

In 2010 the 90 % of offshore wind power was supplied by Siemens and Vestas, while Dong Energy, Vattenfall and E.on were the leading offshore operators [9]. In 2013, offshore wind power contributed to 1,567 MW of the total 11,159 MW of wind power capacity constructed that year [10]. By January 2014, 69 offshore wind farms had been constructed in Europe. By 2015, Siemens Wind Power had installed 63 % of the world's 11 *GW* offshore wind power capacity; Vestas had 19 %, Senvion comes third with 8 % and Adwen 6 % [10]. Since year 2000 installed offshore power has grown from 20 to 3300 MW [10].

Main advantages of installing wind offshore technology are:

- Wind speeds are usually higher, more consistent and less turbulent in the sea than in land. That results in a higher produced energy.
- Size of the wind turbine is not limited by its surroundings, if not by the technology available.
- When turbines are installed far enough from shore, the visual impact and noise disturbances are avoided.
- Since oceans are so vast there are plenty of potential locations where turbines can be placed.

This technology also presents a lot of problems and disadvantages that have slowed down its development and need to be solved:

- The required capital investment is at the moment the biggest problem. This investment is so high because of the cost of the complicated installation of the turbine.
- The operational expenses are higher than those in onshore wind turbines due to the expensive maintenance process required. The offshore environment is a harsh environment and the components of the turbine get deteriorated faster. Besides, offshore installations are less accessible and in case of a fault, the downtime will be higher.

- When offshore wind turbines are designed, other conditions and loads have to be taken into account, such as hydrodynamic loading from waves and sea currents. This results in a more complex design.

Some years after the whole offshore development started, researchers realized that in order to get most of the offshore wind resource potential they should install the turbines in very deep waters (deeper than 30 m). That meant that a new concept of wind turbine needed to be developed, because all installed offshore wind turbines were installed on gravity fixed-bottom concrete based structures, which are not economically feasible in waters deeper than 30 m) [5].

Space frame substructures were proposed for deeps between 30-60 m and for even deeper waters the concept of the floating wind turbine was introduced. A lot of different concepts and floating structures were developed. Since the oil and gas offshore industry was already substantively developed, this technology could be adapted [11].

Owing to the long oil and gas industry tradition, it has been ensured that floating structures can perfectly work in the ocean, so the technical impediment for FOWT has been overcome long time ago. The problem is to develop a cost-effective turbine design which could compete in the electrical market. This is still a challenge that the FOWT industry needs to overcome.

Regardless of this problem the company Statoil plans to build a floating wind farm in the Scottish farm in order to demonstrate the feasibility of multiple floating wind turbines in a region that has optimal wind conditions. It is expected to be finished in 2017. The park will consist on 5 turbines with a total installed power of 30 MW [12].

Three main concepts, which are shown in the Figure 2.5, were specially developed [11].

The spar-buoy concept. It can be moored using catenary or taut lines. The stability is achieved with the use of ballast, which place the center of mass below the center of buoyancy.
The tension leg platform. In order to stabilize this structure mooring-lines are used. These lines are in tension because of the excess buoyancy in the tank.
Buoyancy Stabilized wind turbine. Mooring the barge by catenary lines, the stability is achieved through the use distributed buoyancy, taking advantage of weighted water plane area for righting moment.
Hybrid concepts. Different hybrid concepts can be found as well, which use features from all three classes. Actually, all floating concepts are hybrid design that, even though they have a primary source of stability, they use all three stability methods to differing extents.

In this thesis an in depth analysis of the spar buoy concept will be done, as well as its modeling and design of its operational control. Many advantages can be found in this concept [13]:

- The complexity and cost of the anchors is the lowest one.
- Its simplicity to carry out the on-site installation and decommissioning is a determinant factor.

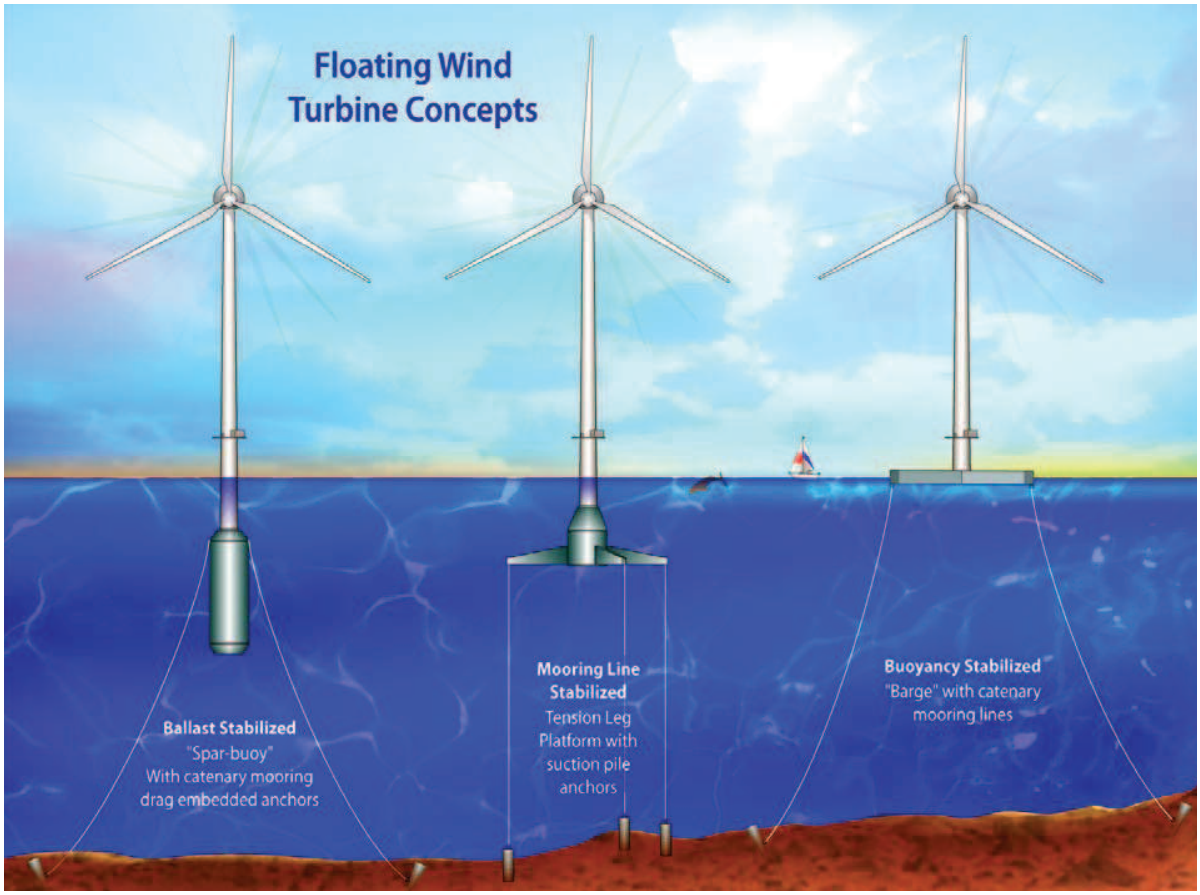

Figure 2.5.: Floating platform concepts for offshore wind turbines. [11]

- Due to its small wave sensitivity and convenient corrosion resistance it requires less maintenance. Besides, this maintenance is easier to carry out.

The most important disadvantages are:

- The complexity and costs of the buoyancy Tank are high. Due to the big dimensions of this tank, a big amount of money must be spend building it. It design can become a complicate task when designing this kind of FOWT.
- The high weight and big dimensions of the tank. In order to achieve the sufficient buoyancy force, a big and heavy buoyancy tank is required. This will suppose an additional problem when transporting and installing the turbine in the ocean.
- The complexity of the control. As later will be explained, the control needed to operate floating wind turbines is not the same as the one used in fixed offshore wind turbines. Different phenomena and conditions must be taken into account. These additional issues will make the control more complex.

3 Floating Offshore Wind Turbine Model

The purpose of this chapter is, first to describe the FOWT on which the mathematical model will be based on, then to deduce the model from the dynamical equations and physical data and finally, to validate this model with a reliable and accurate existing model.

3.1 OC3 Hywind Spar Buoy

The mathematical model of this offshore wind turbine is based on a concept wind turbine developed by NREL, the *OC3 Hywind Spar Buoy* [14]. This concept consists of two main parts: the wind turbine and the floating system.

The wind turbine is a representative utility-scale multimegawatt turbine which is known as the *NREL offshore 5* MW *baseline wind turbine*. This model was created by NREL to support the research on offshore wind technology. The turbine was designed with a heavy emphasis on the *REpower 5* MW machine. This is why most of its physical characteristics are similar [15].

The floating system was designed by NREL as well. In this case, they took also an existing concept from the company Statoil. Having the floating system *Hywind* as a reference, they defined the floating system for the *OC3 Hywind Spar Buoy* [14]. The floating structure consists of a steel cylinder filled with a ballast of water and rocks. The floating system is attached to the seabed by three mooring lines.

The basic working principle of the spar buoy FOWT is illustrated in Figure 3.1. The wind turbine experiences a buoyancy force F_{buoy}, which balances the weight of water displaced by the immersed spar, on the CB, which is place in h_{buoy}. This point is the CM of the displaced water. On the other side, the wind turbine weight F_{weight}, which acts at the CM of the body h_T, is directed opposite to F_{buoy}.

Total weight and buoyancy forces need to be equal in magnitude in order that the wind turbine can float. When CM and CB are aligned, the wind turbine will be in equilibrium. If it leaves this equilibrium position, the misalignment of CM and CB will generate a torque that will restore the equilibrium position. Thus the CB needs to be located above the CM, otherwise the FOWT will be unstable. The spar is always ballasted to ensure the stability by placing the CM below the CB. A more detailed description and all data of the *OC3 Hywind Spar Buoy FOWT* model can be found in [15][14].

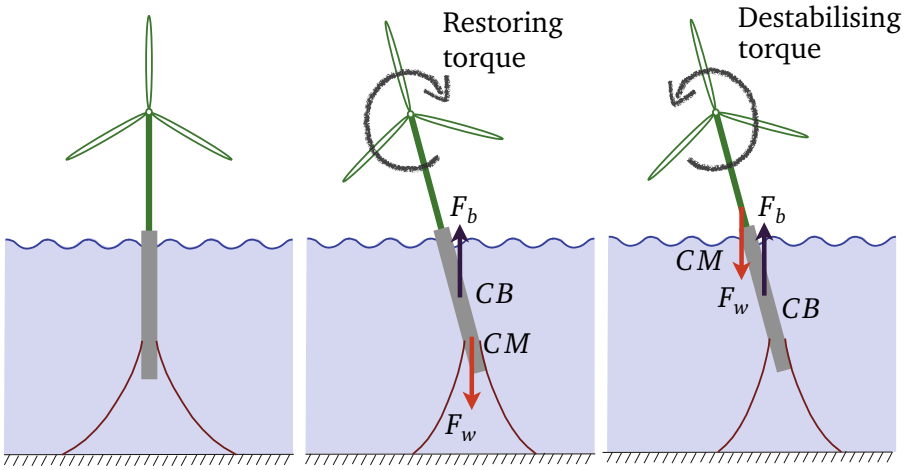

Figure 3.1.: Sketch of a spar buoy FOWT in equilibrium, stable and unstable position. [16]

Table 3.1.: Properties of NREL 5-MW baseline wind turbine [15]

Rating	5 MW
Rotor Orientation, Configuration	Upwind, 3 Blades
Control	Variable Speed, Collective Pitch
Drive-train	High Speed, Multiple-Stage Gearbox
Rotor, Hub Diameter	126 m, 3 m
Hub Height	90 m
Cut-In, Rated, Cut-Out Wind Speed	3 m/s, 11.4 m/s, 25 m/s
Cut-In, Rated Rotor Speed	6.9 rpm, 12.1 rpm
Circumferential Speed	80 m/s
Wind Turbine Mass (without floating platform)	697,000 kg

3.2 Physical Model

The physical problem can be simply described as a rigid body which moves and rotates in several axis and planes respectively, due to some forces that are applied to the body. This is a very simple way of describing the situation, but it is basically what happens in the defined case. In the next section these movements and rotations (DOF) in addition to the applied forces will be derived.

3.2.1 Coordinate system and model degrees of freedom

The system consists on a rigid body with an inertial mass and a mass moment of inertia. No elastic parts will be considered in the model. The coordinate system will be located in the SWL and in the center of the turbine. A reference Galilean system is used as the coordinate system to describe the behavior of the FOWT. Figure 3.2 places the coordinate system and shows the possible translations and rotations of the body.

Table 3.2.: Floating platform structural properties [14]

Depth to Platform Base Below SWL (Total Draft)	120 m
Platform Diameter Below Taper	9.4 m
Platform Mass, Including Ballast	7,466,000 kg
Center of Buoyancy Location Below SWL	62.06 m

Table 3.3.: Wind Turbine and Floating platform together structural properties [11]

Wind Turbine Mass (including floating platform)	8,163,000 kg
Wind Turbine Pitch Inertia about CM(including floating platform)	$1.9731 \cdot 10^{10}$ kg m^2
Wind Turbine Roll Inertia about CM(including floating platform)	$1.9731 \cdot 10^{10}$ kg m^2
Center of Mass Location Below SWL	76.55 m

Six platform motion DOF can be clearly identified: surge, sway and heave translations and pitch, roll and yaw rotations. The x axis direction is the same as the upstream wind. Another degree of freedom has to be taken into account to definitely describe the whole system, rotor azimuth.

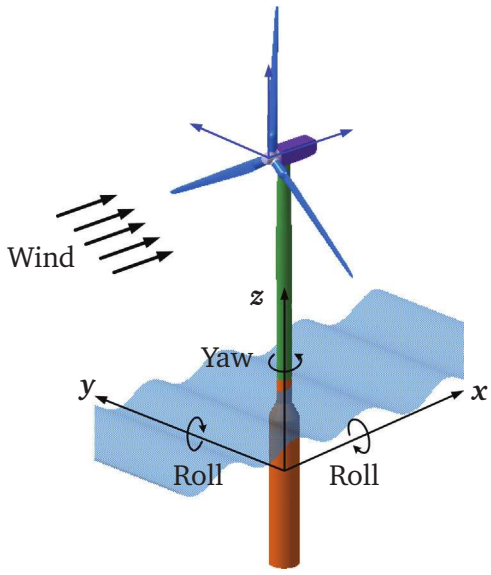

Figure 3.2.: The DOF of a FOWT. [17]

Anyway, when making the FOWT model, heave and yaw DOF will not be taken into account because of their small values in comparison with the other DOF and because of its negligible

relevance for the turbine's control [11]. So, the final model has 5 DOF. Putting all the DOF in vector $\boldsymbol{q}$:

$$\boldsymbol{q} = \begin{bmatrix} x_{CM} \\ y_{CM} \\ \theta_r \\ \theta_P \\ \varphi \end{bmatrix} \tag{3.1}$$

3.2.2 Mechanical model

Based on the above descriptions, the system dynamics are considered as the motion of a rigid body (the FOWT). According to Newton-Euler equations the linear momentum and angular momentum need to be preserved.

$$\boldsymbol{F}^T - m_T \boldsymbol{a} = 0 \tag{3.2}$$

$$\boldsymbol{\tau}^T - I_T \boldsymbol{\alpha} = 0 \tag{3.3}$$

A further developing of Eq. (3.3) will led to the governing motion equations of the system.

Different forces will be applied in the FOWT and these forces will contribute to the linear and angular momentum. In order to develop the governing motion equations, it is necessary to model all the forces applied in the FOWT. All the forces that will act on the FOWT are:

- $\boldsymbol{F_{aero}}$: Aerodynamic forces.
- $\boldsymbol{F_{Hydro}}$: Hydrodynamic forces.
- $\boldsymbol{F_{lines}}$: Mooring lines forces.
- $\boldsymbol{F_{weight}}$: Weight force.
- $\boldsymbol{F_{buoy}}$: Buoyancy force.

Aerodynamics

As it has been mentioned in Section 2.5, the wind will create two resultant forces in the wind turbine: a normal and a tangential force. While the first one contributes to the surge movement and pitch rotation, the tangential one will make the rotor rotate and will contribute to the sway displacement and roll rotation of the FOWT.

Thus, for each blade, the tangential force is defined as

$$F_{\mathrm{t},b} = \frac{\rho}{2}\frac{A}{3} v_b (\dot{\boldsymbol{q}}^T)^2 C_{\mathrm{M}}(\lambda_b, \beta_b) \tag{3.4}$$

and the normal force

$$F_{\mathrm{n},b} = \frac{\rho}{2}\frac{A}{3} v_b (\dot{\boldsymbol{q}}^T)^2 C_{\mathrm{T},b}(\lambda_b, \beta_b) \tag{3.5}$$

with $b = 1,2,3$ the number of the blade on which the force is applied [18]. These forces depend on different variables and non-linear parameters.

The first variable is the relative wind speed. Because of the surge and pitch motions of the FOWT, the wind speed that reaches the wind turbine is not equal to U_∞ and it is varying. So, the defined relative wind speed can be written as a combination of U_∞, $\dot{x}_{CM}$ and $\dot{\theta}_P$.

$$v_b = v_{w,b} - \dot{x}_{CM} - h_b \dot{\theta}_P \tag{3.6}$$

As the wind speed increases nonlinearly with the height above ground [7]

$$v_{w,b} = U_\infty \left(\frac{h}{H}\right)^{0.2} \tag{3.7}$$

being h the height from SWL to the point where the force acts on the blade. This point is located in a distance of 3/4 of the blade radius [7].

$$h_b = H + \frac{3R}{4}\cos\varphi_b \tag{3.8}$$

In the last equation it can be seen that v_b not only depends on surge and pitch, but also on the rotor azimuth. When the rotor rotates the height of the blade changes and the wind speed that this blade sees changes with it.

The rest of the non linear parameters $C_{M,b}$ and $C_{T,b}$ change with the tip speed ratio λ_b and with the blade pitch angle β_b. The coefficients for rotor thrust and torque are depicted for the considered 5 MW reference turbine in Figure 3.3.

Another phenomena must be added to aerodynamic equations, nacelle yaw angle variations. Wind turbine's nacelle is connected to the tower through some drives that allow it to rotate around z axis. This mechanism is used to orientate correctly the wind turbine to the wind direction, as well as to disorientate it. This rotation will cause that the rotor area the wind can cross will be multiplied by the cosine of the yaw angle. This will affect to thrust and axial forces and moments. To properly represent this effect thrust and axial forces are defined like

$$F_{\mathrm{t},b} = \frac{\rho}{2}\frac{A\cos(\theta_{\mathrm{yaw}})}{3} v_b (\dot{\boldsymbol{q}}^T)^2 C_M(\lambda_b, \beta_b) \tag{3.9}$$

$$F_{\mathrm{n},b} = \frac{\rho}{2}\frac{A\cos(\theta_{yaw})}{3} v_b (\dot{\boldsymbol{q}}^T)^2 C_T(\lambda_b, \beta_b) \tag{3.10}$$

In order to get the resultant normal force, which is called thrust force, and the resultant tangential force, which is called axial force, the components of each force in each blade need to be summed

$$F_{\mathrm{ax}} = \sum_{b=1}^{3} F_{\mathrm{n},b} \tag{3.11}$$

$$F_{\mathrm{ss}} = \sum_{b=1}^{3} \cos\varphi_b F_{\mathrm{t},b} \tag{3.12}$$

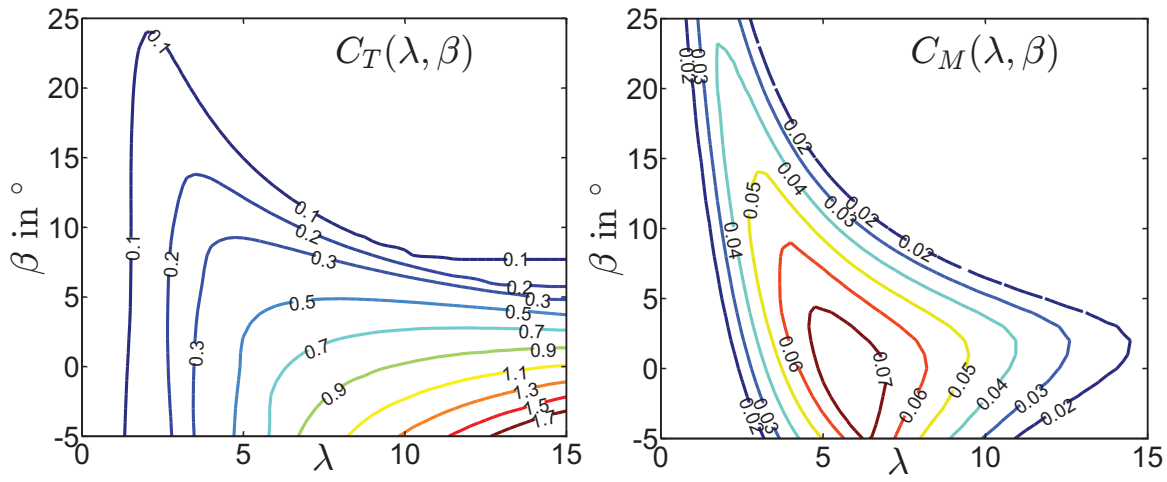

Figure 3.3.: Aerodynamic thrust and moment coefficients. [18]

The moment that these forces create about the CM of the FOWT is

$$M_{\mathrm{n}} = \sum_{b=1}^{3}(h_b - h_{\mathrm{T}})F_{\mathrm{n},b} \tag{3.13}$$

$$M_{\mathrm{t}} = \sum_{b=1}^{3}(h_b - h_{\mathrm{T}})F_{\mathrm{t},b} \tag{3.14}$$

Putting all aerodynamic forces and moments together in a vector with the same number of components as the system DOF, the resultant $\boldsymbol{F_{aero}}$ is:

$$\boldsymbol{F_{aero}} = \begin{bmatrix} F_{\mathrm{ax}} \\ F_{\mathrm{ss}} \\ M_{\mathrm{n}} \\ M_{\mathrm{t}} \\ 0 \end{bmatrix} \tag{3.15}$$

Hydrodynamics

To model the hydrodynamics of the FOWT the hydrodynamic problem will be split into three simpler problems. Radiation, diffraction and hydrostatics problem. Putting all of them together will result on a good hydrodynamical model.

The radiation problem addresses structure-generated radiating waves. When a body oscillates, it generates radiating waves, so no incident waves are present in this problem. This problem includes contributions from added mass and wave radiation damping.

Unlike the previous case, in diffraction problem a fixed structure is assumed. This structure is approached by water waves so that these waves are diffracted when passing the body.

The hydrostatics problem is elementary, but it is truly important in the response on the floating platform.

The first two problems can be modeled by Morison's equation, which is used for hydrodynamic forces. This equation has been used several times to calculate marine architecture [11] [19], besides, Morison's equations meets the necessary conditions to be applied in a FOWT [14].

$$\boldsymbol{F_{Hydro} = F_{mor} + F_{hydrostatic}} \tag{3.16}$$

This equation is written in time domain, and takes added mass and damping terms into account. Morison's equation can be defined as

$$\begin{aligned} \boldsymbol{F_{mor}} = \rho_{water}\frac{\pi D_T^2}{4}\int_0^{h_{buoy}} -C_A\boldsymbol{a_b(z,t)} + (1+C_A)\boldsymbol{a_f(z,t)}dz + \\ +\rho_{water}\frac{D_T}{2}C_D\int_0^{h_{buoy}} \boldsymbol{v_f(z,t)} - \boldsymbol{v_b(z,t)}dz \end{aligned} \tag{3.17}$$

The included parameters added-mass coefficient C_A and viscous drag coefficient C_D are taken from the OC3-Hywind reference FOWT [14]. Applying the linear wave model [20], water particle acceleration and velocity can be described as a sinusoidal function which depend on wave height, period and direction.

$$a_{f,x} = \frac{H_{wave}}{2}\omega^2 \mathrm{e}^{kh_{buoy}}\sin(kx_{CM}-\omega t) \quad \text{and} \quad a_{f,y} = \frac{H_{wave}}{2}\omega^2 \mathrm{e}^{kh_{buoy}}\cos(kx_{CM}-\omega t) \tag{3.18}$$

$$v_{f,x} = \frac{H_{wave}}{2}\omega \mathrm{e}^{kh_{buoy}}\cos(kx_{CM}-\omega t) \quad \text{and} \quad v_{f,y} = \frac{H_{wave}}{2}\omega \mathrm{e}^{kh_{buoy}}\cos(kx_{CM}-\omega t) \tag{3.19}$$

Another parameter that appears in the equations is the wave number k, a non dimensional parameter obtained as well from the linear wave model [20]. On the other side, floating platform acceleration and speed is represented by

$$a_{b,x} = \ddot{x}_{CM}h_{buoy} + \frac{\ddot{\theta}_P}{2}h_{buoy}^2 \quad \text{and} \quad a_{b,y} = \ddot{y}_{CM}h_{buoy} + \frac{\ddot{\theta}_r}{2}h_{buoy}^2 \tag{3.20}$$

$$v_{b,x} = \dot{x}_{CM}h_{buoy} + \frac{\dot{\theta}_P}{2}h_{buoy}^2 \quad \text{and} \quad v_{b,y} = \dot{y}_{CM}h_{buoy} + \frac{\dot{\theta}_r}{2}h_{buoy}^2 \tag{3.21}$$

Operating in Eq. (3.17)

$$\begin{aligned} F_{morx} = &-\rho_{water}\frac{\pi D_T^2}{4}h_{buoy}C_A\ddot{x}_{CM} - \rho_{water}\frac{\pi D_T^2}{8}h_{buoy}^2C_A\ddot{\theta}_P + \\ &+\rho_{water}\frac{D_T}{2}h_{buoy}C_D\dot{x}_{CM} + \rho_{water}\frac{D_T}{4}h_{buoy}^2C_D\dot{\theta}_P + \\ &+\rho_{water}\frac{\pi D_T^2}{4}h_{buoy}(1+C_A)\frac{H_{wave}}{2}\omega^2\mathrm{e}^{kh_{buoy}}\sin(kx_{CM}-\omega t) + \\ &+\rho_{water}\frac{D_T}{2}h_{buoy}C_D\frac{H_{wave}}{2}\omega\mathrm{e}^{kh_{buoy}}\cos(kx_{CM}-\omega t) \end{aligned} \tag{3.22}$$

$$
\begin{aligned}
F_{mory} = &-\rho_{water}\frac{\pi D_T^2}{4}h_{buoy}C_A\ddot{y}_{CM} - \rho_{water}\frac{\pi D_T^2}{8}h_{buoy}^2 C_A\ddot{\theta}_r + \\
&+\rho_{water}\frac{D_T}{2}h_{buoy}C_D\dot{y}_{CM} + \rho_{water}\frac{D_T}{4}h_{buoy}^2 C_D\dot{\theta}_r + \\
&+\rho_{water}\frac{\pi D_T^2}{4}h_{buoy}(1+C_A)\frac{H_{wave}}{2}\omega^2 e^{kh_{buoy}}\cos(kx_{CM}-\omega t) + \\
&+\rho_{water}\frac{D_T}{2}h_{buoy}C_D\frac{H_{wave}}{2}\omega e^{kh_{buoy}}\sin(kx_{CM}-\omega t)
\end{aligned}
\tag{3.23}
$$

And the moments these forces create about the CM is

$$M_{morx} = (h_{buoy} - h_T)F_{mor,x} \tag{3.24}$$

$$M_{mory} = (h_{buoy} - h_T)F_{mor,y} \tag{3.25}$$

Different terms can be clearly identified in these equations: added mass terms (the ones that multiply accelerations), damping terms (the ones that multiply velocities) and non linear terms. In order to have a clearer notation $\mathbf{A}_{ij}^{\mathbf{Hydro}}$ matrix will be define as hydrodynamic added mass matrix , $\mathbf{B}_{ij}^{\mathbf{Hydro}}$ as hydrodynamic damping matrix and $\boldsymbol{F}_i^{\boldsymbol{waves}}$ as wave non linear forces. While first 2 terms are linear, waves forces term is highly non linear and time dependent. Subscripts i and j range from 1 to 5. Each number represents a DOF (1 = surge, 2 = sway, 3 = roll, 4 = pitch, 5 = rotor azimuth). Numerical values of $\mathbf{A}_{ij}^{\mathbf{Hydro}}$ and $\mathbf{B}_{ij}^{\mathbf{Hydro}}$ matrix are included in Appendix A.

$$
\mathbf{A}^{\mathbf{Hydro}} = \frac{\rho_{water}\pi D_T^2 h_{buoy} C_A}{4}
\begin{bmatrix}
-1 & 0 & 0 & -\frac{h_{buoy}}{2} & 0 \\
0 & -1 & -\frac{h_{buoy}}{2} & 0 & 0 \\
0 & -(h_{buoy}-h_T) & -\frac{h_{buoy}(h_{buoy}-h_T)}{2} & 0 & 0 \\
-(h_{buoy}-h_T) & 0 & 0 & -\frac{h_{buoy}(h_{buoy}-h_T)}{2} & 0 \\
0 & 0 & 0 & 0 & 0
\end{bmatrix}
$$

$$
\mathbf{B}^{\mathbf{Hydro}} = \frac{\rho_{water} D_T h_{buoy} C_D}{2}
\begin{bmatrix}
-1 & 0 & 0 & -\frac{h_{buoy}^2}{2} & 0 \\
0 & -1 & -\frac{h_{buoy}}{2} & 0 & 0 \\
0 & -(h_{buoy}-h_T) & -\frac{h_{buoy}(h_{buoy}-h_T)}{2} & 0 & 0 \\
-(h_{buoy}-h_T) & 0 & 0 & -\frac{h_{buoy}(h_{buoy}-h_T)}{2} & 0 \\
0 & 0 & 0 & 0 & 0
\end{bmatrix}
$$

$$
\boldsymbol{F}^{\boldsymbol{waves}} =
\begin{bmatrix}
\frac{\cos(\beta_{waves})\rho_{water} D_T h_{buoy} H_{wave}\omega e^{kh_{buoy}}}{4}\left(\frac{\pi D_T \omega(1+C_A)}{2}\sin(kx-\omega t) + C_D\cos(kx-\omega t)\right) \\
\frac{\sin(\beta_{waves})\rho_{water} D_T h_{buoy} H_{wave}\omega e^{kh_{buoy}}}{4}\left(\frac{\pi D_T \omega(1+C_A)}{2}\cos(kx-\omega t) + C_D\sin(kx-\omega t)\right) \\
\frac{(h_{buoy}-h_T)\cos(\beta_{waves})\rho_{water} D_T h_{buoy} H_{wave}\omega e^{kh_{buoy}}}{4}\left(\frac{\pi D_T \omega(1+C_A)}{2}\sin(kx-\omega t) + C_D\cos(kx-\omega t)\right) \\
\frac{(h_{buoy}-h_T)\sin(\beta_{waves})\rho_{water} D_T h_{buoy} H_{wave}\omega e^{kh_{buoy}}}{4}\left(\frac{\pi D_T \omega(1+C_A)}{2}\cos(kx-\omega t) + C_D\sin(kx-\omega t)\right) \\
0
\end{bmatrix}
$$

The hydrostatics problem is elementary; nevertheless, it is crucial in the overall behavior of a floating platform. These loads are independent of the incident and outgoing waves from the diffraction and radiation problems. The loads on the platform from linear hydrostatics are represented with the $\mathbf{C}_{ij}^{\mathbf{Hydrostatic}}$ restoring matrix.

$$\boldsymbol{F}_{hydrostatic} = \mathbf{C}^{\mathbf{Hydrostatic}}\boldsymbol{q} \tag{3.26}$$

Eq. (3.26) represents the change in both the hydrostatic force and moment due to the platform displacement. It takes into account FOWT weight and buoy forces.

This matrix's values are calculated based on geometry-dependent parameters [14]. Hydrostatic matrix's values for the FOWT can be found in Appendix A.

So, applying everything exposed in this hydro section in Eq. (3.16), forces derived from hydrodynamics and hydrostatics can be expressed as

$$\boldsymbol{F}^{Hydro} = \mathbf{A}^{\mathbf{Hydro}}\ddot{\boldsymbol{q}} + \mathbf{B}^{\mathbf{Hydro}}\dot{\boldsymbol{q}} + \mathbf{C}^{\mathbf{Hydrostatic}}\boldsymbol{q} + \boldsymbol{F}^{waves} \tag{3.27}$$

Mooring lines forces

Mooring lines, that prevent the FOWT from lifting, exert forces and moments on the turbine as well. The three lines are attached to the floating platform with an angle between them of 120 °. According to [11] a linearized model of the mooring system can be used to define mooring forces and moments. This model is composed by a restoring matrix $\mathbf{C}_{ij}^{\mathbf{lines}}$. In order to get this matrix, the elastic stiffness of mooring lines and the effective geometric stiffness brought about by the weight of the lines in water need to be combined [14]. The components of this matrix are attached in Appendix A. The resulting mooring system is described like

$$\boldsymbol{F}^{lines} = -\mathbf{C}^{\mathbf{lines}}\boldsymbol{q} \tag{3.28}$$

Rotor dynamics

To study rotor dynamics fundamental principles of dynamics have to be applied. Using a simple free-body diagram of the drivetrain with a single DOF

$$J_{DT}\frac{\mathrm{d}\Omega}{\mathrm{d}t} = T_{aero} - T_{mec} \tag{3.29}$$

where

$$T_{aero} = \sum_{b=1}^{3}\frac{3R}{4}F_{tan,b} \tag{3.30}$$

$$T_{mec} = i_{GB}T_{Gen} \tag{3.31}$$

3.2.3 state space representation

Summing up all the modeled forces carried out until here, the FOWT mathematical model can be represented as

$$\mathbf{M_{mass}}\ddot{\boldsymbol{q}} = \boldsymbol{F}_{aero} + \boldsymbol{F}_{Hydro} + \boldsymbol{F}_{lines} \tag{3.32}$$

with $\mathbf{M}_{ij}^{\mathbf{mass}}$ containing FOWT mass and mass moment of inertia components. Linear and non linear terms can be differentiated in Eq. (3.32). These linear terms that depend on accelerations will be all put together in a $\mathbf{M}_{ij}$ added mass matrix; terms that depend on velocities will form $\mathbf{D}_{ij}$ damping matrix; finally, terms dependent on displacements will form $\mathbf{K}_{ij}$ stiffness matrix. The only non linear terms are $\boldsymbol{F}_i^{aero}$ and $\boldsymbol{F}_i^{waves}$. Both forces will form $\mathbf{Q_i}$ non linear matrix of generalized forces. All matrix components can be found in Appendix A. Using this notation, the system will be

$$\mathbf{M}\ddot{\boldsymbol{q}} + \mathbf{D}\dot{\boldsymbol{q}} + \mathbf{K}\boldsymbol{q} = \boldsymbol{Q} \tag{3.33}$$

Making some matrix operations

$$\ddot{\boldsymbol{q}} = -\mathbf{M}^{-1}\mathbf{D}\dot{\boldsymbol{q}} - \mathbf{M}^{-1}\mathbf{K}\boldsymbol{q} + \mathbf{M}^{-1}\mathbf{Q} \tag{3.34}$$

Now Eq. (3.34) can be converted to a system of linear first order differential equations.

$$\begin{bmatrix} \ddot{\boldsymbol{q}} \\ \dot{\boldsymbol{q}} \end{bmatrix} = \begin{bmatrix} -\mathbf{M}^{-1}\mathbf{D} & \mathbf{M}^{-1}\mathbf{K} \\ \mathbf{I} & \mathbf{0} \end{bmatrix} + \begin{bmatrix} -\mathbf{M}^{-1} \\ \mathbf{0} \end{bmatrix} \begin{bmatrix} \mathbf{Q} \\ \mathbf{0} \end{bmatrix} \tag{3.35}$$

Naming

$$\mathbf{A} = \begin{bmatrix} -\mathbf{M}^{-1}\mathbf{D} & \mathbf{M}^{-1}\mathbf{K} \\ \mathbf{I} & \mathbf{0} \end{bmatrix} \qquad \mathbf{B} = \begin{bmatrix} -\mathbf{M}^{-1} \\ \mathbf{0} \end{bmatrix} \tag{3.36}$$

$$\boldsymbol{x} = \begin{bmatrix} \ddot{\boldsymbol{q}} \\ \dot{\boldsymbol{q}} \end{bmatrix} \qquad \boldsymbol{f}_u = \begin{bmatrix} \mathbf{Q} \\ \mathbf{0} \end{bmatrix} \tag{3.37}$$

the system can be now represented as a non linear state space system.

$$\begin{cases} \dot{\boldsymbol{x}} = \mathbf{A}\boldsymbol{x} + \mathbf{B}\boldsymbol{f}_u \\ \dot{\boldsymbol{y}} = \mathbf{C}\boldsymbol{x} + \mathbf{D}\boldsymbol{f}_u \end{cases} \tag{3.38}$$

In this system $\boldsymbol{x}$ is the state vector, $\boldsymbol{f}_u$ the non linear input vector and $\boldsymbol{y}$ the output vector. **A** matrix will be the system or state matrix, **B** the input matrix, **C** the output matrix and **D** the feedforward matrix. **C** matrix will be define so that generator speed, tower top velocities and the states are available. **D** will be a zero matrix.

$$\mathbf{C} = \begin{bmatrix} \mathbf{c_{meas}} \\ \mathbf{I} \end{bmatrix} \qquad \mathbf{D} = \begin{bmatrix} \mathbf{0} \end{bmatrix} \tag{3.39}$$

This state space system will be implemented in Simulink in order to have a proper simulation environment and a proper environment to design and implement the control of the FOWT.

3.2.4 Model validation

Once the FOWT model is finished, it is necessary to validate it against an already accepted model. The simulation model that will be used for the validation is known as FAST. FAST is the abbreviation for Fatigue, Aerodynamics, Structures and Turbulence. This nonlinear time domain model employs a combined modal and multibody structural-dynamics to simulate wind turbines.

In order to use the Simulink environment for simulations, this code gives the opportunity to incorporate FAST equations of motion in a S-Function block. Since the previously developed model is implemented in Simulink as well, it will be easy to compare both models using Matlab and Simulink.

The model's outputs that will be compared are:

- Generator torque.
- Generator speed.
- Blade pitch angle.
- Platform pitch angle.
- Platform surge displacement.
- Tower top velocity in x direction.
- Platform roll angle.
- Platform sway displacement.
- Tower top velocity in y direction.

First of all, the designed model will be tested with the calculated parameters, in order to discern how good the outputs match with the outputs from FAST. If the outputs do not match as good as required, some little adjustments will be made in the parameters. These adjustments will be made in the added mass matrix, damping matrix and stiffness matrix parameters.

Selecting a constant wind field of 15 m/s the obtained results from both the designed model and FAST model are represented in Figure 3.5.

In Figure 3.5 can be observed that modifications must be applied in different coefficients.

Regarding to FOWT pitch, a good matching can be appreciated at the beginning, but then designed model pitch signal gets bigger than one in FAST model and the period increases as well. First problem is caused by a disadjustment in damping coefficient and second one because an excessive coupling between surge and pitch frequencies coupling. The adopted solution is to increase damping element related to pitch and decrease added mass term related to the coupling of pitch and surge displacement.

When it comes to surge motion, similar problems to previously appeared ones can be realized. In this case the mismatching of the signals is caused by an excessive coupling between pitch and surge motion. Once the term related to surge movement and pitch coupling is reduced the disadjustment is supposed to be solved.

Roll signals shows the same situation than previously represented pitch signals. Same action will be adopted this time. Incrementing damping term related to roll and decrementing added mass term related to the roll and sway coupling an improvement in the performance of the system is expected.

Regarding to sway motion an additional problem appears. Although sway damping and roll and sway coupling seem to be in the proper value, the steady value of this variable is higher in the designed model than in FAST model. This is caused by the mooring lines, that are limiting the displacement of the FOWT in y direction. Reducing the stiffness term related to sway movement will apparently solve the problem.

Those differences between designed model and FAST model generator torque, generator speed and blade pitch angle will be overcome when solving disadjustments between movements, inasmuch as its dependency. In Table 3.4 adjustments made to different coefficients are shown.

Table 3.4.: Adjustment of added mass, damping and stiffness matrix's values.

Original value		**Adjusted value**
M_{14}	$\Rightarrow$	$1.2 \cdot M_{14}$
M_{32}	$\Rightarrow$	$1.4 \cdot M_{32}$
M_{41}	$\Rightarrow$	$0.6 \cdot M_{41}$
D_{32}	$\Rightarrow$	$0.4 \cdot D_{32}$
D_{33}	$\Rightarrow$	$2.5 \cdot D_{33}$
D_{44}	$\Rightarrow$	$1.8 \cdot M_{44}$
C_{11}	$\Rightarrow$	$0.85 \cdot C_{11}$
C_{22}	$\Rightarrow$	$1.7 \cdot C_{22}$
C_{23}	$\Rightarrow$	$0.7 \cdot C_{23}$

With the different parameters adjusted, the designed model will be tested in different situations and conditions. At the beginning, a constant wind speed of 15 m/s will be used to make the simulations and see the results. Figure 3.4 shows the output signals of the simulation.

It can be seen how most of the previous problems with signals matching have been solved. This time outputs match almost perfectly, both in frequencies and magnitudes. However, some issues are still appearing. Roll and sway displacement are not as accurate as pitch and surge displacement. Principal frequency components almost match though, and the roll is not so inaccurate. The most critical part is the little offset that can be observed in sway movement.

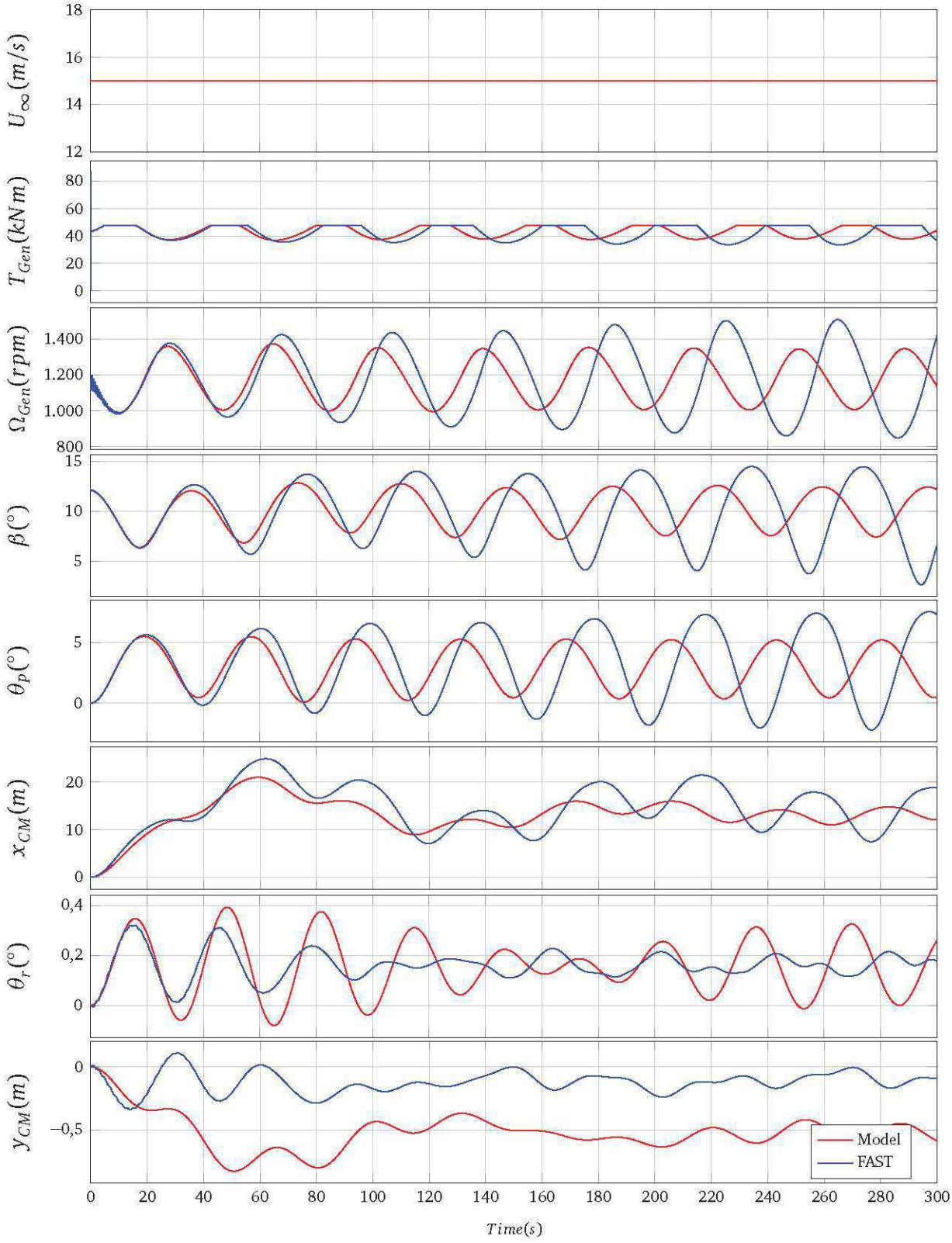

Figure 3.5.: Comparison between original designed model and FAST model outputs for a constant 15 m/s wind speed.

After the previous simulation results, it will be interesting to see how accurate are the results of the model respect FAST in a real turbulent wind field. After all, in this situation is where the

model will work all the time, so it needs to be accurate as well. Turbulent wind field is more demanding and will show real performance of the FOWT. Results are exposed in Figure 3.6.

The results are similar to the previous simulation; good results in pitch and surge but not so good ones in roll and sway. In roll rotation the matching starts truly well but then designed model signal gets retarded. Although the signal gets retarded the period and magnitude of it are truly similar to FAST roll signal. Since roll and sway signals are coupled, the disadjustment in roll gets reflected in sway displacement.

The reason for these inaccuracies are some physic effects that have not been taken into account, such as gyroscopic effects, tower stiffness and mooring non linearities. Anyway, these little errors are assumable when designing and testing the control.

Until now, the model has been tested without any forces related to waves. It can not be forgotten that forces related to waves are very important in FOWT model since a floating structure is more sensible to waves than a fixed one. In the next simulation a regular wave field will be added. The turbulent real wind field will be the same as in the last simulation. A wave height of 6 meters with a period of 10 seconds and direction of 30 ° respect $\boldsymbol{x}$ axis will be chosen. These conditions are harsh enough to test the complete model of the FOWT. Figure 3.7 shows the results of the simulation.

The model represents quite accurate the influence of the waves in the FOWT. Both in surge and sway displacement and pitch and roll rotations. However, and specially in roll rotation, designed model and FAST model do not match perfectly. Anyway, when representing tower top velocities, it can be observed that these signals properly match.

It is important that these signals match because they represent quite well the dynamics of the system, since they are a combination of linear and angular velocities.

$$V_{TTP,x} = \dot{x}_{CM} + H\dot{\theta}_P \tag{3.40}$$

$$V_{TTP,y} = \dot{y}_{CM} + H\dot{\theta}_r \tag{3.41}$$

Besides, these signals are important in the control because they can be used to achieve an augmentation of the FOWT operational life and more efficient power production, thereby it is essential that these signals are as accurate as possible.

Once the FOWT model is tested and validated, different ways of controlling it will be implemented, tested and improved. This task is carried out in the next chapter.

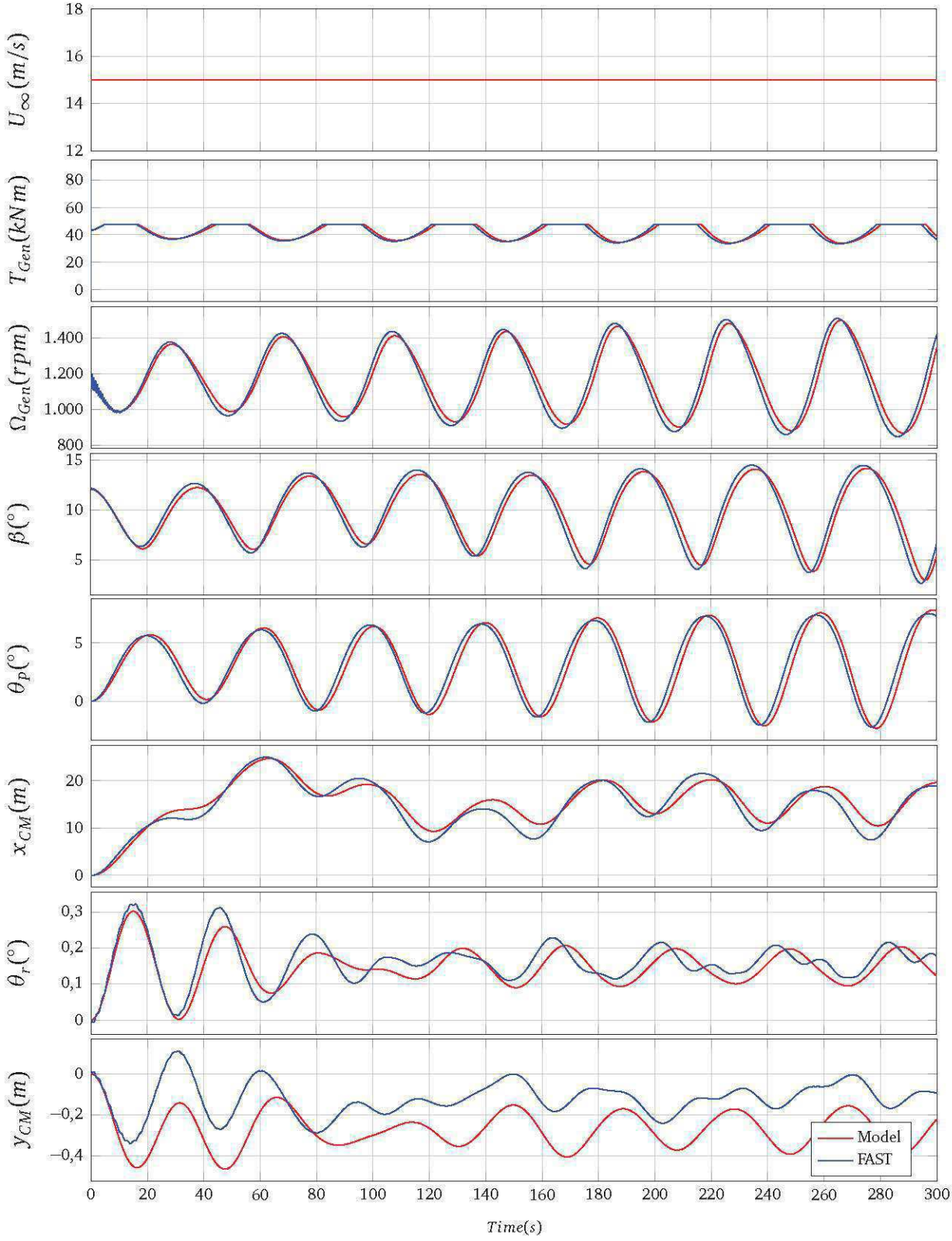

Figure 3.4.: Comparison between adjusted designed model and FAST model outputs for a 15 $\mathrm{m/s}$ wind speed.

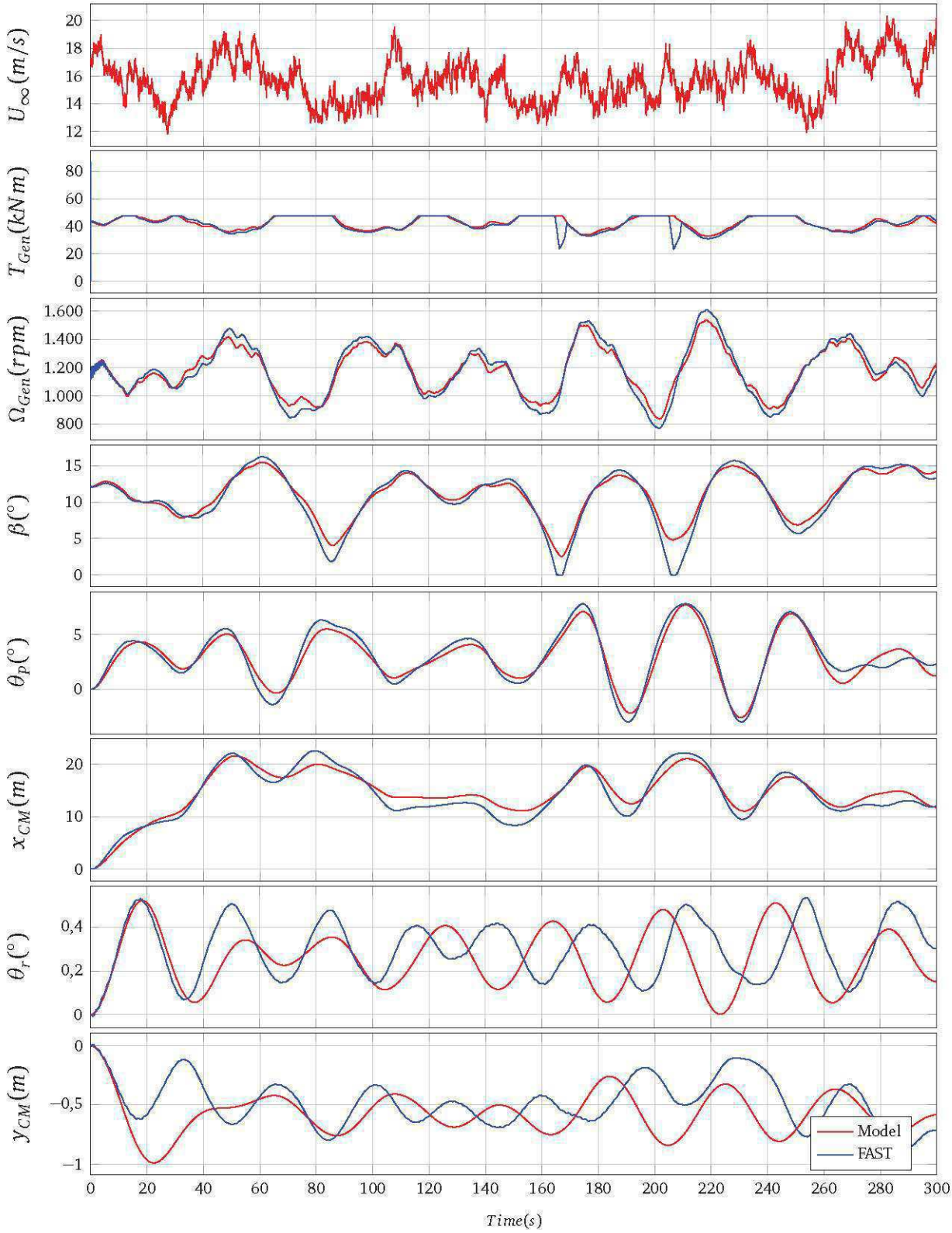

Figure 3.6.: Comparison between adjusted designed model and FAST model outputs for a turbulent real wind field.

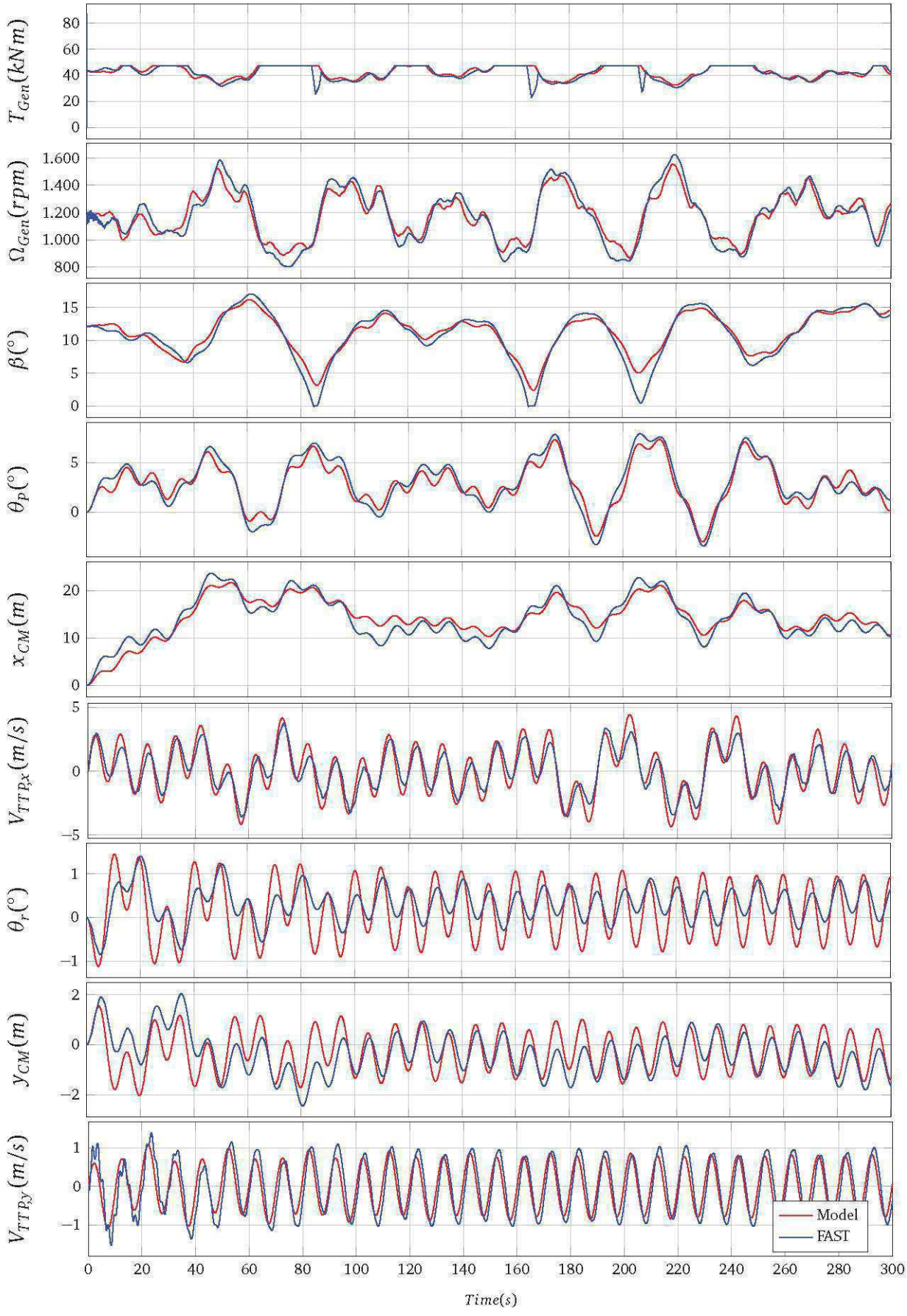

Figure 3.7.: Comparison between adjusted designed model and FAST model outputs for a turbulent real wind field and regular wave field.

4 FOWT control design

In this chapter an introduction to the baseline control of offshore wind turbines will be made and different issues related to the application of this baseline controller on a FOWT will be explained. Some solutions for this problems will be proposed, tested and compared between them.

4.1 Introduction to the control of a wind turbine

Basically, a wind turbine is a system with different sensors and actuators. The hardware and software will process the signals from the sensors and, depending on these signals, some output signals for the actuators will be generated. Depending on the control designed, these variations will be different and they will try to achieve different goals. Most common sensors are [6]:

- An anemometer.
- A wind vane.
- Rotor speed sensor.
- Electrical power sensor.
- Pitch position sensor.
- Tower top accelerometer.
- Temperature and oil level indicators.
- Hydraulic pressure sensors.

The actuators that will change the behavior of the system [6]:

- Hydraulic or electric pitch actuator.
- Generator torque.
- Generator contactors.
- Switches for activating shaft brakes.
- Switches for activating yaw system.

A microprocessor based controller or a computer will process the inputs and carry out the control.

The control system is divided in three main control sequences:

- Supervisory control.
- Safety system control.

- Closed-loop control.

4.1.1 Supervisory control

Supervisory control is the responsible to bring the wind turbine from one operational state to another. It decides both when to move from one state to another and how to do it. Before perform this action, it must be check if the first state was reached successfully. Different operational states can be:

- Stand-by state. External conditions are suitable and the turbine is available to run anytime.
- Start-up state.
- Power production state.
- Shut-down of the wind turbine.
- Stopped of the wind turbine due to a fault.

4.1.2 Safety system control

When a serious event, or an event that can become serious, happens, safety system control brings the wind turbine to a safety operational state. Usually this means stopping the wind turbine and applying the brakes to it.

This control system acts as a back-up to the principal control and when these potentially dangerous events occur, the safety system control takes over. It is highly recommendable to have a safety system control which is independent from the main control [6].

Some dangerous events are:

- Rotor overspeed.
- Generator torque over the limits.
- Pressing of the emergency stop button.
- Other faults that indicate the bad operation of the main controller.

4.1.3 Closed-loop control

This software based system control adjusts the operational state of the turbine so that some pre-defined characteristics and goals can be achieved. The two principal objectives that usually are required are: to maximize the production of electric energy and to extend wind turbine's operational life.

When designing a wind turbine, it is necessary to know in which wind conditions it will work. As it is known, the power a wind turbine can produce depends on the wind speed by a cubic

relation (Eq. (2.4)). This is why cut-in, rated and cut-out wind speeds are defined. These characteristics are set up depending on where the turbine is placed and most common wind fields in that place. It is important to effectively choose these parameters in order to have a successfully economical pay-back of the wind turbine.

The cut-in wind speed defines the wind speed in which the turbine starts generating electrical energy. When the wind speed is below cut-in wind speed the wind turbine will not produce any electricity. Below cut-in wind speed, the available wind will be used to accelerate the turbine.

The rated wind speed defines the wind speed in which the turbine produces its maximum power. Turbines generally are designed so that they yield maximum output power at wind speeds around 12 m/s. Its does not pay to design turbines that maximize their output at stronger winds, because such strong winds are uncommon [6]. In case of stronger winds, part of the excess energy of the wind is wasted in order to avoid damaging the wind turbine.

The cut-out wind speed defines the wind speed in which the turbine stops. This stop of the turbine is because of security reasons. The turbine can not handle for a long time wind speeds bigger than cut-out wind speed and this is why it stops its operation.

It can be deduced that different operation zones between previously defined wind speeds will be needed in the control of the turbine. These operation zones will be controlled by two different control systems and in each operation zone there will be different objectives to achieve.

Different regions will be defined for the operation of the controller. Not always the controllers will act in all the regions in the same way, but different controllers will be used to achieve different objectives. The different controllers that will act in the operation of the wind turbine are the generator torque controller and the collective blade pitch controller. Both of them will maintain the power at its desired value in a different way.

Generator torque controller

The generator torque controller computes the generator torque as a tabulated function of the generator speed. Depending on the generator speed a different torque will be applied.

The relation between the generator speed and the generator torque will be specified by the control region in which the wind turbine is operating.

In region 1, when the wind speed is below cut-in wind speed, the generator torque is set to zero and no power is extracted from the wind. Instead, the wind is used to accelerate the rotor. The turbine control will be operating in this region when the wind speed value is ubicated between 0 and 3 m/s. Generator speed in this region will be between 0 and 670 rpm.

Region 2 is called the region between cut-in and rated wind speed. When the wind blows between 3 and 11.4 m/s the turbine will be operating in this region. The generator speed will be between 670 and 1173.7 rpm in this case. In this region the captured power is the maximum one, so the aim of the generator torque controller is to reach this maximum power.

Eq. (3.29) shows how generator speed can be controlled through generator torque. According to Eq. (2.5), once the generator speed can be fixed, tip speed ratio will be fixed as well. Looking at Figure 2.2, it can be observed how $C_P(\lambda)$ coefficient changes with the tip speed ratio. Hence, changing λ, C_P can be modified, and changing C_P, obtained power can be adjusted to the desired value (Eq. (2.4)).

In order to obtain the maximum power, the maximum Betz coefficient needs to be reached all the time. Since this coefficient is related to the tip speed ratio, there is a value of λ that will always give the maximum C_P. This value is defined as λ_{opt}. For the studied wind turbine, with $\lambda_{opt} = 7.55$ the maximum $C_{P_{opt}} = 0.482$ will be achieved [15].

The generator torque in this region is proportional to the square of the generator speed, so that the tip speed ratio can be maintained in the optimal value. Since $P_{Gen} = T_{Gen}\Omega_{Gen}$, operating in Eq. (2.4) and Eq. (2.5)

$$T_{\text{Gen}} = \frac{\rho}{2} A C_{\text{P,opt}} \Omega_{\text{Gen}}^2 \left(\frac{R}{\lambda_{\text{opt}}} \right)^3 = K_{\text{opt}} \Omega_{\text{Gen}}^2 \tag{4.1}$$

Region 3 is defined as the region above rated wind speed and below cut-out wind speed. This region will be between 11.4 and 25 m/s wind speed. The principal control objective in this region is to maintain the power in a nominal constant value. This goal is reached by the collective blade pitch controller. The generator torque controller will maintain a constant torque value of 43,093.55 Nm and the blade pitch controller will be the responsible to control the generator speed in its nominal value of 1173.7 rpm by changing blade pitch angle.

Between region 1 and region 2, region $1\frac{1}{2}$ can be defined in order to have a linear transition between both regions. The generator torque is proportional to the generator speed, so it will not be possible to obtain the whole available power because λ will not be in its optimal value. Region $1\frac{1}{2}$ is defined to span the range of generators speeds between 670 and 871 rpm.

Another linear transition between region 2 and 3 will be defined as region $2\frac{1}{2}$. Generator speeds between 1161.963 and 1173.7 rpm will be included in this region.

Figure 4.1 shows generator power, torque and speed for each wind speed. In this picture these different zones of the control can be appreciated.

Collective pitch controller

On a pitch controlled wind turbine, the turbine's electronic controller checks the generator speed several times per second. When it becomes too high, the controller sends an order to the blade pitch mechanism which immediately pitches the rotor blades slightly out of the wind. Conversely, the blades are turned back into the wind whenever the wind drops again. The pitch mechanism is usually operated using hydraulics or electrical drives [6].

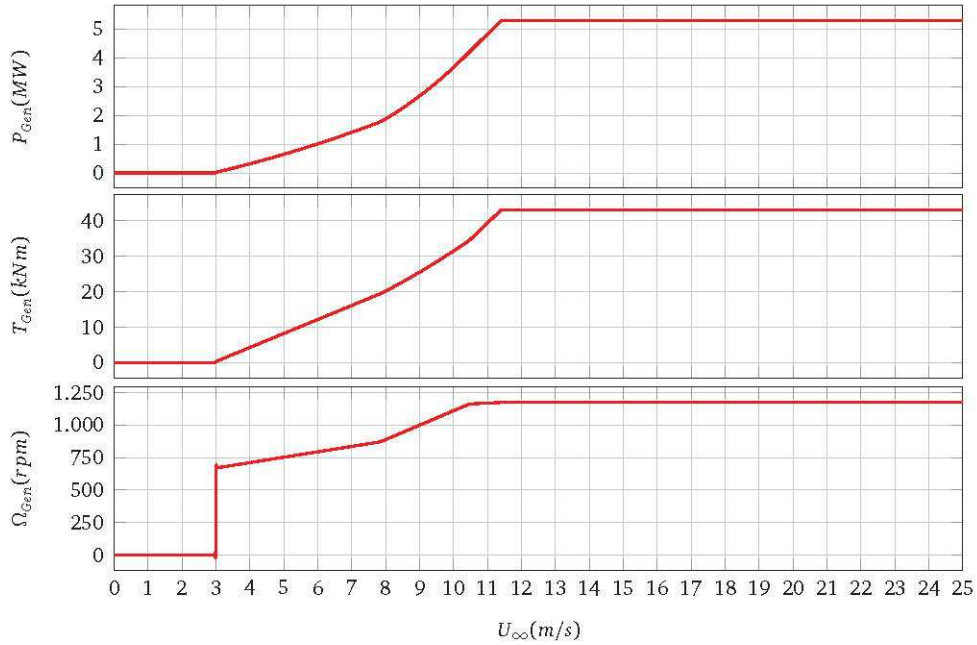

Figure 4.1.: Generator power, torque and speed in each wind speed.

The rotor blades thus have to be able to turn around their longitudinal axis. During normal operation the blades will pitch a fraction of a degree at a time and the rotor will be turning at the same time.

Designing a pitch controlled wind turbine requires some clever engineering to make sure that the rotor blades pitch exactly the amount required. On a pitch controlled wind turbine, the computer will generally pitch the blades a few degrees every time the wind changes in order to keep the rotor blades at the optimum angle in order to maximize output power for all wind speeds.

The commands given to the pitch actuator are the result of a closed loop feedback control which acts depending on the measured generator speed. This loop compares the measured and filtered generator speed and the rated generator speed (1173.7 rpm) and send this error to a PI controller. This PI generates a control action that is sent to the pitch actuator.

Since the goal of the PI controller is to control the generator speed, it will be designed from rotor's dynamics equation Eq. (3.29). Changing this differential equation into the form of infinitesimal increments yields

$$J_{\mathrm{DT}}(\dot{\Omega}_{\mathrm{rated}} + \Delta\dot{\Omega}) = T_{\mathrm{aero}} - i_{\mathrm{GB}} T_{\mathrm{Gen}} \tag{4.2}$$

where $\Delta\Omega$ is the small perturbation of rotor speed and Ω_{rated} is the rated rotor speed.

In region 3 generator torque controller always maintains generator power at its rated value P_{rated}, thereby generator torque must be inversely proportional to generator speed.

$$T_{\mathrm{Gen}} = \frac{P_{\mathrm{rated}}}{i_{\mathrm{GB}}\Omega} \tag{4.3}$$

Assuming that aerodynamic torque does not vary with rotor speed,

$$T_{\text{aero}} = \frac{P(\beta, \Omega_{\text{rated}})}{\Omega_{\text{rated}}} \tag{4.4}$$

P is the mechanical power which depends on blade pitch angle and rated rotor speed.

Expanding Eq. (4.3) and Eq. (4.4) with a first-order Taylor series

$$T_{\text{Gen}} \approx \frac{P_{\text{rated}}}{i_{\text{GB}}\Omega_{\text{rated}}} - \frac{P_{\text{rated}}}{i_{\text{GB}}\Omega_{\text{rated}}^2}\Delta\Omega \tag{4.5}$$

$$T_{\text{aero}} \approx \frac{P_{\text{rated}}}{\Omega_{\text{rated}}} + \frac{1}{\Omega_{\text{rated}}}\frac{\partial P}{\partial \beta}\Delta\beta \tag{4.6}$$

$\frac{\partial P}{\partial \beta}$ term is the sensitivity of power to the blade pitch angle. This is an aerodynamic property of the rotor and it depends on wind and rotor speed and blade pitch angle. Its values are calculated and tabulated for different operational points in [15].

With a proportional-integral control, small perturbation of the blade-pitch angle $\Delta\beta$ about their operating point can be related to rotor speed perturbations.

$$\Delta\beta = K_{\text{P}} i_{\text{GB}}\Delta\Omega + K_{\text{I}}\int_0^t i_{\text{GB}}\Delta\Omega dt \tag{4.7}$$

K_{P} and K_{I} are controller proportional and integral gains. Naming $\Omega = \dot{\varphi}$ and combining Eq. (4.7), Eq. (4.5), Eq. (4.6) and Eq. (4.2) it can be observed that controlled rotor speed error responds as a second order system.

$$J_{\text{DT}}\ddot{\varphi} + \left(\frac{1}{\Omega_{\text{rated}}}\left(-\frac{\partial P}{\partial \beta}\right) i_{\text{GB}}K_{\text{P}} - \frac{P_{\text{rated}}}{\Omega_{\text{rated}}^2}\right)\dot{\varphi} + \left(\frac{1}{\Omega_{\text{rated}}}\left(-\frac{\partial P}{\partial \beta}\right) i_{\text{GB}}K_{\text{I}}\right)\varphi = 0 \tag{4.8}$$

This second order system has a natural $\omega_{\varphi n}$ frequency and $\zeta_{\varphi n}$ damping ratio.

From a second order system natural frecuency and damping equations, and neglecting the negative damping introduced by the generator torque controller [15] (term $-P_{\text{rated}}/\Omega_{\text{rated}}^2$ in Eq. (4.8)) K_{P} and K_{I} gains are calculated.

$$K_{\text{P}} = \frac{2J_{\text{DT}}\Omega_{\text{rated}}\omega_{\varphi n}\zeta_{\varphi n}}{i_{\text{GB}}\left(-\frac{\partial P}{\partial \beta}\right)} \tag{4.9}$$

$$K_{\text{I}} = \frac{J_{\text{DT}}\Omega_{\text{rated}}\omega_{\varphi n}^2}{i_{\text{GB}}\left(-\frac{\partial P}{\partial \beta}\right)} \tag{4.10}$$

Since the pitch sensitivity varies nearly linearly with blade-pitch angle, K_{P} and K_{I} gains will change for different wind speeds. Something needs to be made so proportional and integral gains are adjusted for different operational points.

So that these dynamic gains can be achieved, the pitch sensitivity value is set for a blade pitch angle of 0° and a simple technique for implementing gain scheduling based on blade-pitch angle is implemented to correct K_{P} and K_{I} gains.

Every time the control loop actuates, the gains of the controller will be corrected depending on the previous blade pitch angle. The correction factor is included in a look-up table, which has the blade pitch angle as an input. The values of this table are shown in Figure 4.2. So the new gains will be

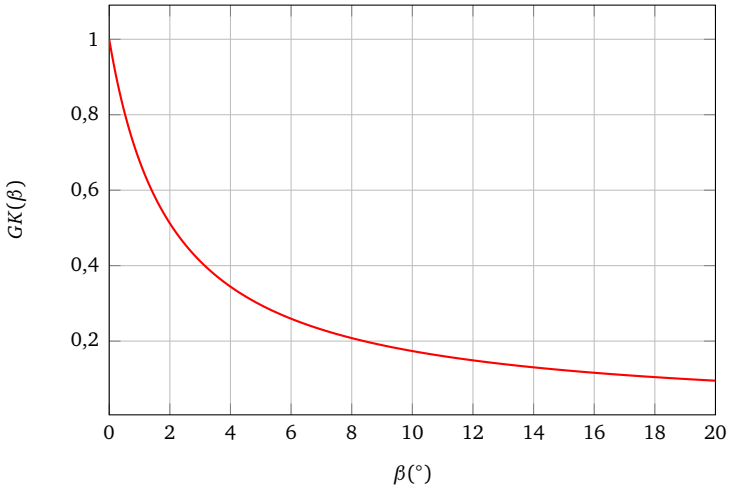

Figure 4.2.: Gain correction factor.

$$K_P = \frac{2J_{DT}\Omega_{rated}\omega_{\varphi n}\zeta_{\varphi n}}{i_{GB}\left(-\frac{\partial P}{\partial \beta}(\beta = 0)\right)} GK(\beta) \tag{4.11}$$

$$K_I = \frac{J_{DT}\Omega_{rated}\omega_{\varphi n}^2}{i_{GB}\left(-\frac{\partial P}{\partial \beta}(\beta = 0)\right)} GK(\beta) \tag{4.12}$$

In order to tune the PI controller the response characteristics need to be selected. According to [21] the damping ratio must be set to 0.7 and the natural frequency about 0.1 Hz (0.6rad/s). Applying these values in Eq. (4.11) and Eq. (4.12), $K_{Po} = 0.0188$ and $K_{Io} = 0.0081$ values are reached. These are the values the controller uses when the blade pitch angle is set to 0. The gain scheduling technique will correct them for different operating points.

Figure 4.3 summarizes the functioning of the whole close loop controller. In this flowchart both generator torque controller and collective blade pitch controller are included.

4.2 Baseline controller applied to a FOWT

The previously designed basic controller was thought to be used in fixed offshore wind turbines [15]. However, this controller will be applied to the modeled FOWT to see how the system

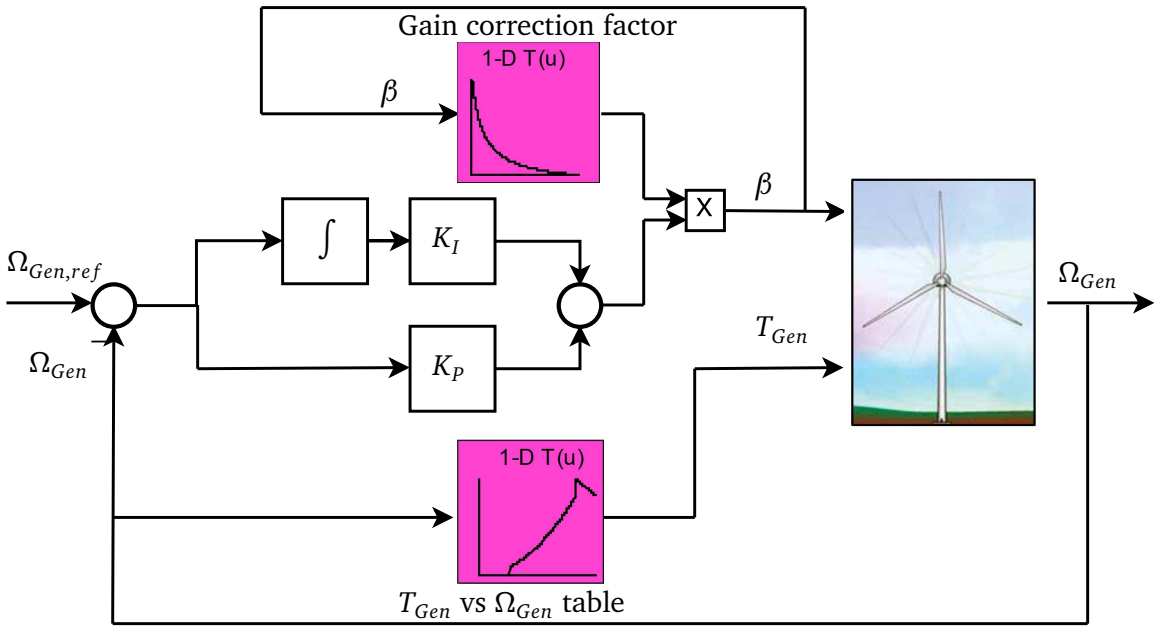

Figure 4.3.: Flowchart of the baseline control system.

works and to have a first attempt of a controller. The obtained results from implementing the controller in the designed model are exposed in Figure 4.4.

It can be observed that the wind turbine works in an stable operation mode when the wind speed is below rated. Once it is exceeded, the operation of the FOWT gets unstable. This situation is due to the existing coupling between blade pitch and tower pitch motion. Since below rated wind speeds blade pitch angle is set to 0, this coupling does not affect the system until wind speed makes blade pitch angle closed loop control actuate.

If a floating foundation, instead of a fixed one, is used to mount the wind turbine, system natural frequencies are significantly reduced. These low natural frequencies avoid any structural vibration mode in the frequency range of wave excitation. This will minimize dynamic load amplifications, but it will cause instability problems if the baseline controller is used.

To properly analyze the system and its natural frequencies, it must be linearized around an operation point. The linearization is carried out for a wind speed of 15m/s, so as to study the performance of the pitch controller and possible instabilities. From this process, a time invariant state-space linear system will result Eq. (4.13). The linearization operation is explained in more detail in Appendix B.

$$\begin{cases} \dot{\boldsymbol{x}} = \mathbf{A}^{\text{lin}}\boldsymbol{x} + \mathbf{B}^{\text{lin}}\boldsymbol{u} \\ \dot{\boldsymbol{y}} = \mathbf{C}^{\text{lin}}\boldsymbol{x} + \mathbf{D}^{\text{lin}}\boldsymbol{u} \end{cases} \tag{4.13}$$

The lowest natural frequency for the fixed foundation offshore wind turbine is the 1st tower frequency. This one is a lateral bending mode that is close to 0.4Hz [22]. When mounting the

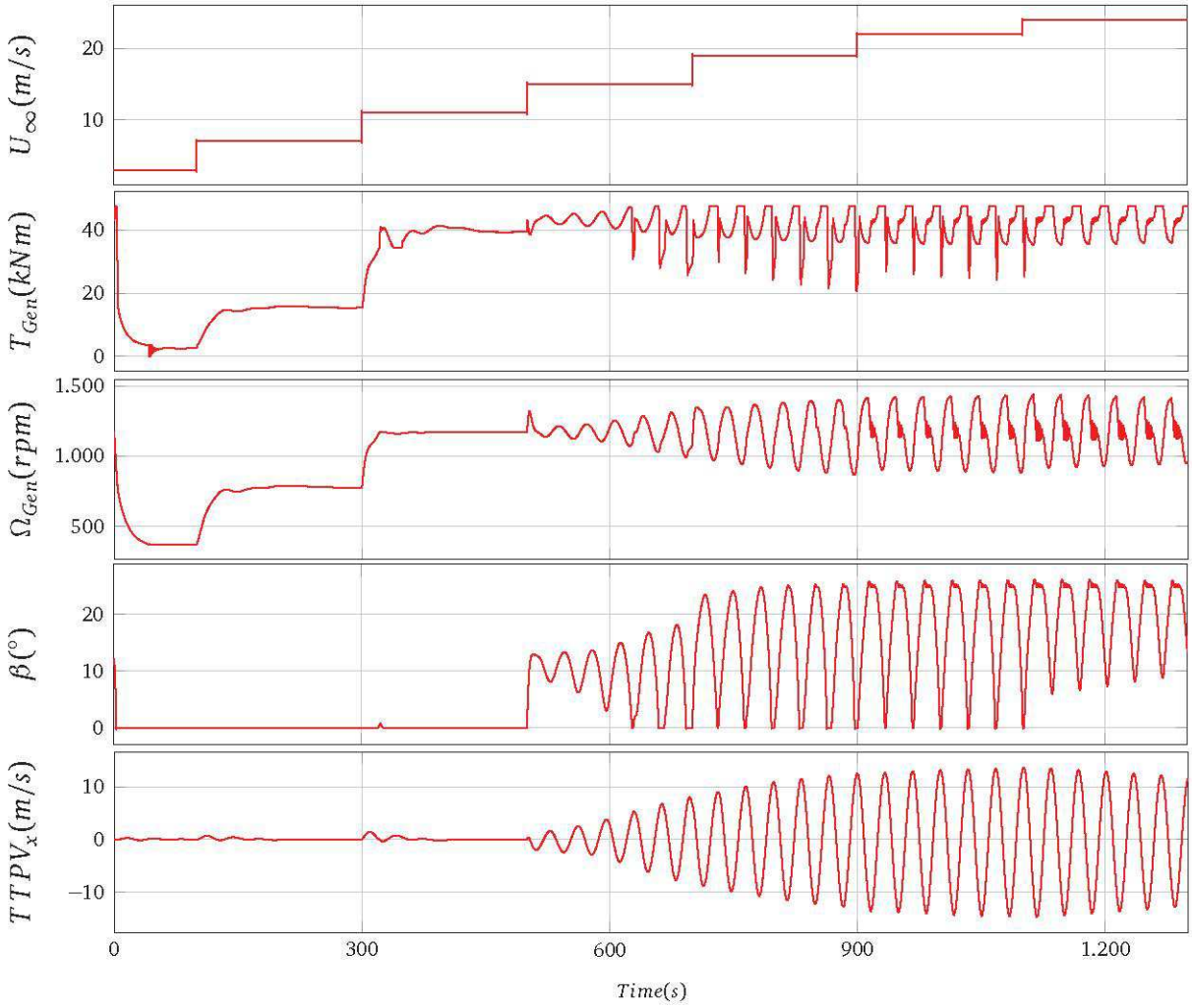

Figure 4.4.: Performance of the PI baseline controller.

turbine on the floating foundation, some new vibration modes appear. Performing an eigen-analysis on the state matrix created from the linearization analysis the natural frequencies of the FOWT are calculated. The 1st tower frequency is an horizontal translation mode of the tower with a natural frequency of 0.0077Hz and the second one a rigid body tilt rotation with a frequency of 0.014Hz.

The baseline controller is designed to have a natural frequency of 0.1Hz, so when this controller is implemented in an offshore wind turbine with fixed foundation the system works stable. The lowest natural frequency of the system is higher than the controller's natural frequency. This means that, comparing with the tower motion, the pitch controller is slow and will not cause this problematic coupling between blade pitch and tower pitch motion.

The problem appears when the baseline controller is mounted on a FOWT. Now, due to the system's lower natural frequencies, a coupling between blade pitch and tower pitch motion appears. This coupling produces a negative damping, which leads to instability of the system.

So that this negative damping concept can be better understood, the steady-state rotor thrust as a function of wind speed is represented in Figure 4.5.

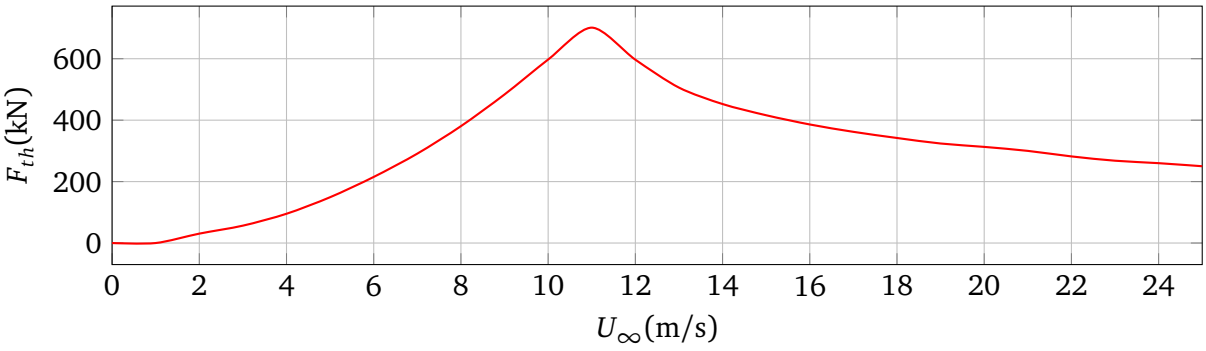

Figure 4.5.: Steady-state rotor thrust as a function of wind speed for the NREL 5-MW baseline wind turbine.

Above rated wind speed, the thrust force exerted by the wind on the wind turbine decreases, because of the rise of blade pitch angle. When this angle augments, the thrust force decreases. Every time the FOWT pitches in the sense of θ_p positive and is displaced in the sense of x positive, Eq. (3.6) shows how the relative wind speed reaching the turbine is decreased. In order to maintain the generator speed in the rated value, the blade pitch angle will be decreased. This blade pitch angle reduction will result in an increment of the thrust force and, consequently, a higher tower pitch angle. The contrary effect will be produced when the FOWT pitches in the sense of θ_p negative and is displaced in the sense of x negative. The relative wind speed that reaches the turbine will increase, resulting on a growth of blade pitch angle to maintain the rated generator speed. As a consequence, the thrust force will be smaller and the backward motion will be encouraged. This cyclic event will continually augment the tower pitch angle, making the system unstable.

Analyzing the closed loop formed by PI controller transfer function and the transfer function from collective pitch angle to generator speed this instability can be confirmed. $G(s)_{\Omega_{Gen}\beta}$ transfer function is obtained from the state space system Eq. (4.13). The poles of the closed loop system are:

$$\boldsymbol{poles} = \begin{bmatrix} 0.0683 \\ -0.0151 \pm 0.1907i \\ -0.0122 \pm 0.0477i \\ -0.2076 \end{bmatrix}$$

Inasmuch as a pole with positive real part can be found, the instability of the closed loop system is confirmed. A solution need to be found for this instability problem.

4.3 Derated baseline controller

The instability in the system is caused by the negative damping, which is a consequence of having such high controller natural frequency, if compared with the system natural frequencies.

While the vibration mode with the lowest frequency of 0.0077Hz has a positive damping from the hydrodynamic loads and the catenary lines, the rotational mode of the tower at 0.014Hz has no damping from the catenary lines and very little damping from the hydrodynamic loads. When the motion is towards the wind, due to the low natural frequency, the pitch controller will adjust the pitch angle and reduce the thrust as a consequence. The aerodynamic damping is therefore negative when the pitch control is fast.

Therefore, a valid solution to avoid the unstable operation of the system above rated wind speeds is to derate the controller, so its natural frequency can be lowered.

Since the rotational mode of the turbine is the one causing problems, the new gains of the PI controller will be calculated for a natural frequency lower than this frequency. This way, the effect of the negative damping is avoided.

Solving Eq. (4.11) and Eq. (4.12) with the new parameters $\omega_n = 0.014Hz$ and $\zeta = 0.7$,a resultant $K_{Po} = 0.002636$ and $K_{Io} = 0.001134$ are obtained. Original gains have been reduced to 14% of its original value. This calculus has been made from the designed model though, that is to say that this gain reduction may not be optimum in FAST model. In order to find the optimum value that stabilizes the system, the behavior of generator torque, generator speed, blade pitch angle and platform pitch angle for different gains is shown in Figure 4.6.

Although a little error between designed model optimum derated value and FAST model derated value exists, it can be appreciated how the instability problem has been successfully solved derating controller's gain to 10% of their values and how this problem persist for smaller gain reductions. However, the parameters of the current controller are not the optimal parameters for a wind turbine's blade pitch controller. Reducing the gains of the PI controller, the closed-loop bandwidth is reduced as well. This reduction will cause a more sensitive response of the generator speed to disturbances. For a FOWT with reduced bandwidth, the generator speed can reach values higher than 30 % of the nominal speed [23]. Typical values in onshore wind turbines are up to 10 %. The difference is truly considerable. The probability of shut downs owing to overspeed is increased. This problem is specially censorious for wind turbines with doubly fed induction because they are designed with a variable speed range of ±30 % around the synchronous speed [23].

4.4 Feedback of tower top velocity in generator torque

Although the instability problem has been solved with the previous controller, a new solution must be found in order to overcome the generator speed high variability issues. Analyzing the

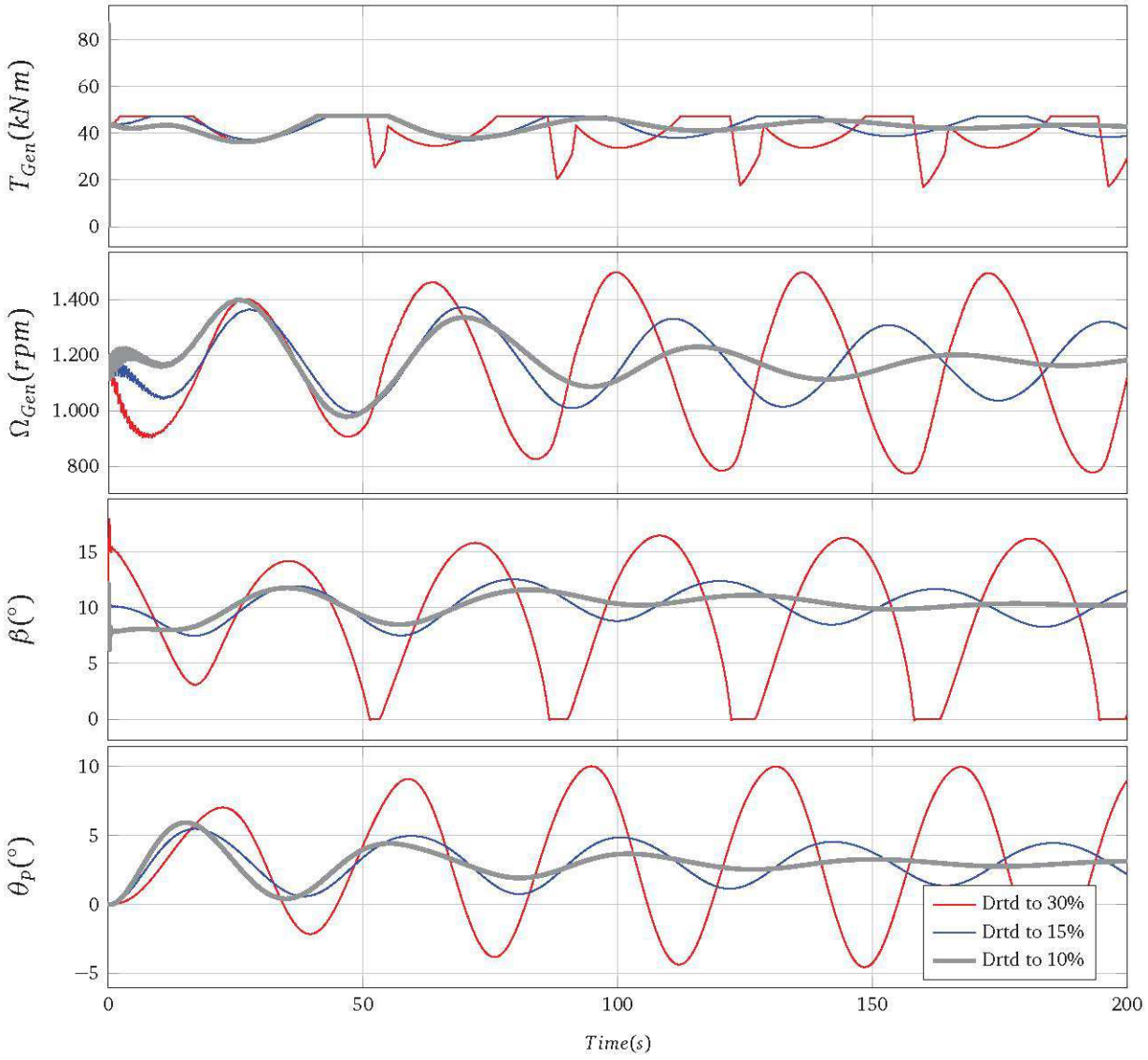

Figure 4.6.: Performance of the PI derated controller for a constant wind speed of 15m/s and different derated factors.

the transfer function from the blade pitch angle to the generator speed, obtained from the linear system Eq. (4.13), a complex pair of non-minimum phase zeros (NMPZ) is found:

$$\boldsymbol{zeros} = \begin{bmatrix} 0.0019 \pm 0.1910i \\ 0 \\ -0.0113 \pm 0.0472i \end{bmatrix} \tag{4.14}$$

The existence of these zeros is the cause of the instability appearance. To understand where they come from, a reduced 2 DOF FOWT model is represented. This model focuses only on the pitch rotation and rotor dynamics. With 2nd order differential equations the system is described. For the reduced model, the coupling between pitch and surge motion will not be considered. For the pitch mode:

$$M_{44}\ddot{\theta}_P + D_{44}\dot{\theta}_P + K_{44}\theta_P = L_T F_{th} \tag{4.15}$$

Rotor dynamics will be described in the same way as in the original model.

$$J_{DT}\frac{\mathrm{d}\Omega}{\mathrm{d}t} = T_{aero} - T_{Gen}, \tag{4.16}$$

where

$$F_{th} = c_{T,U_\infty}\left(U_\infty - H\dot{\theta}_P\right) + c_{T,\dot{\varphi}}\dot{\varphi} + c_{T,\beta}\beta \tag{4.17}$$

$$T_{aero} = c_{P,U_\infty}\left(U_\infty - H\dot{\theta}_P\right) + c_{P,\dot{\varphi}}\dot{\varphi} + c_{P,\beta}\beta \tag{4.18}$$

In order to have a linear thrust force and a linear aerodynamic torque, gradients of different variables will be used. Gradients of thrust force and aerodynamic torque with respect to effective local wind speed (c_{T,U_∞} and c_{P,U_∞}), to blade-pitch angle ($c_{T,\beta}$ and $c_{P,\beta}$) and to rotor speed ($c_{T,\dot{\varphi}}$ and $c_{P,\dot{\varphi}}$) can be found. These gradients are calculated around the same operation point as before, wind speed of 15m/s. Values for these parameters are shown in Symbols list .

Previously defined differential equations are transformed into a linear and invariant in time state space system.

$$\begin{cases} \dot{\boldsymbol{x}} = \mathbf{A}^{\mathbf{red}}\boldsymbol{x} + \mathbf{B}^{\mathbf{red}}\boldsymbol{u} \\ \dot{\boldsymbol{y}} = \mathbf{C}^{\mathbf{red}}\boldsymbol{x} + \mathbf{D}^{\mathbf{red}}\boldsymbol{u} \end{cases} \tag{4.19}$$

$$\mathbf{A}^{\mathbf{red}} = \begin{bmatrix} 0 & 1 & 0 & 0 \\ \frac{-K_{44}}{M_{44}} & \frac{-D_{44}}{M_{44}} - \frac{c_{T,U_\infty}H^2}{M_{44}} & \frac{c_{T,\dot{\varphi}}H}{M_{44}} & 0 \\ 0 & 0 & 0 & 1 \\ 0 & \frac{-c_{P,U_\infty}H}{J_{DT}} & \frac{c_{T,\dot{\varphi}}}{J_{DT}} & 0 \end{bmatrix} \mathbf{B}^{\mathbf{red}} = \begin{bmatrix} 0 & 0 & 0 \\ \frac{c_{T,U_\infty}H}{M_{44}} & \frac{c_{T,\beta}H}{M_{44}} & 0 \\ 0 & 0 & 0 \\ \frac{c_{P,U_\infty}}{J_{DT}} & \frac{c_{P,\beta}H}{J_{DT}} & \frac{-1}{J_{DT}} \end{bmatrix}$$

$$\mathbf{C}^{\mathbf{red}} = \begin{bmatrix} 1 & 0 & 0 & 0 \\ 0 & 1 & 0 & 0 \\ 0 & 0 & 1 & 0 \\ 0 & 0 & 0 & 1 \end{bmatrix} \qquad \mathbf{D}^{\mathbf{red}} = \mathbf{0_{4x4}}$$

From this state space system the transfer function from blade pitch input to generator speed output is obtained. Taking the numerator of it, a second order equation that will define the zeros of the system is used to explain the occurrence of the NMPZ.

$$s^2 + \frac{1}{M_{44}}\left(D_{44} + c_{T,U_\infty}H^2 - c_{P,U_\infty}H^2\frac{c_{T,\beta}}{c_{P,\beta}}\right)s + \frac{C_{44}}{M_{44}} = 0 \tag{4.20}$$

From Eq. (4.20), the term that will determine if NMPZ exist on the system is the one multiplying s. When the condition exposed in Eq. (4.22) is accomplished, NMPZ will make unstable the operation of the system with a baseline controller.

$$\left(c_{T,v} - c_{P,v}\frac{c_{T,\beta}}{c_{P,\beta}}\right)H^2 < -D_{44} \tag{4.21}$$

So that the performance of the controller can be improve, a method to compensate these NMPZ is proposed. A method known as parallel path modification is implemented for this purpose. This method has been proposed by B. Fischer in [23]. According to his research, the zeros between one input and one output of the plant can be compensated by using a second input and a second output.

Feeding back the nacelle velocity to the generator torque, the NMPZ included in the transfer function from blade-pitch to generator speed can be modified. This feeding is performed by a simple proportional controller. A block scheme is represented in Figure 4.7.

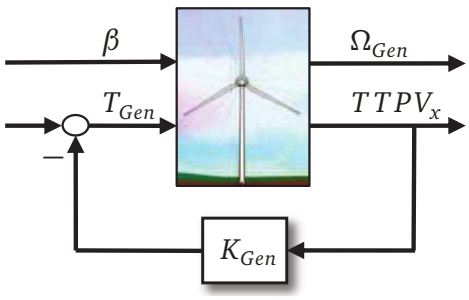

Figure 4.7.: Block schematic of the proportional parallel feedback.

One of the inconveniences of this control method is that the tower top velocity is not directly available. Instead of this variable, tower top acceleration is measured by an accelerometer. Integrating this signal tower top velocity variable will be obtained.

Since the aim of this compensator is to allow a higher bandwidth of the collective blade-pitch control loop, there is no sense on using it below rated wind speed, where the blade-pitch controller is shutdown. A simple switching logic will be implemented to avoid the compensator of working where it must not work. When the blade pitch angle is not 0 the compensator will be working and with an angle of 0 it will stop.

With this new signal feedback, the state space matrices will change. With this new modification, $T_{Gen} = -K_{Gen}\dot{\varphi}H$. Replacing that in the state space matrices

$$\mathbf{A^{red}} = \begin{bmatrix} 0 & 1 & 0 & 0 \\ \frac{-K_{44}}{M_{44}} & \frac{-D_{44}}{M_{44}} - \frac{c_{T,U_\infty}H^2}{M_{44}} & \frac{c_{T,\dot{\varphi}}H}{M_{44}} & 0 \\ 0 & 0 & 0 & 1 \\ 0 & \frac{-c_{P,U_\infty}H}{J_{DT}} - \frac{K_{Gen}H^2}{J_{DT}} & \frac{c_{T,\dot{\varphi}}}{J_{DT}} & 0 \end{bmatrix} \mathbf{B^{red}} = \begin{bmatrix} 0 & 0 & 0 \\ \frac{c_{T,U_\infty}H}{M_{44}} & \frac{c_{T,\beta}H}{M_{44}} & 0 \\ 0 & 0 & 0 \\ \frac{c_{P,U_\infty}}{J_{DT}} & \frac{c_{P,\beta}H}{J_{DT}} & \frac{-1}{J_{DT}} \end{bmatrix}$$

$$\mathbf{C^{red}} = \begin{bmatrix} 1 & 0 & 0 & 0 \\ 0 & 1 & 0 & 0 \\ 0 & 0 & 1 & 0 \\ 0 & 0 & 0 & 1 \end{bmatrix} \qquad \mathbf{D^{red}} = \mathbf{0_{4x4}}$$

Transfer function NMPZ are modified and this time its occurrence depends on proportional gain K_{Gen} as well.

$$\left(c_{T,v} - (c_{P,v} - K_{Gen})\frac{c_{T,\beta}}{c_{P,\beta}}\right)H^2 < -(D_{44}) \tag{4.22}$$

Aerodynamic coefficients and the damping of the FOWT will determine the minimum value o K_{Gen}. When $K_{Gen} \approx 2500$ or bigger, NMPZ will be compensated and the system will operate stable. Same as before, this value is calculated from a reduced linear model instead of calcultating it from FAST model. However, in this case $K_{Gen} \approx 2500$ stabilize FAST model as well. Generator torque, generator speed, blade pitch angle and platform pitch angle response for different gains around this value are represented in Figure 4.8.

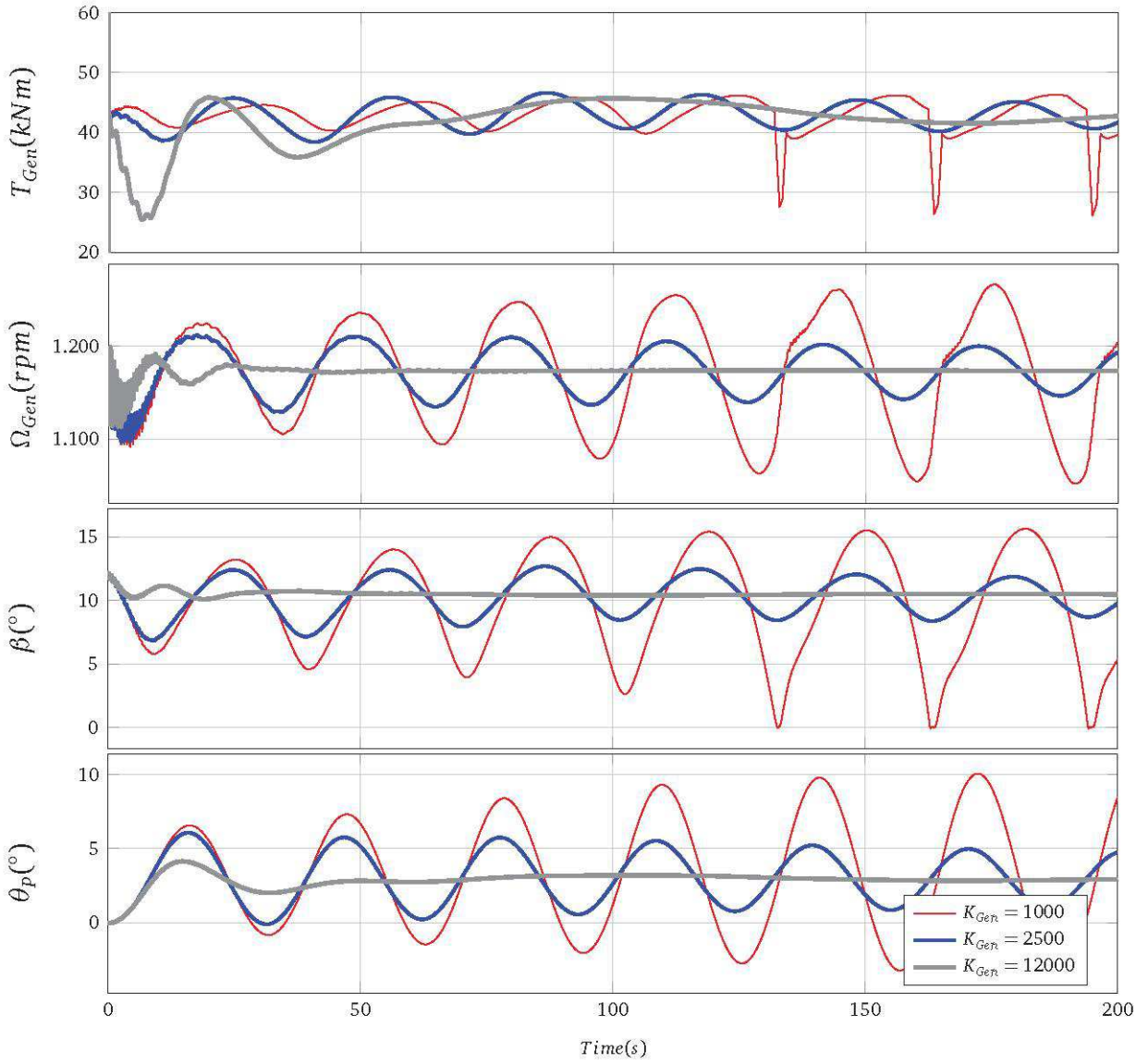

Figure 4.8.: Performance of the NMPZ compensator for a constant wind speed of 15m/s with different K_{Gen}.

With $K_{Gen} = 1000$ the system gets unstable, so the limit has been succesfully calculated. Although the systems is stabilized with $K_{Gen} = 2500$, the response is not as good as desired with. It takes too long to mitigate pitch velocity, thereby generator speed, blade pitch angle, generator torque and produced power will notably vary. So that a faster mitigation of the tower top velocity is produced proportional gain will be increased and it will take a value of $K_{Gen} = 12000$. The performance of the compensator with the new gains is shown in Figure 4.8.

Despite of the increase of bandwidth respect to the derated PI controller and reduction of generator speed variations, an increase in main shaft torsion will be produced. This inconvenience is a result of the higher use of the generator torque. Besides, if value of K_{Gen} is augmented, both tower top velocity and generator speed variations will be reduced. On the contrary, generated power will be more fluctuating and the increase in main shaft torsion will be even higher.

4.5 Feedback of tower top velocity in generator torque and nacelle yaw angle

Implementing an additional parallel path modification, a new attempt to stabilize the system and improve controller's performance is done. On the one side, a feedback of tower top velocity to the generator torque is realized and on the other side, the same output is fed back to the nacelle yaw angle. The zeros between blade pitch angle input and generator speed output will be modified by the yaw angle and generator torque input and tower top velocity output. Same way as in Section 4.4, tower top velocity will be multiplied by a proportional gain in both feedbacks and the compensator will be shutdown below rated wind speeds.

Adding the collaboration of another actuator, the nacelle yaw angle, a reduction in the activity of generator torque is desired. So that main shaft torsion can be reduced.

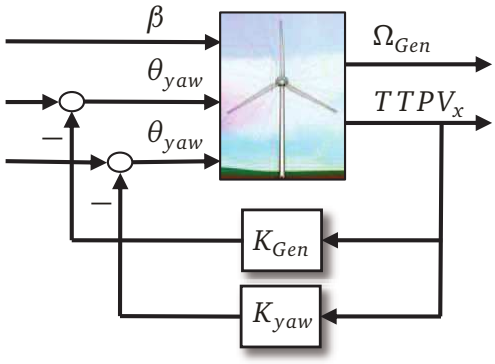

Figure 4.9.: Block schematic of the proportional parallel feedback

Using the same reduced model as the one used in Eq. (4.19), gradients of thrust force and aerodynamic torque with respect to nacelle yaw angle need to be added. The values of these gradients can be found in Symbols list as well.

$$F_{th} = c_{T,U_\infty}\left(U_\infty - H\dot{\theta}_P\right) + c_{T,\dot{\varphi}}\dot{\varphi} + c_{T,\beta}\beta + c_{T,\theta_{yaw}}\theta_{yaw} \tag{4.23}$$

$$T_{aero} = c_{P,U_\infty}\left(U_\infty - H\dot{\theta}_P\right) + c_{P,\dot{\varphi}}\dot{\varphi} + c_{P,\beta}\beta + c_{P,\theta_{yaw}}\theta_{yaw} \tag{4.24}$$

With the addition of these terms, state, input, output and feedforward matrices for the linear time invariant state space system will be

$$\mathbf{A}=\begin{bmatrix} 0 & 1 & 0 & 0 \\ \frac{-K_{44}}{M_{44}} & \frac{-D_{44}}{M_{44}}-\frac{c_{T,U_\infty}H^2}{M_{44}}-\frac{K_{yaw}H^2}{M_{44}} & \frac{c_{T,\dot{\varphi}}H}{M_{44}} & 0 \\ 0 & 0 & 0 & 1 \\ 0 & \frac{-c_{P,U_\infty}H}{J_{DT}}-\frac{K_{yaw}H}{J_{DT}}-\frac{K_{Gen}H}{J_{DT}} & \frac{c_{T,\dot{\varphi}}}{J_{DT}} & 0 \end{bmatrix} \mathbf{B}=\begin{bmatrix} 0 & 0 & 0 & 0 \\ \frac{c_{T,U_\infty}H}{M_{44}} & \frac{c_{T,\beta}H}{M_{44}} & 0 & \frac{c_{T,\theta yaw}H}{M_{44}} \\ 0 & 0 & 0 & 0 \\ \frac{c_{P,U_\infty}}{J_{DT}} & \frac{c_{P,\beta}H}{J_{DT}} & \frac{-1}{J_{DT}} & \frac{c_{P,\theta yaw}H}{J_{DT}} \end{bmatrix}$$

$$\mathbf{C}=\begin{bmatrix} 1 & 0 & 0 & 0 \\ 0 & 1 & 0 & 0 \\ 0 & 0 & 1 & 0 \\ 0 & 0 & 0 & 1 \end{bmatrix} \qquad \mathbf{D}=\mathbf{0_{4x4}}$$

From the state space system, the transfer function from the blade-pitch angle to the rotor speed is obtained. The zeros of this transfer function will be calculated from the second order Eq. (4.25)

$$s^2+\frac{1}{M_{44}}\left(D_{44}+c_{T,U_\infty}H^2+K_{yaw}H^2-K_{yaw}H^2\frac{c_{T,\beta}}{c_{P,\beta}}-K_{Gen}H^2\frac{c_{T,\beta}}{c_{P,\beta}}-c_{P,U_\infty}H^2\frac{c_{T,\beta}}{c_{P,\beta}}\right)s+\frac{C_{44}}{M_{44}}=0 \tag{4.25}$$

So that the are no MNPZ in the system, this relation must be fulfilled:

$$D_{44}>c_{T,U_\infty}H^2+K_{yaw}H^2-K_{yaw}H^2\frac{c_{T,\beta}}{c_{T,\beta}}-K_{Gen}H^2\frac{c_{T,\beta}}{c_{P,\beta}}-c_{P,U_\infty}H^2\frac{c_{T,\beta}}{c_{P,\beta}} \tag{4.26}$$

In order to tune the proportional controllers, a new strategy will be followed. It is proved that the stability of the system can be achieved with the K_{Gen} used in Section 4.4. Since a reduction of main shaft torsion is desirable and the dynamical limits of the nacelle yaw actuator are established, K_{Gen} will be reduced and from Eq. (4.26) K_{yaw} will be calculated. The limit for K_{yaw} will be set by nacelle yaw's actuator dynamics and its velocity. The nominal nacelle-yaw rate is 0.3 °/s, so a value of K_{yaw} that does not provoque the trespassing of this limit must be chosen. After an iterative process K_{Gen} and K_{yaw} are chosen and set to $K_{Gen}=1170$ and $K_{yaw}=0.4$. It can be notice that torque proportional gain is almost equal to the previous controller and nacelle yaw angle proportional gain is very small. Due to the values of the gains, it can be deduced that the system behavior will not be very different to the one implemented in Section 4.4. Figure 4.10 represents platform pitch behavior when both controllers are implemented for a constant wind speed of 15m/s.

In Figure 4.11 velocity of the nacelle yaw actuator is shown. As it is required, the maximum velocity can not exceed 0.3 °/s.

Performance of this controller is quite similar to the one without tower top velocity feedback to nacelle yaw angle. The reason is that nacelle yaw angle actuator's dynamic conditions are so

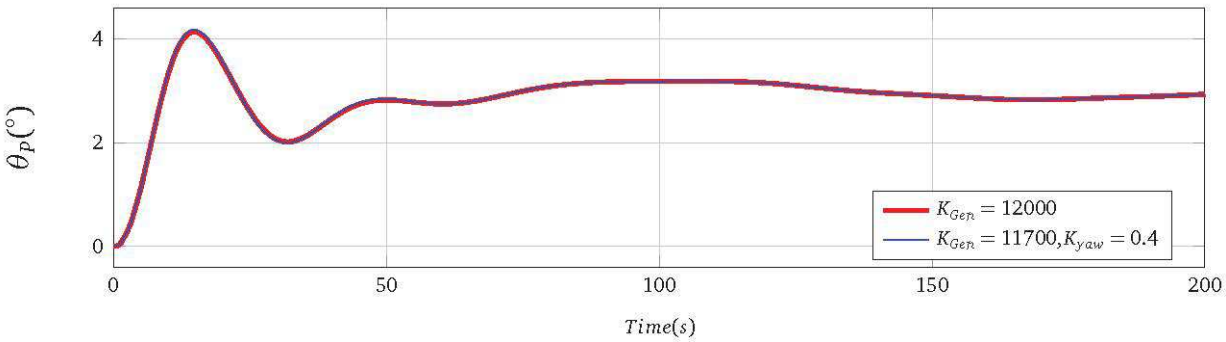

Figure 4.10.: Platform pitch angle when NMPZ controller is implemented for a constant wind speed of 15m/s. Both without using yaw angle with $K_{Gen} = 12000$, and using yaw angle with $K_{Gen} = 11700$ and $K_{yaw} = 0.4$.

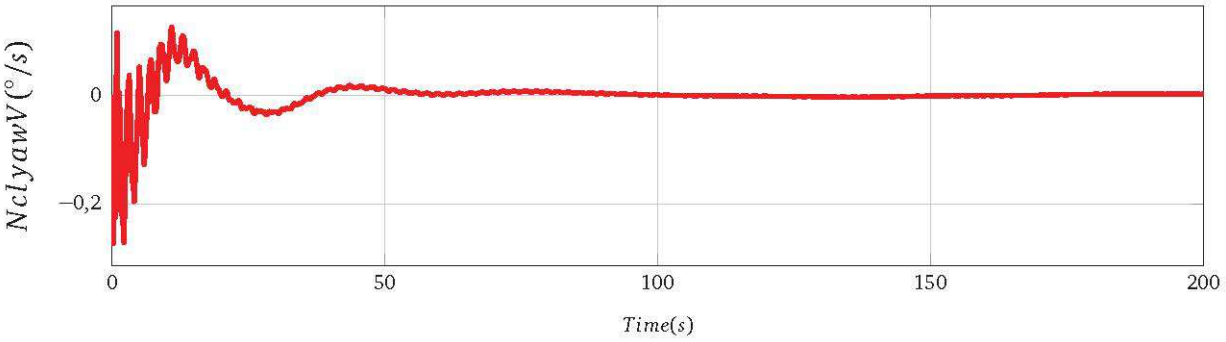

Figure 4.11.: Nacelle yaw rotation velocity for a constant wind speed of 15m/s, $K_{Gen} = 11700$ and $K_{yaw} = 0.4$.

restrictive that K_{yaw} value must be very low, making K_{Gen} almost equal to the one previously chosen. This means that although theoretically is possible to reach a stable operation and to achieve a main shaft torsion reduction with this control method, in reality the drive that operates nacelle yaw is not fast enough to follow given actuation orders. Due to that, this control will be discarded for the further comparison between controllers. It is worth mentioning that commercial turbines only use nacelle yaw angle to properly orient the turbine to the wind direction, instead of using it to maximize power generation or reduce loads in the wind turbine. With new improvements on this actuators, maybe this control concept can be implemented.

4.6 States feedback linear quadratic regulator controller

Once the results and performance of previous controllers have been studied, a last attempt of a new controller is made subsequently. This one is a more complex state feedback controller. The aim of this controller is to shape the behavior of the system through feedback of the system's states like it is shown in Figure 4.12.

To implement this controller a linear and time invariant system is necessary. Since the developed FOWT model is non-linear, the linearized model developed in Appendix B is used.

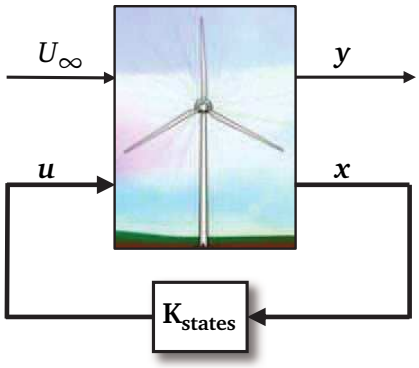

Figure 4.12.: Block schematic of the states feedback control

Before applying the states feedback control to the system, some conditions need to be checked. First of all, the system must be stable. A state space system is stable when all the eigenvalues of the state matrix have a negative real part. Using Matlab and the implemented command `eig(A)`. it can be assured that this condition is accomplished for this system.

Controlability of the system needs to be check as well. A system is controllable if, applying adequate inputs, it is able to change from one state to a different one. Mathematical relation shown in Eq. (4.27) need to be fulfilled to ensure system's controlability.

$$rank\begin{bmatrix} \mathbf{B} & \mathbf{AB} & \mathbf{A}^2\mathbf{B} & \cdots & \mathbf{A}^n\mathbf{B} \end{bmatrix} = n \tag{4.27}$$

Where n is the system's number of states. Studied system is perfectly controllable.

When a states feedback wants to be done, it has to be possible to obtain these states' values. Since measuring all the states is a harsh and very expensive task, these values are often obtained through an estimator. So that the estimator can be implemented in the system, the system itself needs to be observable.

Observability is a measure for how well internal states of a system can be inferred by knowledge of its external outputs. Observability provides that knowing an output trajectory provides enough information to predict the initial state of the system. Observability of the system is possible if and only if

$$rank\begin{bmatrix} \mathbf{C} \\ \mathbf{CA} \\ \vdots \\ \mathbf{CA}^{n-1} \end{bmatrix} = n \tag{4.28}$$

Once all necessary conditions are ensure, a $\mathbf{K}_{\mathbf{states}}$ matrix can be found so that, multiplying system's states with this matrix and feedbacking the result, the behavior of the system can be shape to the required necessities. For the studied case of the FOWT, system states will be obtained through a Kalman filter estimator and the result of multiplying them with the $\mathbf{K}_{\mathbf{states}}$

matrix will be fed back. The part concerned to Kalman filter will not be treated in this thesis, but a Kalman filter which provides the correct values of the states is supposed in order to design the control.

$\mathbf{K_{states}}$ will be designed using the linear quadratic regulator method. This is an optimization control theory which determines the control signals that will cause a process to minimize some cost criterion. In order to reduce the cost function, some weight factor, that the designer will provide, are needed. To calculate $\mathbf{K}_{LQR}$, first, a cost function that will be minimized is specified

$$J = \int_0^\infty \boldsymbol{x}^T \mathbf{Q}\boldsymbol{x} + \boldsymbol{u}^T \mathbf{R}\boldsymbol{u} + 2\boldsymbol{x}^T \mathbf{N}\boldsymbol{u}\, dt \tag{4.29}$$

$\mathbf{Q}$, $\mathbf{R}$ and $\mathbf{N}$ are symmetric and positive defined weight matrices that are given by the designer. The first term of the cost function Eq. (4.29) minimize the deviation of states while the second one is related to the energy expended by the control. Coupling between states and control commands is represented by the last term. According to this, choosing a different relation between $\mathbf{Q}$ and $\mathbf{R}$, it can be put more emphasis on reducing states deviation or on using less energy in control commands.

The feedback control law that minimizes the value of this cost is given by

$$\boldsymbol{u} = -\mathbf{K_{LQR}}\boldsymbol{x}, \tag{4.30}$$

where $\mathbf{K_{LQR}}$ is given by

$$\mathbf{K_{LQR}} = \mathbf{R}^{-1}\left(\mathbf{B}^T\mathbf{P} + \mathbf{N}^T\right) \tag{4.31}$$

and $\mathbf{P}$ is found by solving continuous time algebraic Riccati equation [24].

$$\mathbf{A}^T\mathbf{P} + \mathbf{P}\mathbf{A} - (\mathbf{P}\mathbf{B} + \mathbf{N})\,\mathbf{R}^{-1}\left(\mathbf{B}^T\mathbf{P} + \mathbf{N}^T\right) + \mathbf{Q} = 0 \tag{4.32}$$

In the studied case of the FOWT the quadratic cost function will be defined as the sum of the power deviations from rated value, surge, sway, roll and pitch velocities and control inputs use. So the objective of the controller will be divided in three parts: First objective will be to reduce power losses, produced by a turbine operation far form the operating point, and keep the power at its rated value, avoiding as well as possible power fluctuations. Second objective will be to minimize FOWT displacements and rotations. The third objective will be to reduce the use of control inputs, such as generator torque and blade pitch angle.

$$\begin{aligned} J &= \int_0^\infty \boldsymbol{x}^T \mathbf{Q}\boldsymbol{x} + \boldsymbol{u}^T \mathbf{R}\boldsymbol{u} + 2\boldsymbol{x}^T \mathbf{N}\boldsymbol{u}\ dt = \\ &= \int_0^\infty (P - P_{rated})^2 + \dot{x}_{CM}^2 + \dot{y}_{CM}^2 + \dot{\theta}_P^2 + \dot{\theta}_r^2 + T_{Gen}^2 + \beta^2\ dt \end{aligned} \tag{4.33}$$

Weight matrices will be provided by FOWT model will provide weight matrices. In order to find these **Q**, **R** and **N** matrices attached to the cost function, this cost function must be expressed in terms of states and inputs. Power term is the only term of the cost function that is not expressed this way. In order to achieve an states and inputs dependent expression, power equation is developed.

$$P = \frac{\rho_{air} A}{2} C_P(\lambda,\beta)(U_\infty - \dot{x}_{CM} - H\dot{\theta}_P)^3 \tag{4.34}$$

Power coefficient can be obtained from torque coefficient using tip speed ratio.

$$C_P(\lambda,\beta) = \lambda C_M(\lambda,\beta) \tag{4.35}$$

So that the dependance of the power coefficient with respect to blade collective pitch angle and tip speed ratio in the current operation point can be seen, a linearization of power coefficient around this point is done by making a Taylor series expansion until first order derive. The first term is the power coefficient in the operation point and the two next terms are gradients of the power coefficient with respect to tip speed ratio and blade pitch angle in the selected operation point as well.

$$C_P(\lambda,\beta) = C_{Po} + \left.\frac{\partial C_P}{\partial \beta}\right|_0 (\beta - \beta_0) + \left.\frac{\partial C_P}{\partial \lambda}\right|_0 (\lambda - \lambda_0) \tag{4.36}$$

where

$$\lambda = \frac{R\Omega}{U_\infty - \dot{x}_{CM} - H\dot{\theta}_P} \tag{4.37}$$

Incorporating Eq. (4.36) and Eq. (4.37) into Eq. (4.34)

$$P = \frac{\rho_{air} A_{rotor}}{2} \left(C_{Po} + \left.\frac{\partial C_P}{\partial \beta}\right|_0 (\beta - \beta_0) + \left.\frac{\partial C_P}{\partial \lambda}\right|_0 \left(\frac{R\Omega}{U_\infty - \dot{x}_{CM} - H\dot{\theta}_P} - \lambda_0 \right) \right) (U_\infty - \dot{x}_{CM} - \dot{\theta}_P)^3 \tag{4.38}$$

Finally, Eq. (4.38) is incorporated in the cost function Eq. (4.33) and this whole cost function is expanded. Expanding Eq. (4.33) those terms related to **Q**, **R** and **N** matrices can be found.

Since in the cost function **Q** is multiplying the transpose of the states vector and the states vector, its terms will be those terms of Eq. (4.38) that multiply a state to the power of 2 and those terms that multiply the multiplication of 2 states.

$$
\begin{aligned}
Q_{11} &= 3C_{Po}U_{\infty} + 1 \\
Q_{22} &= 1 \\
Q_{33} &= 1 \\
Q_{44} &= 3C_{Po}U_{\infty}H^2 + 1 \\
Q_{14} &= 6C_{Po}U_{\infty}H\dot{\theta}_P \\
Q_{41} &= 6C_{Po}U_{\infty}H\dot{\theta}_P \\
Q_{15} &= -2RU_{\infty}\left.\frac{\partial C_P}{\partial \lambda}\right|_0 \\
Q_{51} &= -2RU_{\infty}\left.\frac{\partial C_P}{\partial \lambda}\right|_0 \\
Q_{45} &= -2RU_{\infty}\left.\frac{\partial C_P}{\partial \lambda}\right|_0 \\
Q_{54} &= -2RU_{\infty}\left.\frac{\partial C_P}{\partial \lambda}\right|_0
\end{aligned}
$$

The rest of **Q** matrix will be completed with zeros.

R matrix terms will be those terms multiplying a control input (β,T_{Gen}) to the power of 2 and the multiplication of two control commands. Since there is no term that multiply two control inputs, **R** matrix non zero terms will be only located in the diagonal.

$$
\begin{aligned}
R_{11} &= 1 \\
R_{22} &= 1
\end{aligned}
$$

Finally, **N** matrix terms will be those terms multiplying the multiplication of a state with a control command.

$$
\begin{aligned}
N_{11} &= -3U_{\infty}^2\left.\frac{\partial C_P}{\partial \beta}\right|_0 \\
N_{41} &= -3U_{\infty}^2\left.\frac{\partial C_P}{\partial \beta}\right|_0
\end{aligned}
$$

Now that all the terms from the function cost are defined, $\mathbf{K_{LQR}}$ can be calculated with Riccati equation. This task is carried out with a Matlab function known as `lqr(A,B,Q,R,N)`. $\mathbf{K_{LQR}}$ Numerical values are detailed in Appendix B.

Once $\mathbf{K_{LQR}}$ is obtained the control set up can be implemented. The collective pitch angle set-point value is the pitch control outgoing signal from the LQR controller, while the generator torque set-point value is the addition of the generator torque control outgoing signal from the

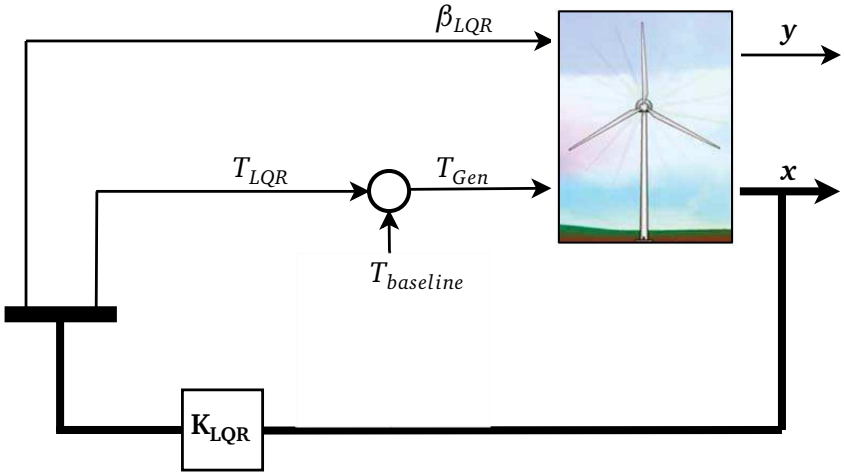

Figure 4.13.: Block schematic of the states feedback LQR control

LQR controller and the generator torque baseline controller value in the above rated zone. Figure 4.13 shows the control diagram.

This control architecture has an issue though. A reduced linearized model has been used to design the LQR controller; this model even if sophisticated and able to account for a number of dynamics, is an approximation of the real thing. Moreover, the blade's aero characteristic coefficients such as C_M, C_T and C_P are measured or estimated from suitable models- Hence they are affected by errors. Chosen weight matrices have attached errors as well, thereby a control law trying to keep the machine at an specific point may not succeed in exactly trimming the machine at the correct pitch, torque and generator speed. At the end, all this comes down to an incorrect average power output and an inefficient produce of energy.

An elegant solution to this hassle is to implement an integral action ϵ that will act on the error between desired output r and actual output y. Keeping generator speed at its rated value will maintain generated power at its optimum value, since generator torque value is set up in control region 3, . Hence, integral action will be applied into generator speed error. The flow chart diagram shown in Figure 4.14 describes the implementation.

New blade pitch angle control input will be

$$\beta_{LQR} = -\mathbf{K_{LQR},1,j}\boldsymbol{x} - K_{I,LQR}\epsilon \tag{4.39}$$

K_{int} must be the maximum value that keeps the system stable. To calculate this, new system closed loop zeros are analyzed. Since the integral action corrects generator speed error acting on blade pitch angle, only terms of $\mathbf{B^{lin}}$ and $\mathbf{C^{lin}}$ are included in the system, $\mathbf{B^{lin}_{i1}}$ and $\mathbf{C^{lin}_{5j}}$

$$\dot{\epsilon} = \Omega_{Gen,ref} - \Omega_{Gen} = \Omega_{Gen,ref} - \mathbf{C^{lin}_{5j}}\boldsymbol{x} \tag{4.40}$$

$$\dot{\boldsymbol{x}} = \mathbf{A^{lin}}\boldsymbol{x} + \mathbf{B^{lin}_{i1}}\boldsymbol{\beta} \tag{4.41}$$

$$\beta = K_{I,LQR}\epsilon + \mathbf{K_{LQR},1,j}\boldsymbol{x} = \begin{bmatrix} K_{I,LQR} & \mathbf{K_{LQR},1,j} \end{bmatrix} \begin{bmatrix} \epsilon \\ \boldsymbol{x} \end{bmatrix} \tag{4.42}$$

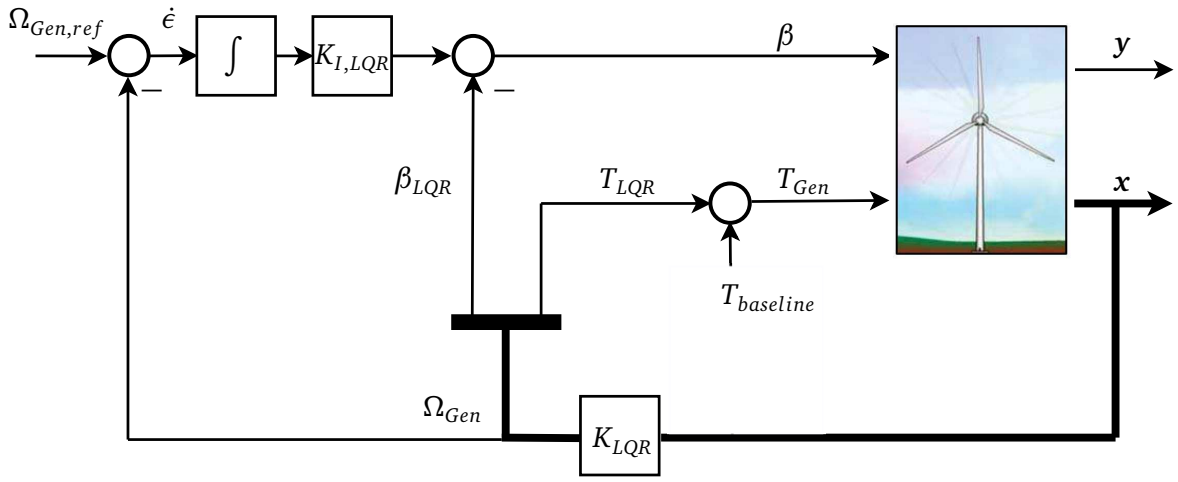

Figure 4.14.: Block schematic of the states feedback LQR control with integral action.

This means that the system is augmented and the integral action is added as a new state.

$$\begin{bmatrix} \dot{\epsilon} \\ \boldsymbol{x} \end{bmatrix} = \begin{bmatrix} 0 & -\mathbf{C}^{\mathbf{lin}} \\ \mathbf{0} & \mathbf{A}^{\mathbf{lin}} \end{bmatrix} \begin{bmatrix} \epsilon \\ \boldsymbol{x} \end{bmatrix} + \begin{bmatrix} 0 \\ \mathbf{B}^{\mathbf{lin}}_{i1} \end{bmatrix} \beta + \begin{bmatrix} 1 \\ 0 \end{bmatrix} \Omega_{Gen,ref} = \tag{4.43}$$

$$= \begin{bmatrix} 0 & -\mathbf{C}^{\mathbf{lin}} \\ \mathbf{0} & \mathbf{A}^{\mathbf{lin}} \end{bmatrix} \begin{bmatrix} \epsilon \\ \boldsymbol{x} \end{bmatrix} + \begin{bmatrix} 0 & 0 \\ \mathbf{B}^{\mathbf{lin}}_{i1} K_{I,LQR} & \mathbf{B}^{\mathbf{lin}}_{i1} \mathbf{K}_{\mathbf{LQR},1,j} \end{bmatrix} \begin{bmatrix} \epsilon \\ \boldsymbol{x} \end{bmatrix} + \begin{bmatrix} 1 \\ 0 \end{bmatrix} \Omega_{Gen,ref} \tag{4.44}$$

$$= \begin{bmatrix} 0 & -\mathbf{C}^{\mathbf{lin}} \\ \mathbf{B}^{\mathbf{lin}}_{i1} K_{I,LQR} & \mathbf{B}^{\mathbf{lin}}_{i1} \mathbf{K}_{\mathbf{LQR},1,j} \end{bmatrix} \begin{bmatrix} \epsilon \\ \boldsymbol{x} \end{bmatrix} + \begin{bmatrix} 1 \\ 0 \end{bmatrix} \Omega_{Gen,ref} \tag{4.45}$$

From this new augmented system state matrix is defined as

$$\tilde{\mathbf{A}}_{\mathbf{r}} = \begin{bmatrix} 0 & -\mathbf{C}^{\mathbf{lin}} \\ \mathbf{B}^{\mathbf{lin}}_{i1} K_{I,LQR} & \mathbf{B}^{\mathbf{lin}}_{i1} \mathbf{K}_{\mathbf{LQR},1,j} \end{bmatrix} \tag{4.46}$$

Since $\mathbf{K}_{\mathbf{LQR},1,j}$ has been previously obtained, $K_{I,LQR}$ will be calculated so that all poles of the augmented system have a negative real part, making the system stable. Solving state matrix eigenvalue problem, $K_{I,LQR}$ will be obtained.

$$\left| s\mathbf{I} - \tilde{\mathbf{A}}_{\mathbf{r}} \right| = \mathbf{0} \tag{4.47}$$

The maximum value of $K_{I,LQR}$ that makes the system stable (only negative real part polos) will is $K_{I,LQR} = 0.05$. This value is calculated from the designed model, so it needs to be tested in FAST model in order to know if the value needs to be modified. Figure 4.15 shows FAST model behavior with different $K_{I,LQR}$.

Due to the modeling errors, $K_{I,LQR} = 0.05$ makes FAST model unstable. However, if this parameter is reduced to $K_{I,LQR} = 0.02$ the system gets stabilize. This stabilization limit can be ensured simulating the system with a smaller gain, $K_{I,LQR} = 0.008$. From simulations it can be deduced that the limit is in $K_{I,LQR} = 0.004$.

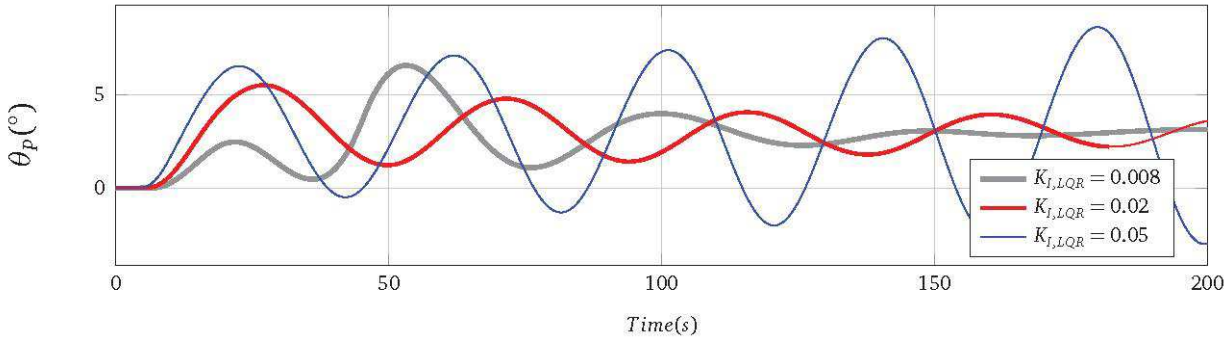

Figure 4.15.: Performance of the LQR controller for a constant wind speed of 15m/s and different $K_{I,LQR}$ values*.

It is worth mentioning that LQR control will operate the turbine above rated wind speed, being shut down when the wind blows below this value. Due to the impossibility of measuring directly wind speed, another technique must be implemented to detect whether wind is above or below rated speed.

The functioning of this switch is the following. When wind speed is above rated wind speed, blade pitch angle will be greater than zero and generator speed will be around 1173.7rpm, rated Ω_{Gen}. If suddenly wind speed decreases below rated wind speed, generator speed will drop and blade pitch controller will decrement blade pitch angle to try to maintain generator speed at its rated value. Since wind is below rated wind speed, the controller will not be able to do that and while pitch angle gets stuck in 0 °, generator speed will continue dropping. Once generator speed gets lower than 1150rpm, switch logic will detect that wind speed is below rated speed and will deactivate LQR controller, passing to control produced power with generator torque (control region 2).

4.7 States feedback linear quadratic regulator controller with gain scheduling

The controller developed in Section 4.6 was designed to work around an operational point. This is not most efficient way of actuating, since wind speed means trend to vary around different values. The best actuation strategy is to adapt the controller to work in the different operational points that wind speed imposes. In order to do so, a gain scheduling is applied to gains $\mathbf{K_{LQR}}$ and $K_{I,LQR}$. Thanks to that, the controller will have an efficient operation above rated wind speed.

The functioning of this gain scheduling is the following. $\mathbf{K_{LQR}}$ and $K_{I,LQR}$ gains will be calculated for different operating point above rated wind speeds. The computation method is the same as the one explained Section 4.6. The operation point is the only thing that changes. These operation points will be the ones reached with $U_\infty = 12,14,16,18,20m/s$. As a result 5 different $\mathbf{K_{LQR}}$ and $K_{I,LQR}$ will be obtained. All $\mathbf{K_{LQR}}$ matrices can be found in Appendix A.

Finally, gain scheduling logic will choose the value of $\mathbf{K_{LQR}}$ and $K_{I,LQR}$ depending on existing wind speed. Chosen operation point will be the one which is the closest to the existing wind speed. For instance, if $U_\infty = 13.2$m/s the controller will operate with gains that have been calculated for $U_\infty = 14$. There is no interpolation between scheduling points, so that a less complicate computation of the controller can be implemented. This gain scheduling operation is implemented when analyzing LQR controller performance in Chapter 5.

5 Controllers comparison

In this chapter blade pitch PI derated controller, NMPZ compensator and states feedback LQR controller performance is shown and compared, making a proper analysis in order to determine how well they manage to accomplish defined objectives. Different tests with diverse conditions will be carried out. Both time plots and fatigue analysis will be exposed and analyzed.

5.1 Time plots

Time plots of system's response give a very good idea of the implemented controller's performance. In this section, FOWT model and implemented controllers will deal with turbulent real wind fields. Each wind field will have a different mean wind speed so that diverse operating point and LQR gain scheduling can be tested.

Exposed outputs will be generator power, generator torque, generator speed, tower top velocity in x and y directions and blade pitch angle. These are very relevant variables when comparing the controllers, which provide big amount of system's behavior information.

- **Generator power**. It is important to maintain the generator power as close as possible to rated value in order to produce a higher amount of energy. Its variability is very important as well. If the produced power is very fluctuating, the grid will suffer more than if the produced power is more constant and non fluctuating.
- **Generator torque**. The more generator torque fluctuates, the bigger will be main shaft torsion and its operational life will be reduced.
- **Generator speed**. Keeping generator speed value close to rated value is essential as well. The wind turbine will have limits for generator speed, so it can not largely vary.
- **Tower top velocity in x and y directions**. This variable will give us an idea of FOWT's movement. The more it moves, the bigger will be the fatigue and the smaller operational life.
- **Blade pitch angle**. It is important to know how much blade pitch angle varies, so that an idea of blade fatigue can be have. If implemented control makes an exhausting use of blade pitch, that will negatively affect in its operational life. This variable will give us an idea of FOWT's movement. The more it moves, the bigger will be the fatigue and the smaller operation life.

In Figure 5.3 first test results are exposed. A turbulent wind field with a mean wind speed of 15m/s is simulated in this case. This mean wind speed can be a very common working condition for the FOWT and it is interesting to see how different controllers handle the situation.

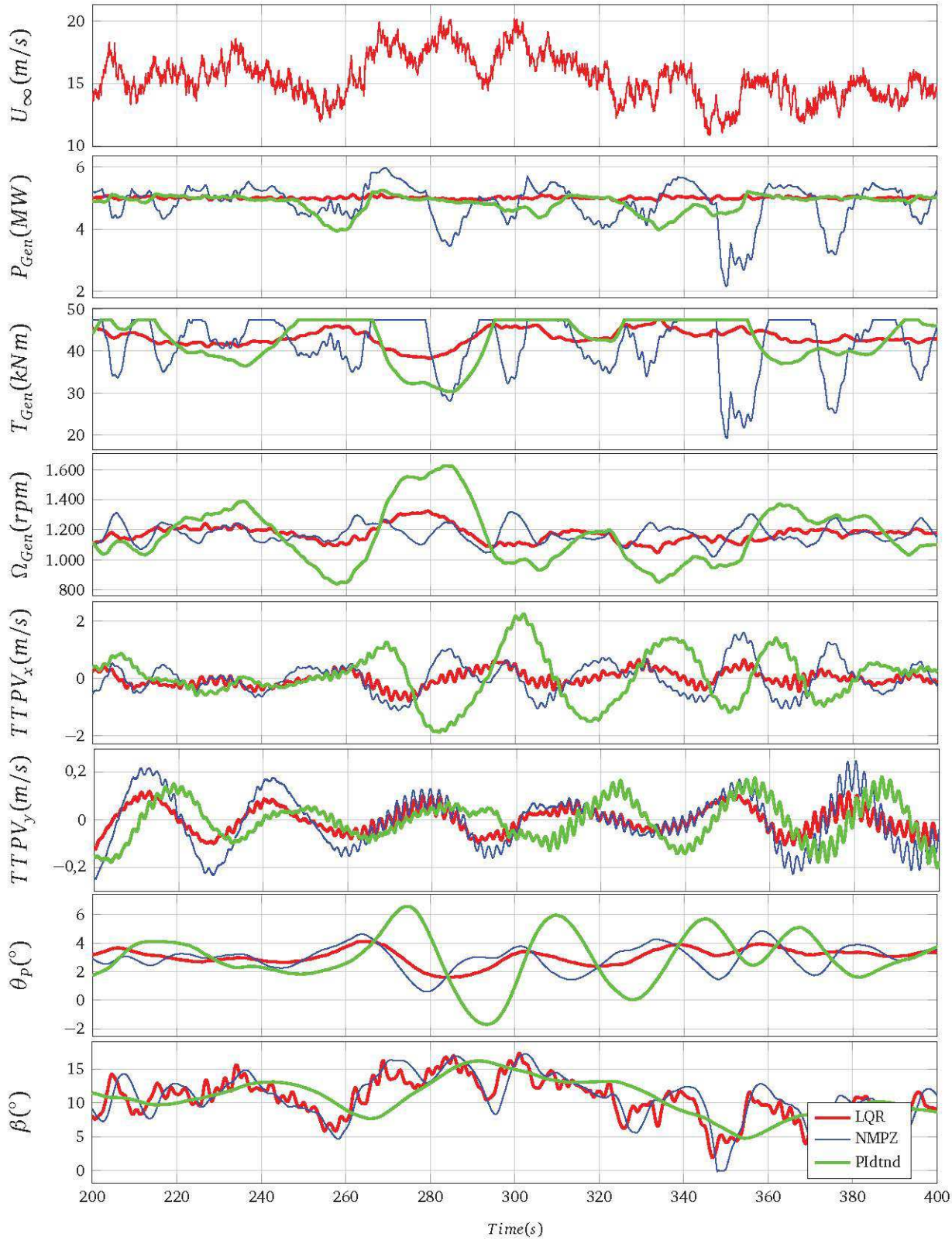

Figure 5.1.: Comparison between derated PI blade pitch controller, NMPZ compensator and LQR controller for a turbulent wind field with a mean wind speed of 15m/s.

Looking at the graphics shown in Figure 5.3 a first analysis can be carried out. LQR state feedback controller really improves power production comparing with other two controllers.

In this aspect, NMPZ compensator has the worst results , and although PI derated controller has not such a bad performance, still produces remarkable power fluctuations. The reason why NMPZ compensator has such a bad result trying to maintain a non fluctuating power is because of its big use of generator torque. PI derated controller performs not so good as LQR regarding to generated power because of the reduction of the bandwidth produced by the lessening of controller's gains. Due to this bandwidth reduction, generator speed largely varies and it makes power varying as well.

Regarding to FOWT tower top velocities, it can be said that both LQR and NMPZ compensator controllers reduce tower top velocities in x direction comparing with the PI derated controller. However, in y direction, this reduction is not so remarkable and only LQR controller achieves a mentionable decrease in this variable. Indeed, PI derated controller gets better results in this output than NMPZ compensator. The reason for this is that in LQR controller's cost function, surge, sway, roll and pitch velocities' terms were included in weight matrices. Therefore the controller will try to minimize them. Anyway, since weights in surge and pitch velocities are bigger, the controller will make a bigger effort reducing these variables. On the contrary in NMPZ compensator, when feeding back tower top velocity in x direction, only FOWT damping in this direction is augmented. This produces a reduction of tower top velocity in x direction, but it does not affect to y direction velocities.

Finally, looking at blade pitch use it can be easily seen that while NMPZ compensator and LQR controller make an exhaustive use of this control input, PI derated controller does not vary it so frequently. This is a consequence of the bandwidth reduction.

Another interesting FOWT working condition is when wind speed is around rated wind speed. Studying controllers performance in this point is interesting because it can be analyze how good is controllers performance when control regions are constantly changing. In Figure 5.2 can be seen how each controller act in this situation.

The good performance of LQR controller can be confirmed in this working condition as well. LQR controller manages to maintain the less fluctuating power when wind speed is above rated and reduces tower top velocities. The only inconveniences that it presents are higher tower top velocities in y direction below rated wind speed (due to the change to baseline generator torque controller) and the higher use of blade pitch angle. On the other hand, MNPZ compensator solves these problems but it produces a more fluctuating power and bigger tower top velocities in x direction. However, generator speed is the less fluctuating of the three controllers.

Finally, controllers performance is tested for turbulent wind fields with higher mean wind speed, 18 m/s in this case. Once again, the good operation of the LQR controller is confirmed, checking the good operation of the controller gain scheduler.

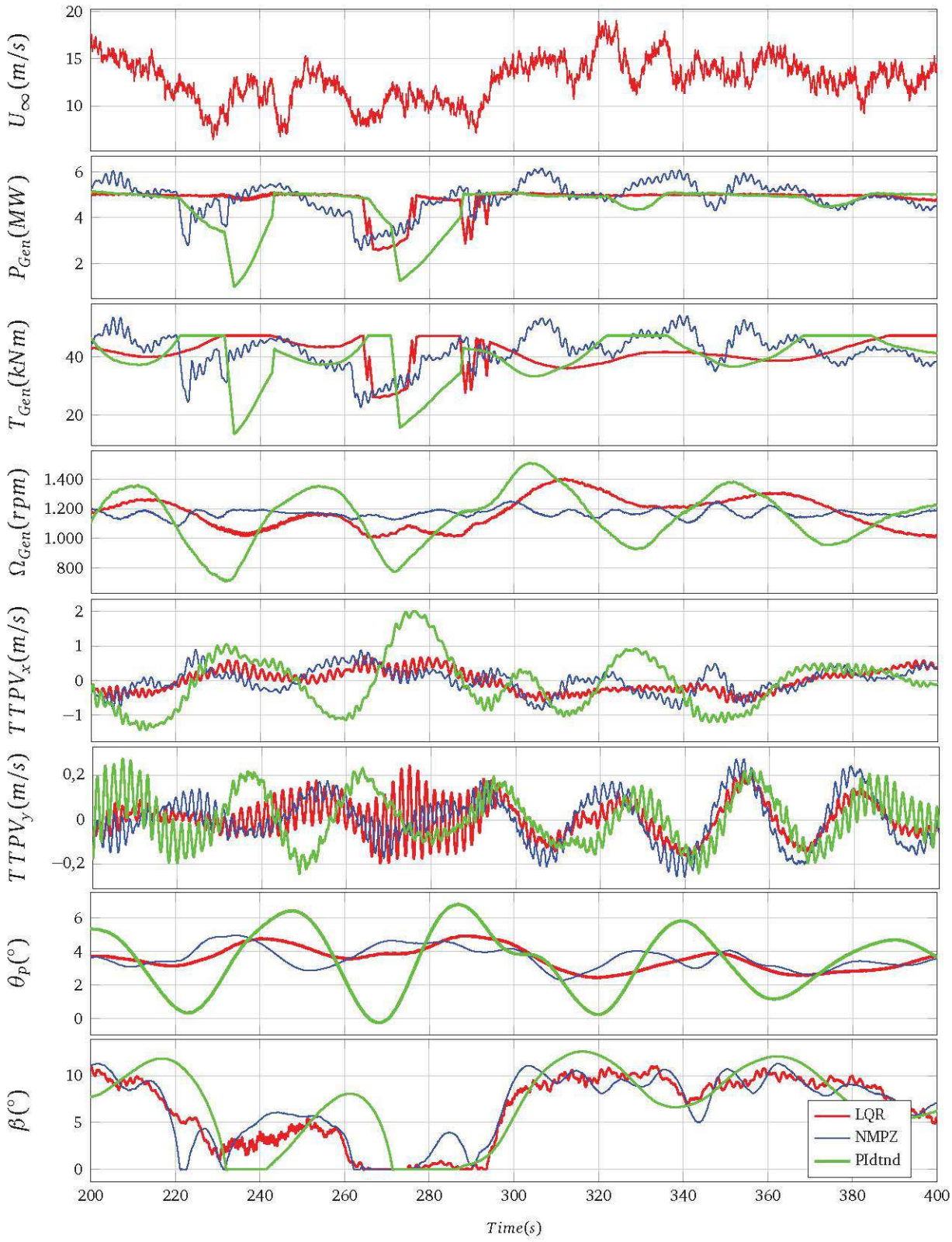

Figure 5.2.: Comparison between derated PI blade pitch controller, NMPZ compensator and LQR controller for a turbulent wind field with a mean wind speed of 12m/s.

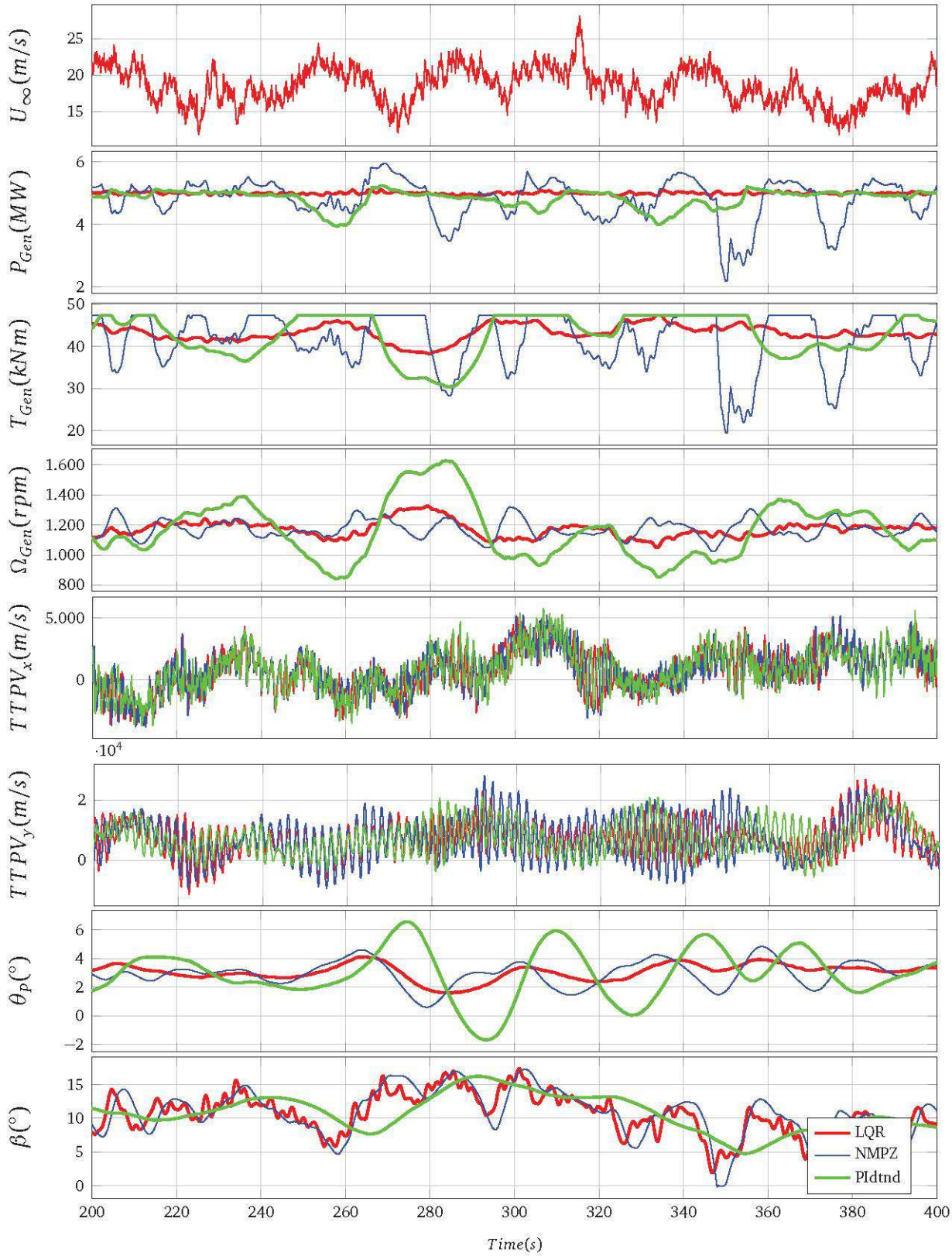

Figure 5.3.: Comparison between derated PI blade pitch controller, NMPZ compensator and LQR controller for a turbulent wind field with a mean wind speed of 18m/s.

5.2 Fatigue analysis

Comparing implemented controllers through a fatigue analysis can give relevant information. This analysis is carried out with Mlife tool [25]. This is a MATLAB based tool created to post-process results from FAST simulation tests. MLife computes statistical information and fatigue estimates for one or more time-series.

As it has been previously done, the analysis will be done for different working conditions. First one will be a turbulent wind field with a 15m/s mean wind speed, then a turbulent wind field with a 12m/s mean wind speed will be tested and finally a turbulent wind field with a 18m/s mean wind speed. The idea is to translate previously exposed time series into different statistical results and fatigue measurements. The variables that will be plotted are:

- Generated mean power.
- Generated power variance.
- Generator mean speed.
- Generator speed variance.
- Tower base roll moment $TwrBsM_x$.
- Tower base pitch moment $TwrBsM_y$.
- Tower top roll moment $TTPM_x$.
- Tower top pitch moment $TTPM_y$.
- Low-speed shaft torque T_{Rot}.

To develop an adequate statistical analysis with Mlife, first four different wind fields with the same mean wind speed are chosen. Afterwards, simulation time is set to 630 seconds. Finally, one simulation for each wind field is carried out for all controllers. With all of this data Mlif carries out the statistical analysis.

All variables are represented as per-unit values, taking PI controller's values as the base . This way, different controllers results will be easily compared.

In the first scenario of a mean wind speed of 15m/s, Figure 5.4 shows how NMPZ compensator and LQR controller improve produced mean power and its variance, specially LQR controller. Besides, generator speed variance is remarkably reduced.

Regarding to different moments, it can be seen how moments related to pitch moments decrease in a bigger way than those related to roll moments. That is because of the weight matrices chosen in the cost function of the LQR controller and because of the feedback of the tower top velocity in x direction. Indeed, although tower base and tower top pitch moments are reduced, roll moments do not achieve that. Low shaft torsion is reduced in the NMPZ compensator but augmented for the LQR controller.

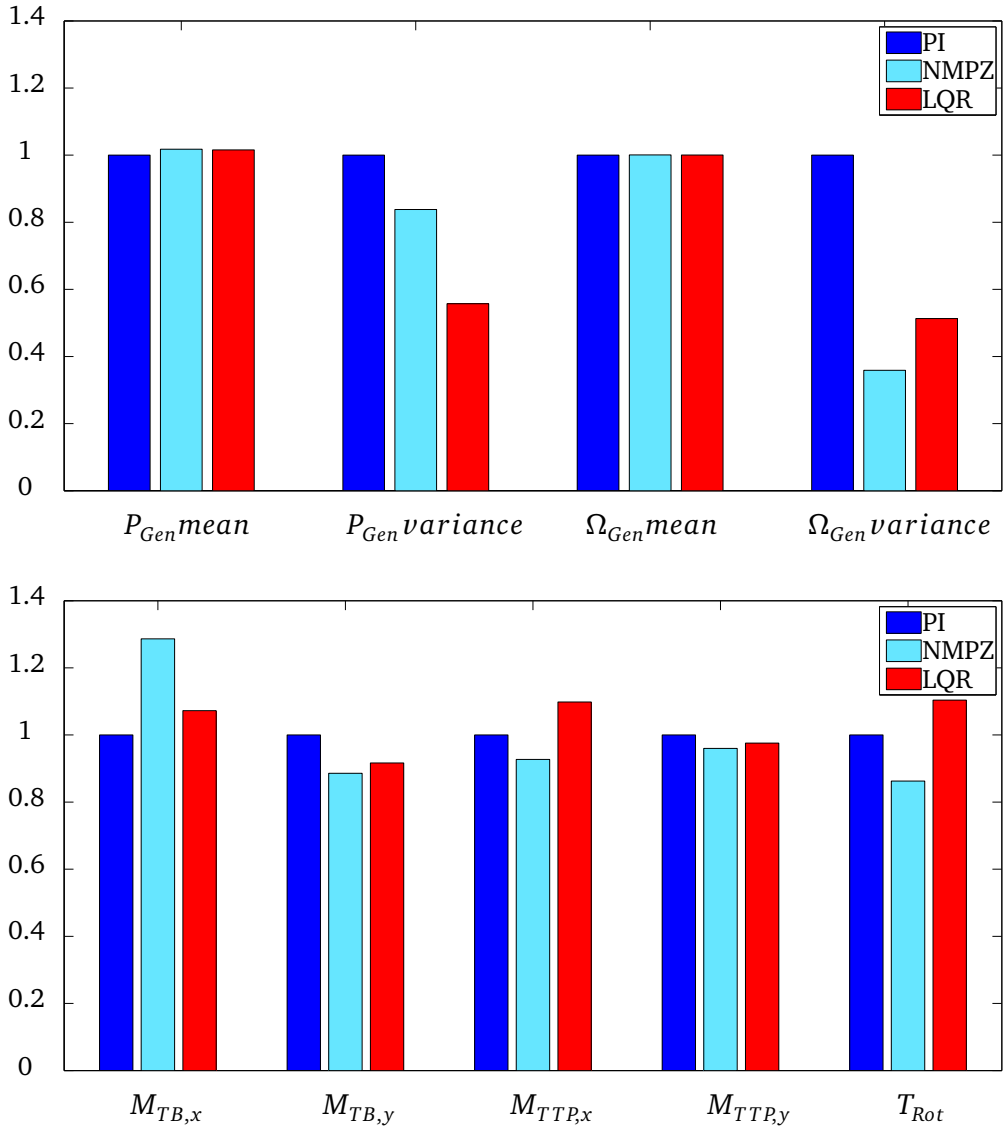

Figure 5.4.: Mlife fatigue analysis tool results for a real turbulent wind field with a mean wind speed of 15m/s.

When working condition imposes a mean wind speed of 12m/s, Figure 5.4 shows how NMPZ compensator and LQR controller improvements are not so remarkable. Since control region is frequently changing and improved controllers are switching on and off every time, their benefits are not as exploited as in the previous case. Although NMPZ compensator gets some good results in moment reduction, LQR controller can not make such a good improvement.

For higher wind speeds, a turbulent wind field with a mean wind speed of 18m/s, Figure 5.4 shows similar results to those obtained for a mean wind speed of 15m/s. However, NMPZ compensator performance is notably worst than in the previous case. Generated power variance achieve a very bad result. Generator speed variance is reduced in both NMPZ compensator and LQR controller though. In moments reduction LQR maintain more ore less its results, but NMPZ compensator achieve worst results than those achieved for a mean wind speed of 15m/s.

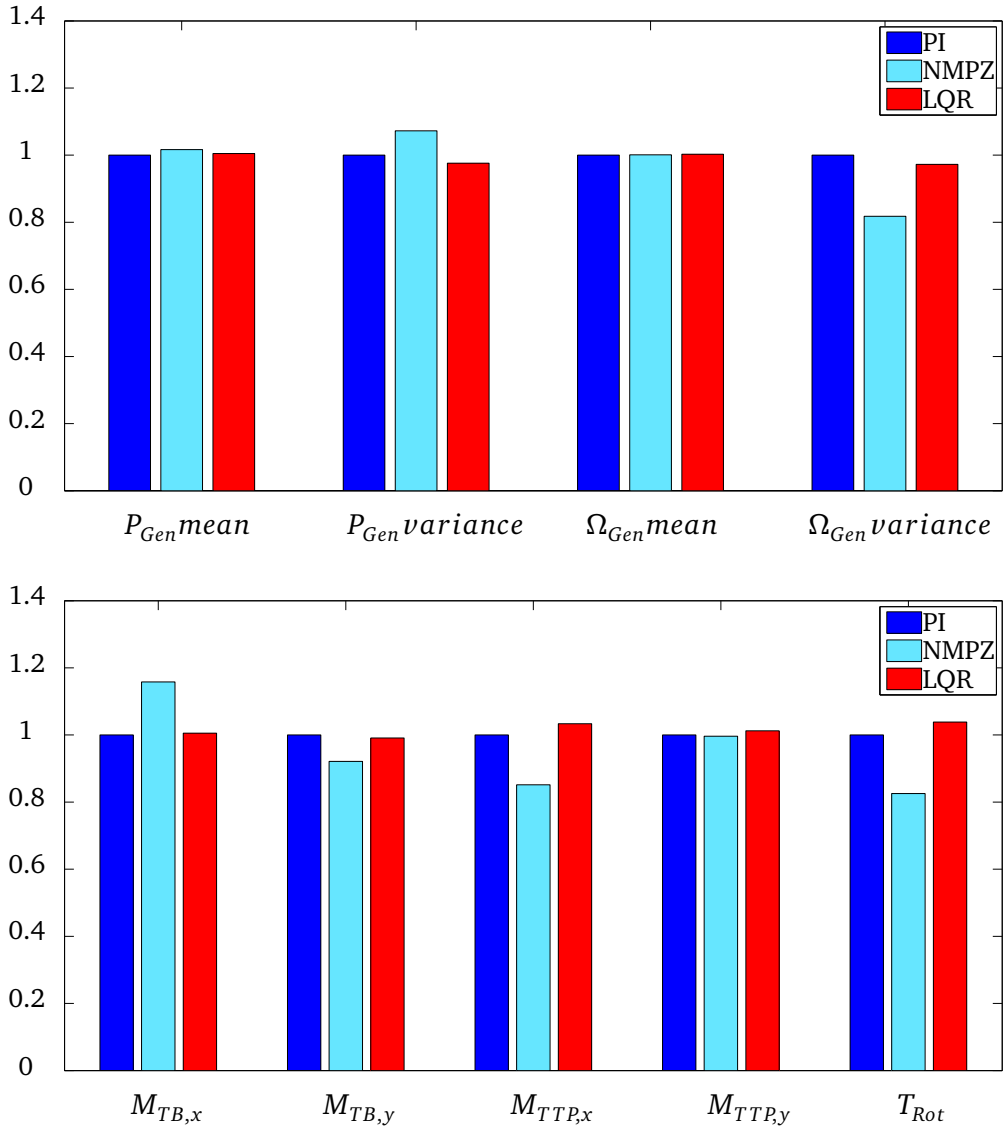

Figure 5.5.: Mlife fatigue analysis tool results for a real turbulent wind field with a mean wind speed of 12m/s.

Table 5.1, Table 5.2 and Table 5.3 summarize fatigue test results. In this table NMPZ compensator and LQR results are compared with PI derated controller fatigue test results. "✓✓" means that an excellent improvement has been achieved, "✓" that a good but not excellent improvement has been made, "=" that the result is the same and "X" means that the result is worst.

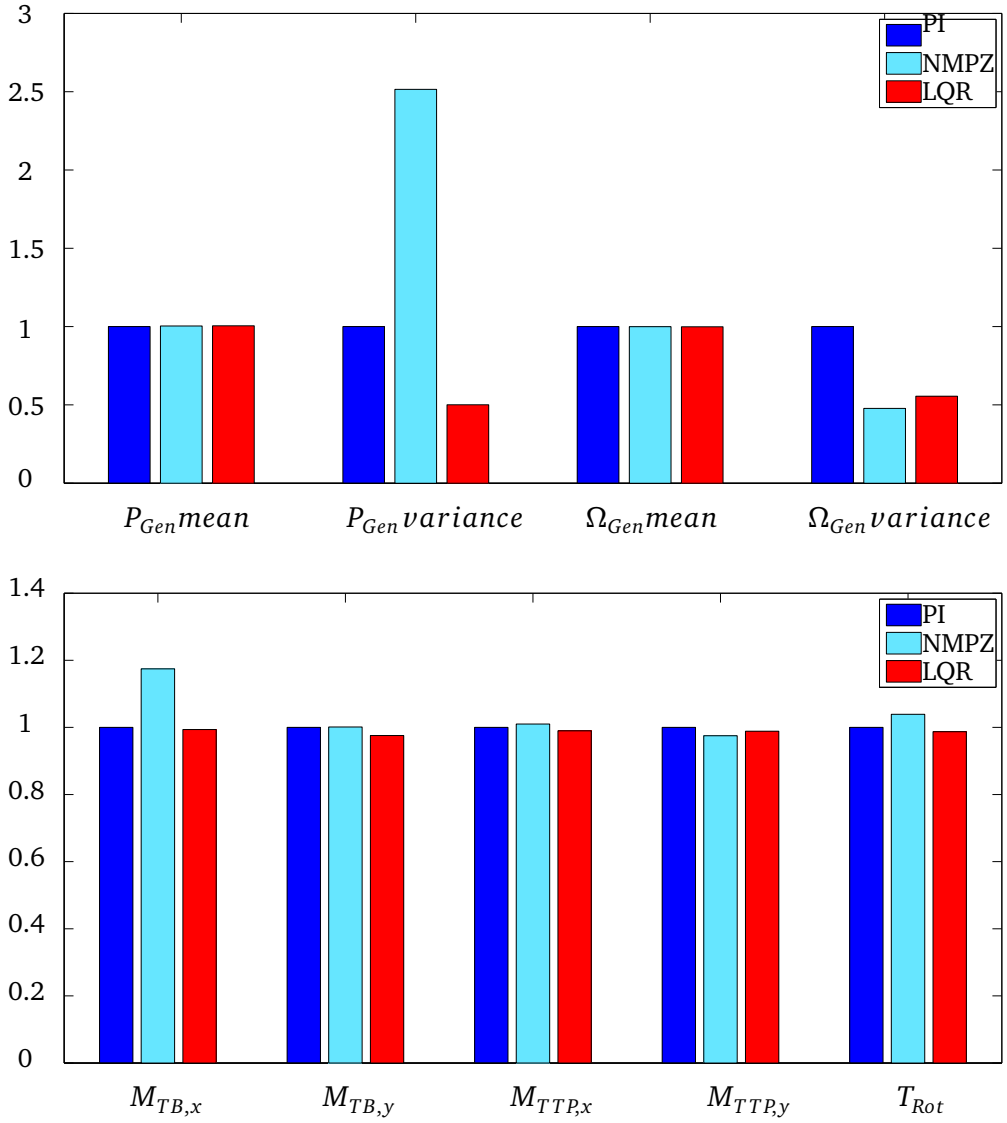

Figure 5.6.: Mlife fatigue analysis tool results for a real turbulent wind field with a mean wind speed of 18m/s.

Table 5.1.: Summary of the fatigue test results for a mean wind speed of 15m/s.

	NMPZ compensator	LQR controller
Generated mean power	✓	✓
Generated power variance	✓✓	✓✓
Generator mean speed	=	=
Generator speed variance	✓✓	✓✓
Tower base roll moment	X	X
Tower base pitch moment	✓	✓
Tower top roll moment	✓	X
Tower top pitch moment	✓	✓
Low speed shaft torque	✓✓	X

Table 5.2.: Summary of the fatigue test results for a mean wind speed of 12m/s.

	NMPZ compensator	LQR controller
Generated mean power	✓	✓
Generated power variance	X	✓
Generator mean speed	=	=
Generator speed variance	✓✓	✓
Tower base roll moment	X	=
Tower base pitch moment	✓	✓
Tower top roll moment	✓	X
Tower top pitch moment	✓	X
Low speed shaft torque	✓✓	X

Table 5.3.: Summary of the fatigue test results for a mean wind speed of 18m/s.

	NMPZ compensator	LQR controller
Generated mean power	✓	✓
Generated power variance	X	✓✓
Generator mean speed	=	=
Generator speed variance	✓✓	✓✓
Tower base roll moment	X	=
Tower base pitch moment	=	✓
Tower top roll moment	X	✓
Tower top pitch moment	✓	✓
Low speed shaft torque	X	✓

6 Conclusion

This chapter summarizes what has been done and what can be done from now on.

6.1 Summary

This thesis constitutes an approach to the modeling and control of floating offshore wind turbines. After getting familiar with some basic concepts and data of onshore and offshore wind energy, the work focuses on spar buoy floating offshore wind turbine concept, analyzing and modeling it in detail. Taking into account all the phenomena and working conditions related to FOWT the mathematical equations are derived. Using these equations a nonlinear complex model is developed. Once the model is designed, it is implemented in Simulink and tested. Since this model must be validated against an existing nonlinear model (FAST code), using a simulation environment that compares the results between both models the accuracy of the designed model is tested. In order to validate the model, some parameters are adjusted.

Afterwards, an introduction to turbine control and control objectives is done. Once a proper model is obtained, this model has to be properly controlled, so that the operation of the floating wind turbine is the adequate and reaches all the proposed objectives. Problems of instability when implementing the baseline classic controller in a floating turbine are shown and analyzed. Alternatives to the classic baseline controller are proposed, such as PI derated controller, NMPZ compensator and LQR controller. These controllers are calculated, developed and implemented so that appeared issues can be overcome. Finally, controllers performances when applying different working conditions are compared through time plots and fatigue analysis, showing the improvements that there have been achieved and the aspects that still need to be amended.

6.2 Accomplished Goals

The main objective of this thesis can be divided in two groups. First one, the design and validation of the floating offshore wind turbine model. The other objective is to achieve an stable operation of the turbine. In order to that different control strategies are developed and implemented.

Both objectives have been achieved. The model has been successfully designed and validated against FAST model. This designed model has been used to develop new controllers that overcome baseline controller issues and add improvements, such as better power quality or fatigue reduction, acomplishing the second objective of the stable operation of floating the wind turbine.

These controllers has been successfully implemented, tested and compared in FAST model. From made analysis of controllers performance in FAST model, it can be deduced the good results for NMPZ compensator and state feedback LQR controller comparing to PI derated controller.

From the simulation results it can be summarized that although the three tested controllers achieve an stable operation, for different working conditions advantages and inconveniences may appear with each controllers. It is clear that comparing with the derated PI controller, both NMPZ compensator and LQR controller have a better operation. Although NMPZ compensator achieve a higher moment reduction for a mean wind speed of 15m/s, when this value rises the results get worst. On the other hand LQR controller achieves smaller moment reductions, but these reductions stay very similar no matter the mean wind speed. In addition, LQR controller achieves a less fluctuating generated power, which is a very good advantage. Both controllers performance is deteriorated when the turbine operates close to the rated wind speed.

Table 6.1 summarized this results comparing NMPZ compensator and LQR controller with derated PI controller. "✓✓" means that an excellent result has been achieved, "✓" that a good but not excellent result has been made and "X" means that a bad result is achieved.

Table 6.1.: Summary of the controllers performance.

	NMPZ compensator	LQR controller
Nonfluctuating power	X	✓✓
Moment reduction near rated wind speed	✓	X
Moment reduction for common wind speed	✓✓	✓
Moment reduction for high wind speed	X	✓

6.3 Outlook to further research

The presented work opens new paths to further research and improvements, such as

- Implementation of improvements in the designed model. Addition of heave displacement and yaw movement.
- Design of new controllers: individual blade pitch controller, H infinite norm reduction controller, Non linear model predictive controller...
- Implementation of an observer in the system, in order to have the full system.
- Generating C code to implement control strategies in a micro-controller.
- Design of new mathematical models for different floating offshore wind turbine concept, such as ballast stabilized , mooring line stabilized or hybrid concepts.

A Matrices

In this appendix matrices contained in the system are summarized.

Added mass hydrodynamic matrix obtained from hydro model.

$$\mathbf{A}_{ij}^{\mathbf{Hydro}} = \begin{bmatrix} 1.6357 \cdot 10^{7} & 0 & 0 & -5.9 \cdot 10^{8} & 0 \\ 0 & 8.1787 \cdot 10^{6} & 4.9167 \cdot 10^{8} & 0 & 0 \\ 0 & 1.3767 \cdot 10^{9} & 2.1257 \cdot 10^{11} & 0 & 0 \\ -5.9 \cdot 10^{8} & 0 & 0 & 1.7321 \cdot 10^{11} & 0 \\ 0 & 0 & 0 & 0 & 0 \end{bmatrix}$$

Damping hydrodynamic matrix obtained from hydro model.

$$\mathbf{B}_{ij}^{\mathbf{Hydro}} = \begin{bmatrix} -3.4686 \cdot 10^{5} & 0 & 0 & 2.0812 \cdot 10^{7} & 0 \\ 0 & -1.3874 \cdot 10^{5} & -2.0812 \cdot 10^{7} & 0 & 0 \\ 0 & -1.6649 \cdot 10^{7} & -5.4922 \cdot 10^{8} & 0 & 0 \\ 4.1623 \cdot 10^{7} & 0 & 0 & -1.5490 \cdot 10^{8} & 0 \\ 0 & 0 & 0 & 0 & 0 \end{bmatrix}$$

Stiffness hydrodynamic matrix obtained from hydro model.

$$\mathbf{C}_{ij}^{\mathbf{Hydro}} = \begin{bmatrix} 3.5003 \cdot 10^{4} & 0 & 0 & 9.8735 \cdot 10^{6} & 0 \\ 0 & 7.0006 \cdot 10^{4} & 1.9747 \cdot 10^{6} & 0 & 0 \\ 0 & 2.816 \cdot 10^{6} & 5.3103 \cdot 10^{9} & 0 & 0 \\ 2.816 \cdot 10^{6} & 0 & 0 & 5.3103 \cdot 10^{9} & 0 \\ 0 & 0 & 0 & 0 & 0 \end{bmatrix}$$

Stiffness hydrostatic matrix obtained from hydro model.

$$\mathbf{C}_{ij}^{\mathbf{Hydrostatic}} = \begin{bmatrix} 0 & 0 & 0 & 0 & 0 \\ 0 & 0 & 0 & 0 & 0 \\ 0 & 0 & -4.99918 \cdot 10^{9} & 0 & 0 \\ 0 & 0 & 0 & -4.99918 \cdot 10^{9} & 0 \\ 0 & 0 & 0 & 0 & 0 \end{bmatrix}$$

Stiffness lines matrix obtained from mooring lines model.

$$\mathbf{C}_{ij}^{\mathbf{lines}} = \begin{bmatrix} 4.118 \cdot 10^{4} & 0 & 0 & -2.816 \cdot 10^{6} & 0 \\ 0 & 4.118 \cdot 10^{4} & 2.816 \cdot 10^{6} & 0 & 0 \\ 0 & 2.816 \cdot 10^{6} & 3.111 \cdot 10^{8} & 0 & 0 \\ -2.816 \cdot 10^{6} & 0 & 0 & 3.111 \cdot 10^{8} & 0 \\ 0 & 0 & 0 & 0 & 0 \end{bmatrix}$$

Model added mass matrix.

$$\mathbf{M}_{ij} = \begin{bmatrix} m_T + A_{11}^{Hydro} & 0 & 0 & A_{14}^{Hydro} & 0 \\ 0 & m_T + A_{22}^{Hydro} & A_{23}^{Hydro} & 0 & 0 \\ 0 & A_{32}^{Hydro} & I_T + A_{33}^{Hydro} & 0 & 0 \\ A_{41}^{Hydro} & 0 & 0 & I_T + A_{44}^{Hydro} & 0 \\ 0 & 0 & 0 & 0 & J_{DT} \end{bmatrix}$$

Model damping matrix.

$$\mathbf{D}_{ij} = \begin{bmatrix} B_{11}^{Hydro} & 0 & 0 & B_{14}^{Hydro} & 0 \\ 0 & B_{22}^{Hydro} & B_{23}^{Hydro} & 0 & 0 \\ 0 & B_{32}^{Hydro} & B_{33}^{Hydro} & 0 & 0 \\ B_{41}^{Hydro} & 0 & 0 & B_{44}^{Hydro} & 0 \\ 0 & 0 & 0 & 0 & 0 \end{bmatrix}$$

Model stiffness matrix.

$$\mathbf{K}_{ij} = \begin{bmatrix} C_{11}^{lines} & 0 & 0 & C_{14}^{lines} & 0 \\ 0 & C_{22}^{lines} & C_{23}^{lines} & 0 & 0 \\ 0 & C_{32}^{lines} & C_{33}^{Hydrostatic} + C_{33}^{lines} & 0 & 0 \\ C_{41}^{Hydro} & 0 & 0 & C_{44}^{Hydrostatic} + C_{44}^{lines} & 0 \\ 0 & 0 & 0 & 0 & 0 \end{bmatrix}$$

State space system state matrix.

$$\mathbf{A} = \begin{bmatrix} -\mathbf{M}^{-1}\mathbf{D} & \mathbf{M}^{-1}\mathbf{K} \\ \mathbf{I} & \mathbf{0} \end{bmatrix}$$

State space system input matrix.

$$\mathbf{B} = \begin{bmatrix} -\mathbf{M}^{-1} \\ \mathbf{0} \end{bmatrix}$$

State space system output matrix.

$$\mathbf{C} = \begin{bmatrix} \mathbf{c_{meas}} \\ \mathbf{I} \end{bmatrix}$$

State space system feedforward matrix.

$$\mathbf{D} = \begin{bmatrix} \mathbf{0_{5x3}} \end{bmatrix}$$

Measurement matrix.

$$\mathbf{c}^{\mathbf{meas}} = \begin{bmatrix} 1 & 0 & 0 & H-h_T & 0 & 0 & 0 & 0 & 0 & 0 \\ 0 & 1 & H-h_T & 0 & 0 & 0 & 0 & 0 & 0 & 0 \\ 0 & 0 & 0 & 0 & 0 & 0 & 0 & 0 & 0 & 0 \\ 0 & 0 & 0 & 0 & 0 & 0 & 0 & 0 & 0 & 0 \\ 0 & 0 & 0 & 0 & i_{GB}\frac{60}{2\pi} & 0 & 0 & 0 & 0 & 0 \end{bmatrix}$$

State feedback LQR controller matrix for the operating point reached with 15m/s.

$$\mathbf{K_{LQR}} = \begin{bmatrix} -6.61 & -16.85 & 6.22 & -1230 & -61.95 & -1.11 & -3.88 & 326.65 & -509.25 & -10 \\ 0.09 & 0.05 & 1.43 & -3.08 & 0.07 & -0.00045 & -0.002 & -0.025 & 0.29 & 0 \end{bmatrix}$$

State feedback LQR controller matrix for the operating point reached with 12m/s.

$$\mathbf{K_{LQR}} = \begin{bmatrix} -12.02 & -30.7 & -762.3 & -0.0016 & -81.03 & -2.9 & -7.2 & 390.6 & -802.7 & -10 \\ 0.39 & 0.18 & 6.9 & -16 & -0.49 & -0.01 & -0.01 & 0.16 & -1.6 & 0 \end{bmatrix}$$

State feedback LQR controller matrix for the operating point reached with 14m/s.

$$\mathbf{K_{LQR}} = \begin{bmatrix} -26.07 & -42 & -740 & -0.002 & -77.3 & -2.5 & -7.8 & 481 & -769.8 & -10 \\ 0.2 & 0.14 & 4.17 & -7.9 & -0.17 & -0.003 & -0.005 & -0.1 & -0.59 & 0 \end{bmatrix}$$

State feedback LQR controller matrix for the operating point reached with 16m/s.

$$\mathbf{K_{LQR}} = \begin{bmatrix} -39.8 & -59.9 & -378 & -0.002 & -86.8 & -2.64 & -8.38 & 407.6 & -617.8 & -10 \\ 0.16 & 0.1 & 3.3 & -6.02 & -0.1 & -0.003 & -0.003 & -0.33 & -0.18 & 0 \end{bmatrix}$$

State feedback LQR controller matrix for the operating point reached with 18m/s.

$$\mathbf{K_{LQR}} = \begin{bmatrix} -50.2 & -72.3 & -321.3 & -0.002 & -84.9 & -2.8 & -8.7 & 311 & -449.3 & -10 \\ 0.11 & 0.08 & 2.8 & -4.86 & -0.05 & -0.003 & -0.0008 & -0.4 & 0.06 & 0 \end{bmatrix}$$

State feedback LQR controller matrix for the operating point reached with 20m/s.

$$\mathbf{K_{LQR}} = \begin{bmatrix} -62 & -87.2 & 483.5 & -0.002 & -88 & -3.2 & -9.1 & 32.5 & -54.9 & -10 \\ 0.07 & 0.07 & 3.6 & -5.8 & -0.008 & -0.002 & 0.001 & -0.48 & 0.32 & 0 \end{bmatrix}$$

B Linearization

FOWT model is a system with high non linearities. For control design purpose or even to study the system, the global model can be linearized around an operating point. Due to the complexity of the designed FOWT model, it would be very tedious to make the linearization for it. Instead of that, a reduced model of the FOWT is used. The only difference between both models is a change of the aerodynamic model and the suppression of waves forces.

Regarding to aerodynamics, the dependance on relative high h is eliminated from wind speed. This way, in lieu of using Eq. (3.7),

$$v_{w,b} = U_{\infty} H^{0.2} \tag{B.1}$$

is used to define wind speed [7]. This simplification will make that tangential and normal forces will not depend on rotor azimuth. Hence, the forces in each blade will be the same.

$$F_{tan,1} = F_{tan,2} = F_{tan,3} \tag{B.2}$$

$$F_{nor,1} = F_{nor,2} = F_{nor,3} \tag{B.3}$$

From Eq. (3.12) thrust force total component will remain as

$$F_{th,red} = \frac{\rho A}{2} v(q)^2 C_M(\lambda,\beta) \tag{B.4}$$

and from Eq. (3.12), as well, axial total component will be 0 (three identical forces forming an angle of 120 °between them).

These modifications will lead to a non linear reduced state space model. System matrices will remain identical, the only change will be in non linear inputs.

$$\mathbf{A}^{\mathbf{red}} = \mathbf{A}, \qquad \mathbf{B}^{\mathbf{red}} = \mathbf{B}, \qquad \mathbf{C}^{\mathbf{red}} = \mathbf{C}, \qquad \mathbf{D}^{\mathbf{red}} = \mathbf{D},$$

Defining $\boldsymbol{u}$ as the linear inputs vector

$$\boldsymbol{u}^T = \begin{bmatrix} \beta & T_{Gen} \end{bmatrix} \tag{B.5}$$

$$\begin{cases} \dot{\boldsymbol{x}} = \mathbf{A}^{\mathbf{red}} \boldsymbol{x} + \mathbf{B}^{\mathbf{red}} \boldsymbol{f}_{\boldsymbol{u}}^{red}(\boldsymbol{x}^T, \boldsymbol{u}^T) \\ \boldsymbol{y} = \mathbf{C}^{\mathbf{red}} \boldsymbol{x} + \mathbf{D}^{\mathbf{red}} \boldsymbol{f}_{\boldsymbol{u}}^{red}(\boldsymbol{x}^T, \boldsymbol{u}^T) \end{cases} \tag{B.6}$$

This model will be the starting point to carry out the linearization, which will be locally valid around the chosen operating point. Eq. (B.6) can be written in compact form as

$$\begin{cases} \dot{\boldsymbol{x}} = \boldsymbol{f}(\boldsymbol{x}^T, \boldsymbol{u}^T) \\ \boldsymbol{y} = \boldsymbol{g}(\boldsymbol{x}^T, \boldsymbol{u}^T) \end{cases} \tag{B.7}$$

Since $\mathbf{D} = \mathbf{0}$ and $\mathbf{C}$ is a linear matrix, non linear parts related to outputs is zero. Letting

$$\begin{cases} \dot{\boldsymbol{x}} = \boldsymbol{f}(\boldsymbol{x}^T, \boldsymbol{u}^T) \\ \boldsymbol{y} = \mathbf{C}\boldsymbol{x} \end{cases} \tag{B.8}$$

This nonlinear reduced model can be easily linearized for a given equilibrium point, defined by a given state and input set point corresponding to an assigned value of the wind speed U_∞. The point around whom the system will be linearized will be the one reached when wind speed is 15m/s. This wind speed has been chosen because it is above rated wind speed, instability issues occur and it is a very common wind speed for offshore wind energy. States and linear inputs values are defined for this working stage as $\boldsymbol{x}_o$ and $\boldsymbol{u}_o$. Running a simulation with the designed model for this wind speed, steady state values can be found in this equilibrium point.

$$\boldsymbol{x}_o^T = \begin{bmatrix} 0 & 0 & 0 & 0 & 1.267 & 20.84 & 0 & 0 & 0.0334 & 0 \end{bmatrix}$$
$$\boldsymbol{u}_o^T = \begin{bmatrix} 0.1824 & 43093.55 \end{bmatrix}$$

Thus, the equilibrium point can be defined as

$$\boldsymbol{p}_s = \begin{bmatrix} \boldsymbol{x}_o^T & \boldsymbol{u}_o^T \end{bmatrix}$$

In order to linearized the system around the operation point, it is expanded with Taylor series until first derived.

$$\dot{\boldsymbol{x}} = \boldsymbol{f}(\boldsymbol{x}^T, \boldsymbol{u}^T) \tag{B.9}$$

$$\boldsymbol{f}(\boldsymbol{x}^T, \boldsymbol{u}^T) \approx \boldsymbol{f}(\boldsymbol{p}_s) + \left.\frac{\partial \boldsymbol{f}}{\partial \boldsymbol{x}}\right|_{p_s} \hat{\boldsymbol{x}} + \left.\frac{\partial \boldsymbol{f}}{\partial \boldsymbol{u}}\right|_{p_s} \hat{\boldsymbol{u}} \tag{B.10}$$

Since p_s is a steady state point $\dot{\boldsymbol{x}}(\boldsymbol{p}_s) = 0$ and $\boldsymbol{f}(\boldsymbol{p}_s) = 0$. Thus

$$\boldsymbol{f}(\boldsymbol{x}^T, \boldsymbol{u}^T) \approx \left.\frac{\partial \boldsymbol{f}}{\partial \boldsymbol{x}}\right|_{p_s} \hat{\boldsymbol{x}} + \left.\frac{\partial \boldsymbol{f}}{\partial \boldsymbol{u}}\right|_{p_s} \hat{\boldsymbol{u}} \tag{B.11}$$

Where $\hat{\boldsymbol{x}}$, $\hat{\boldsymbol{u}}$ and $\hat{U}_\infty$ are little variations respect to the equilibrium point. Now a linear state space system can be defined.

$$\frac{\mathrm{d}\boldsymbol{x}}{\mathrm{d}t} = \mathbf{A}^{\text{lin}}\hat{\boldsymbol{x}} + \mathbf{B}^{\text{lin}}\hat{\boldsymbol{u}} \tag{B.12}$$

$$\tag{B.13}$$

Where

$$\frac{\mathrm{d}\boldsymbol{x}}{\mathrm{d}t} = \begin{bmatrix} \frac{\mathrm{d}\dot{x}_T}{\mathrm{d}t} \\ \frac{\mathrm{d}\dot{y}_T}{\mathrm{d}t} \\ \frac{\mathrm{d}\dot{\theta}_r}{\mathrm{d}t} \\ \frac{\mathrm{d}\dot{\theta}_P}{\mathrm{d}t} \\ \frac{\mathrm{d}\dot{\varphi}}{\mathrm{d}t} \\ \frac{\mathrm{d}x_T}{\mathrm{d}t} \\ \frac{\mathrm{d}y_T}{\mathrm{d}t} \\ \frac{\mathrm{d}\theta_r}{\mathrm{d}t} \\ \frac{\mathrm{d}\theta_P}{\mathrm{d}t} \\ \frac{\mathrm{d}\varphi}{\mathrm{d}t} \end{bmatrix}, \qquad \hat{\boldsymbol{x}} = \begin{bmatrix} \hat{\dot{x}}_T \\ \hat{\dot{y}}_T \\ \hat{\dot{\theta}}_r \\ \hat{\dot{\theta}}_P \\ \hat{\dot{\varphi}} \\ \hat{x_T} \\ \hat{y_T} \\ \hat{\theta}_r \\ \hat{\theta}_P \\ \hat{\varphi} \end{bmatrix}, \qquad \hat{\boldsymbol{u}} = \begin{bmatrix} \hat{\beta} \\ \hat{T_{Gen}} \end{bmatrix}, \tag{B.14}$$

$$\mathbf{A}^{\mathbf{lin}} = \begin{bmatrix} \frac{\partial f_1}{\partial \dot{x}_T}\Big|_{p_s} & \cdots & \frac{\partial f_1}{\partial \varphi}\Big|_{p_s} \\ \vdots & \ddots & \vdots \\ \frac{\partial f_{10}}{\partial \dot{x}_T}\Big|_{p_s} & \cdots & \frac{\partial f_{10}}{\partial \varphi}\Big|_{p_s} \end{bmatrix}, \mathbf{B}^{\mathbf{lin}} = \begin{bmatrix} \frac{\partial f_1}{\partial \beta}\Big|_{p_s} & \frac{\partial f_1}{\partial T_{Gen}}\Big|_{p_s} \\ \vdots & \vdots \\ \frac{\partial f_{10}}{\partial \beta}\Big|_{p_s} & \frac{\partial f_{10}}{\partial T_{Gen}}\Big|_{p_s} \end{bmatrix}, \mathbf{B}_{\mathbf{w,lin}} = \begin{bmatrix} \frac{\partial f_1}{\partial U_\infty}\Big|_{p_s} \\ \vdots \\ \frac{\partial f_{10}}{\partial U_\infty}\Big|_{p_s} \end{bmatrix} \tag{B.15}$$

Using Matlab these derives are calculated numerically, given the resultant matrices

$$\mathbf{A}^{\mathbf{lin}} = \begin{bmatrix} 0.0335 & 0 & 0 & -1.3110 & -0.0664 & -0.0018 & 0 & 0 & -1.9489 & 0 \\ 0 & -0.0201 & -0.6973 & 0 & 0 & 0 & -0.0127 & 2.0638 & 0 & 0 \\ 0 & 5.1648 \cdot 10^{-5} & -0.0307 & 0 & 0 & 0 & 6.9081 \cdot 10^{-5} & -0.0383 & 0 & 0 \\ -3.5304 \cdot 10^{-6} & 0 & 0 & -0.0418 & -6.7296 \cdot 10^{-4} & 1.0225 \cdot 10^{-5} & 0 & 0 & -0.0373 & 0 \\ -0.0267 & 0 & 0 & -2.3516 & -0.1526 & 0 & 0 & 0 & 0 & 0 \\ 1 & 0 & 0 & 0 & 0 & 0 & 0 & 0 & 0 & 0 \\ 0 & 1 & 0 & 0 & 0 & 0 & 0 & 0 & 0 & 0 \\ 0 & 0 & 1 & 0 & 0 & 0 & 0 & 0 & 0 & 0 \\ 0 & 0 & 0 & 1 & 0 & 0 & 0 & 0 & 0 & 0 \\ 0 & 0 & 0 & 0 & 1 & 0 & 0 & 0 & 0 & 0 \end{bmatrix}$$

$$\mathbf{B}^{\mathbf{lin}} = \begin{bmatrix} -0.0161 & 0 \\ 0 & 0 \\ 0 & -2.3898 \cdot 10^{-6} \\ -1.6307 \cdot 10^{-4} & 0 \\ -0.0159 & 0 \\ 0 & 0 \\ 0 & 0 \\ 0 & 0 \\ 0 & 0 \\ 0 & 0 \end{bmatrix}, \qquad \mathbf{C}^{\mathbf{lin}} = \mathbf{C}, \qquad \mathbf{D}^{\mathbf{lin}} = \mathbf{D}$$

The final result is an invariant in time linear state space system.

$$\begin{cases} \dot{\boldsymbol{x}} = \mathbf{A}^{\mathbf{lin}}\boldsymbol{x} + \mathbf{B}^{\mathbf{lin}}\boldsymbol{u} \\ \boldsymbol{y} = \mathbf{C}^{\mathbf{lin}}\boldsymbol{x} + \mathbf{D}^{\mathbf{lin}}\boldsymbol{u} \end{cases} \tag{B.16}$$

Stability of the system is check performing a $\mathbf{A}^{\mathbf{lin}}$ matrix eigenvalues analysis. Introducing the Matlab command `eig(A)`.

$$\boldsymbol{eig} = \begin{bmatrix} 0 \\ -0.0099 \pm 0.0889i \\ -0.0139 \pm 0.0454i \\ -0.0151 \pm 0.1907i \\ -0.0172 \pm 0.1865i \\ -0.1658 \end{bmatrix}$$

Since there is no eigenvalue with positive real part, the system is stable.

Controlability of the system needs to be check as well. A system is controllable if, applying adequate inputs, it is able to change from one state to a different one. Mathematical relation shown in Eq. (4.27) need to be fulfilled to ensure system's controlability.

$$rank\begin{bmatrix} \mathbf{B}^{\mathbf{lin}} & \mathbf{A}^{\mathbf{lin}}\mathbf{B}^{\mathbf{lin}} & \mathbf{A}^{\mathbf{lin}^2}\mathbf{B}^{\mathbf{lin}} & \cdots & \mathbf{A}^{\mathbf{lin}^n}\mathbf{B}^{\mathbf{lin}} \end{bmatrix} = n \tag{B.17}$$

Where n is the system's number of states. Studied system is perfectly controllable.

List of Figures

List of Tables

Bibliography

[1] *BP Statistical Review of World Energy 2015*. Technical Report, BP p.l.c, 2016.

[2] *Renewables 2016. Global Status Report.* Technical Report, REN 21, 2016.

[3] Hau, Eric: *Wind Turbines. Fundamentals, Technologies, Application, Economics*. Springer, Third, translate edition edition, 2013.

[4] *Global Wind Report. Annual Market Update 2015*. Technical Report, Global Wind Energy Council, 2016.

[5] *Renewable Energy Technologies: Cost Analysis Series*. Technical Report, IRENA, 2012.

[6] Bossanyi., Tony Burton. David Sharpe. Nick Jenkins. Ervin: *Wind Energy Handbook*. John Wiley & Sons, LTD, 2001.

[7] Hansen, O. L.: *Aerodynamics of Wind Turbines*. EARTHSCAN, Second edition edition, 2008.

[8] *Offshore Wind Energy*. Technical Report, Enviromental and Energy Study Institute, 2010.

[9] Krogsgaard, Madsen &: *Offshore Wind Power 2010*. Technical Report, BTM Consult, 2011.

[10] *The European offshore wind industry key trends and statistics 2015*. Technical Report, The European Wind Energy Association, 2016.

[11] Jonkman, J.M.: *Dynamics Modeling and Loads Analysis of an Offshore Floating Wind Turbine*. PhD thesis, National Renewable Energy Laboratory, 2007.

[12] *Hywind Scotland Pilot Park Project*. Technical Report, Statoil Wind Limited (SWL), 2013.

[13] Sclavounos, S. Butterfield W. Musial J. Jonkman P. and L. Wayman: *Engineering Challenges for Floating Offshore Wind Turbines*. 2005.

[14] Jonkman, J.: *Definition of the Floating System for Phase IV of OC3*. Technical Report, NREL, 2010.

[15] J. Jonkman, S. Butterfield, W. Musial and G. Scott: *Definition of a 5-MW Reference Wind Turbine for Offshore System Development*. Technical Report, NREL, 2009.

[16] Vire, Axelle: *How to float a wind turbine*. Science Career, 2012.

[17] Thanh-Toan Tran, Dong-Hyun Kim: *The platform pitching motion of floating offshore wind turbine: A preliminaryun steady aerodynamic analysis*. Journal ofWindEngineering and IndustrialAerodynamics, 2015.

[18] Bastian Ritter, Holger Fürst, Ulrich Konigorski and Mike Eichhorn: *Multivariable Model for Simulation and Control Design of Wind Turbines*. 2015.

[19] Chandrasekaran, Srinivasan: *Dynamic Analysis and Design of Offshore Structures*. Springer, 2015.

[20] Sandner, Frank: *Reduced Model Design of a Floating Wind Turbine*. Master's thesis, University of Stuttgart, 2012.

[21] Hansen, M. H., Hansen A. Larsen T. J. Oye S. Sorensen and P. Fuglsang: *Control Design for a Pitch-Regulated, Variable-Speed Wind Turbine*. Riso National Laboratory, 2005.

[22] Larsen, T. J. and T. D. Hanson: *A method to avoid negative damped low frequent tower vibrations for a floating, pitch controlled wind turbine*. IOP science, 2007.

[23] Fischer, Boris: *Reducing rotor speed variations of floating wind turbines by compensation of non-minimum phase zeros*. IET Renewable Power Generation, 2012.

[24] Skogestad, Sigurd and Ian Postlethwaite: *Multivariable Feedback Control. Analysis and design*. John Wiley & Sons, LTD, 2001.

[25] Hayman, G. J. and Jr. M. Buhl: *MLife User's Guide for Version 1.00*, 2012.